Embedding a Grid of Load Cells into a Dining Table for Automatic Monitoring and Detection of Eating Events

A Dissertation
Presented to
the Graduate School of
Clemson University

In Partial Fulfillment
of the Requirements for the Degree
Doctor of Philosophy
Electrical Engineering

by
Mohammad Mayyan
August 2022

Accepted by:
Dr. Adam Hoover, Committee Chair
Dr. Harlan Russell
Dr. Jacob Sorber
Dr. Ian Walker

Abstract

This dissertation describes a "smart dining table" that can detect and measure consumption events. This work is motivated by the growing problem of obesity, which is a global problem and an epidemic in the United States and Europe. Chapter 1 gives a background on the economic burden of obesity and its comorbidities. For the assessment of obesity, we briefly describe the classic dietary assessment tools and discuss their drawback and the necessity of using more objective, accurate, low-cost, and in-situ automatic dietary assessment tools. We explain in short various technologies used for automatic dietary assessment such as acoustic-, motion-, or image-based systems. This is followed by a literature review of prior works related to the detection of weights and locations of objects sitting on a table surface. Finally, we state the novelty of this work.

In chapter 2, we describe the construction of a table that uses an embedded grid of load cells to sense the weights and positions of objects. The main challenge is aligning the tops of adjacent load cells to within a few micrometer tolerance, which we accomplish using a novel inversion process during construction. Experimental tests found that object weights distributed across 4 to 16 load cells could be measured with 99.97±0.1% accuracy. Testing the surface for flatness at 58 points showed that we achieved approximately 4.2±0.5 um deviation among adjacent 2x2 grid of tiles. Through empirical measurements we determined that the table has a 40.2 signal-to-noise ratio when detecting the smallest expected intake amount (0.5 g) from a normal meal (approximate total weight is 560 g), indicating that a tiny amount of intake can be detected well above the noise level of the sensors.

In chapter 3, we describe a pilot experiment that tests the capability of the table to monitor eating. Eleven human subjects were video recorded for ground truth while eating a meal on the table using a plate, bowl, and cup. To detect consumption events, we describe an algorithm that analyzes the grid of weight measurements in the format of an image. The algorithm segments the

image into multiple objects, tracks them over time, and uses a set of rules to detect and measure individual bites of food and drinks of liquid. On average, each meal consisted of 62 consumption events. Event detection accuracy was very high, with an F1-score per subject of 0.91 to 1.0, and an F1 score per container of 0.97 for the plate and bowl, and 0.99 for the cup. The experiment demonstrates that our device is capable of detecting and measuring individual consumption events during a meal.

Chapter 4 compares the capability of our new tool to monitor eating against previous works that have also monitored table surfaces. We completed a literature search and identified the three state-of-the-art methods to be used for comparison. The main limitation of all previous methods is that they used only one load cell for monitoring, so only the total surface weight can be analyzed. To simulate their operations, the weights of our grid of load cells were summed up to use the 2D data as 1D. Data were prepared according to the requirements of each method. Four metrics were used to evaluate the comparison: precision, recall, accuracy, and F1-score. Our method scored the highest in recall, accuracy, and F1-score; compared to all other methods, our method scored 13-21% higher for recall, 8-28% higher for accuracy, and 10-18% higher for F1-score. For precision, our method scored 97% that is just 1% lower than the highest precision, which was 98%.

In summary, this dissertation describes novel hardware, a pilot experiment, and a comparison against current state-of-the-art tools. We also believe our methods could be used to build a similar surface for other applications besides monitoring consumption.

Dedication

With all my love to my wonderful wife, Noha, and to my children, Areez and Moayad.

Acknowledgments

I would like to express my deepest and sincere appreciation to my academic adviser Dr. Adam Hoover for his guidance and advice through the steps of scientific research and academic writing. Dr. Hoover's mentorship, starting from the practical and project-based classes through the time I was writing this dissertation, has greatly impacted various aspects of my life. I would also like to extend my deepest gratitude to my committee members: Dr. Harlan Russell, Dr. Jacob Sorber, and Dr. Ian Walker, for their time and effort spent reviewing my dissertation. I am also grateful to Dr. Christopher Post for an assistantship and the chance he gave me to work on his research project, which broadened my Ph.D. experience.

Words can never express my gratitude and thanks to my wife, Noha Alzahrani, for everything she has done for me to achieve and deliver this work. I would not have been able to reach this milestone in my academic journey without her love, care, and support.

Special thanks to Mr. David Moline, the Holcombe Department of Electrical and Computer Engineering lab technologist, for his help in supporting my hardware development and data collection. His knowledge and expertise were very helpful and allowed me to overcome technical issues. I am also grateful to Mr. Wayne Chao from the Forestry and Environmental Conservation Department for his help in cutting lumber that was used to complete the surface of the dining table presented in this work.

I must also thank and acknowledge the help I received from Dr. Ryan S. Mattfeld and Dr. Vasileios Papapanagiotou to complete the comparison of algorithms. I also must thank all subjects who participated in the study and whose voluntary participation was an important part of this study.

Table of Contents

List of Tables

List of Figures

Chapter 1

Introduction

This dissertation describes a new method for automatic monitoring of eating activities taking place on a dining table. The motivating problem is obesity, which is a growing global health problem [4]. In the United States, obesity is a national epidemic and associated with some of the leading causes of death [5, 6]. After the Americas, Europe comes next in the prevalence of obesity, where 59% of adults and almost 1 in 3 children are overweight or obese. The study and treatment of obesity involves acquiring information about daily eating habits. Classic tools used to acquire this information, such as a 24-hour dietary recall (24HR), can be inaccurate and biased; patients tend to forget or might report false information [21, 34]. New tools are being developed to overcome this problem by automatic the monitoring of eating behaviors to provide more objective and accurate information [96]. Some examples include wearable sensors, cameras, and smart utensils. This dissertation considers a new method for automatic monitoring of eating taking place on a dining table. This tool is ideal for monitoring behaviors in a home or other fixed setting where a lot of eating may occur.

In this work, we describe the construction of a 2D grid of load cells in the form of a dining table. The instrument is constructed using a grid of load cells to produce an image of weight measurements giving weights and positions of objects resting on the grid surface. Processing a stream of these frames enables continuous tracking of changes in weight and position of the objects. The load cells are mounted on a metal sheet which is placed on a wooden box that encloses an electronic system. Signals produced by the load cells are digitized by the electronic system and sent to a computer for image processing and tracking of objects, and hence eating events are detected.

Performance of the instrument was evaluated for accurate weight measurements and for correct spatial representation of footprints of objects placed on the grid surface. After getting an approval from the Institution Review Board (IRB) of Clemson University, a pilot study was conducted to collect data of 11 human subjects eating on the dining table. Using the data collected from this pilot study, an algorithm was developed to process the data. The algorithm consists of two parts: image segmentation using geometric information of the objects placed on the table surface, and a rule based algorithm, which analyzes the sequence of weight changes in the weight profile of each object, to detect intake events. More human subjects — total of 32 — were recorded to compare the developed algorithm against other state-of-the-art methods in related prior studies. Similar instruments have been developed that use far less load cells per unit area and provide less information. The work done by Mattfeld *et al.*, for example, uses only 1D measurements produced by one load cell, representing total weight of a food tray on which food and beverage were placed [127]. For this case, the 2D measurements produced by the grid of load cells were summed up into 1D weight profile that was fed to Mattfeld's algorithm.

The rest of this chapter provides background on the medical problems associated with obesity, classic tools for the measurement of eating behaviors, and related research on new tools for automating the eating monitoring process. We also provide background on load cell sensors. Finally, the chapter concludes with a statement of novelty and specific questions that this work endeavors to answer.

1.1 Obesity

Overweight and obesity is alarmingly increasing worldwide and has grown to epidemic proportions. In 2019, the Global Burden of Disease Study identified dietary habits among the top five risks for global deaths (second for females, third for males) [136,200]. According to the World Health Organization (WHO), overweight and obesity are defined as abnormal or excessive fat accumulation that may impair health [4]. An adult person (18 years of age and older) is classified to have obesity or overweight by using the body mass index (BMI). The BMI is defined as a person's weight in kilograms divided by the square of their height in meters (kg/m^2). An adult with BMI from 25 to 30 is classified to have overweight. Obesity is a BMI larger than 30. In 2016, 39% of the world's adult population were over weight and 13% were obese. The problem of obesity and overweight is

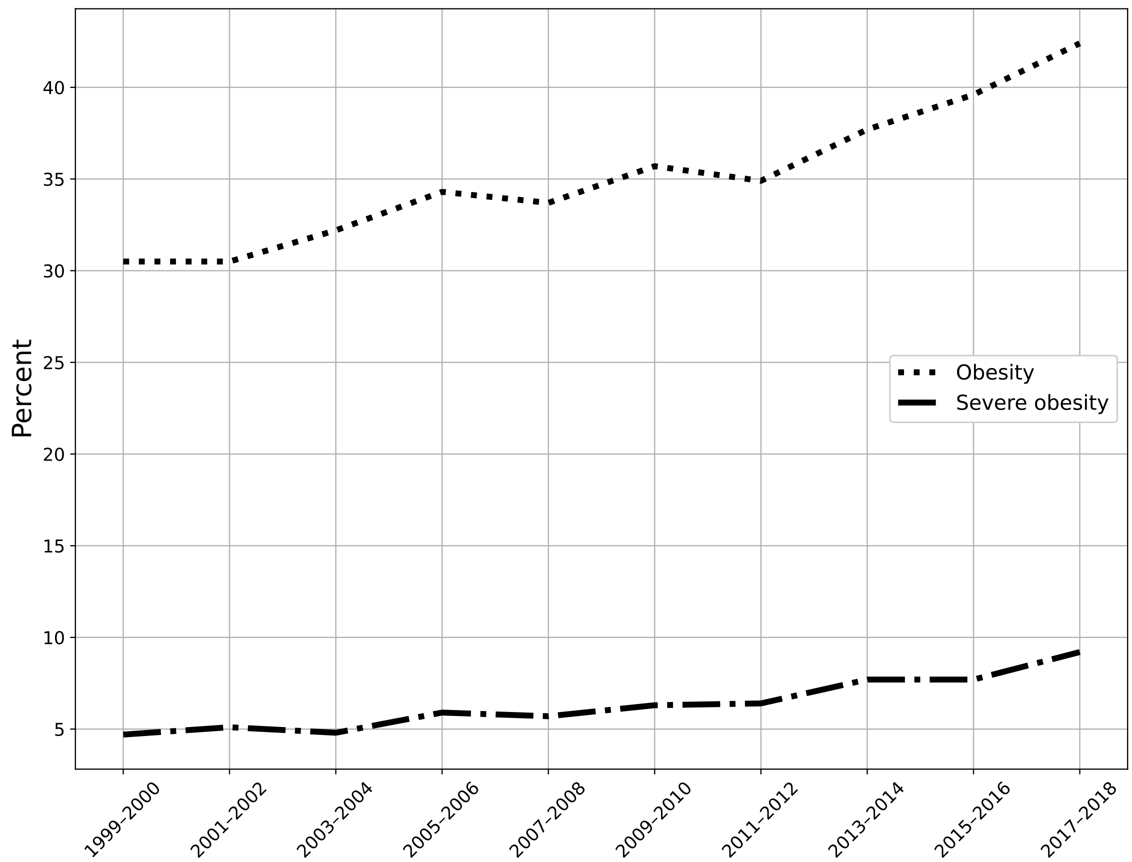

Figure 1.1: Trend of increasing obesity over the last two decades for a sample size of 4,989±582 people with age-adjustment [66]. Y axis is the percentage of the population. X axis is the time period.

affecting even children, and is not limited to high-income countries but even low and middle-income countries. The number of deaths as a result of obesity and overweight is larger than that of underweight. Overweight and obesity are responsible of the death of at least 4 million people every year. The National Health and Nutrition Examination Survey (NHANES) shows an age-adjusted trends of increasing obesity and severe obesity (BMI at or above 40.0) of American adults 20–74 years old from the years 1960–1962 through 2017–2018 [66]. Fig.1.1 illustrates the increasing trend of obesity over the last two decades for a sample size of 4,989±582 people with age-adjustment.

Obesity has a direct and indirect economic burden to patients, their families, and nations [25, 43, 175, 196]. For direct economic burden, several studies agree that higher BMI translates to a higher medical expenditure [209]. It was found that, for example, there was 1.9% higher in median medical spending for each one-unit increase of BMI during 18-months period when studying a stratified random sample of 5,689 people [158]. Obese and overweight people are charged higher for healthcare and health-insurance premiums [175]. Increases in body weight due to obesity would likely imply more costs for transportation; vehicles consume more fuel when loaded with heavier weights, and people having larger bodies would likely need bigger vehicles. Several studies have investigated the increased costs due to obesity and overweight for commercial and non-commercial passengers [50, 90]. A study, for example, found that each additional one pound increase in the average passenger weight in the United States results in over 39 million gallons of annual fuel consumption in passenger vehicles for noncommercial purposes [91].

Indirect costs include, but are not limited to, unproductivity and human capital. In the United States, the national productivity losses as a result of absenteeism due to morbid obesity range from $13.4 to $26.8 billion in 2016 [39]. Several studies used different measures, methods, and approaches, however, they agree that absenteeism and obesity have positive correlations with statistical significance [101, 162]. Attending workplace while suffering morbid obesity that lowers productivity is known as presenteeism, which was found to have a higher cost than absenteeism [61]. Premature mortality caused by obesity-related health problems is a loss of investment on professional training and skill developments that employers provide to their employees [74, 79]. Obesity hinders education outcomes as observed by several studies investigating the effect of obesity on human capital in childhood [174]. Educational attainment of both males and females are negatively affected by obesity but the impact is stronger on females [152, 167]. The same negative impact of obesity was also observed on cognitive performance for children [19,28]. Obesity is associated with higher hazard ratios for unemployment than that of people with normal BMI [33].

Comorbidities associated with obesity contribute to high mortality rates especially at higher levels of BMI [4, 7, 13]. Cardiovascular diseases (CVD), Type 2 Diabetes Mellitus (T2DM), hypertension, and cancer are major comorbidities of obesity. Tha vast majority of epidemiological studies consider obesity as an independent CVD predictor [75, 89, 100, 107, 123, 126, 159, 198]. Obesity is associated with a spectrum of cardiovascular diseases including coronary artery disease, congestive heart failure, hypertension, stroke, arrhythmias, and sudden cardiac death [40, 67, 80, 100, 100, 109, 123, 130, 153, 155, 159, 169, 203]. Obesity was classified by the American Heart Association as major risk factor for coronary heart disease [56].

Obesity is associated with alterations in immune function [138]. Observational studies have linked obesity to 13 types of cancer [8]. It was shown that absence of body fatness lowers cancer risk of different types of cancer [115]. Obesity suppresses anti-tumor immunity through impairing function of $CD8^{+}$ T cells, which are vital for killing cancerous or virally infected cells, thereby accelerating tumor growth [165, 215]. In humans and animals, numerous studies have shown that obesity alters T cells steady-state number, function, and maintenance [99, 149, 182]. Obese people were at risk to suffer severe COVID-19 disease and obesity was found to be a strong and independent determinant of increased risk of mortality in COVID-19 infected patients [186].

The prevalence of T2DM is projected to reach 25% to 28% by 2050 in the US adult population [32]. Obesity is associated with the development of T2DM [9]. Independently of family history of diabetes, BMI was found to be the dominant predictor of risk for T2DM for adult women and men [41, 47, 48, 106]. Risk for T2DM increased with BMI > 23 [41, 47]. In an observational study of 22,171 male health professionals, who were observed for 12 years, weight gain was monotonically related to risk for T2DM, and the risk increased by 7.3% for every kilogram of weight gained [106]. There is no clear understanding of causal relationships [214]. Moreover, there is no consensus for a clear understanding of the complex relationship between obesity and metabolic diseases or what first triggers the other [14, 95, 122, 214]. Nevertheless, accumulating evidence suggests that even small weight loss improves several diabetes risk parameters [17, 20, 210].

1.1.1 Obesity Treatment and Prevention

The prevalence of obesity is driven by adoption of modern lifestyles, in which many people follow sedentary habits and eat high calorie foods. Treatment of obesity includes losing weight through eating healthy foods, more physical activities, and adopting changes in lifestyle [10]. Energy imbalance between the intake and expenditure of calories can be measured as a cause of overweight and obesity [4]. Cheap, energy-dense, low nutritional value foods contribute to more energy intake and to gaining more weight. Engagement in multidisciplinary weight loss programs and increasing daily physical activities helps to reverse and prevent the development of obesity. A doctor may consider adding other treatments for the cases when some patients cannot lose weight through the aforementioned ways. These treatments including weight-loss medicines, weight-loss devices, or bariatric surgery [10,191]. Although bariatric surgery can improve obesity related comorbidities [18], it is associated with higher complication rates such as abdominal pain, gastroduodenal ulcers, and iron deficiency [92].

1.2 Classic Dietary Assessment Tools

Monitoring of eating behavior and energy intake helps people to gain awareness and adopt healthy eating practices and improve their diet [35, 36]. Dietitians and researchers also use dietary assessment tools to keep records of eating behavior for individuals or populations. Currently, the most widely used dietary assessment tools are classical such as dietary records, 24-hour dietary recall, and food frequency questionnaire (FFQ) [193, 194]. An overview of each of the classical tools is presented in this section.

With dietary records, respondents record the types and amounts, and timings of the foods and beverages consumed over one or more days on open-ended or close-ended forms [141] Respondents are supposed to record the information concurrently when they eat their meals. They need to be trained to provide detailed information about what they eat such as names of foods, preparation methods, recipes, and portion sizes. In some cases, an investigator contacts the respondents to review the records. At the end of the recording period a reviewer checks with the respondents to clarify the records.

Collected information using dietary records decreases over more recording days due to forgetfulness or fatigue [71]. This method might fail to measure the actual energy intake as it could alert the respondents while they measure and record their foods and beverages. As a result, this process could alter their actual dietary behavior, which is meant to be monitored and measured accurately. Although numerous smartphone apps are being used as a convenient way for data entry, respondents still need to manually log their dietary information into such mobile apps. This method might be burdensome and is subject to biases and inaccuracy. Several studies reported that dietary records underestimate energy intake in the range of 4% to 37% compared to energy intake measured using doubly labeled water [72,195]. The doubly labeled water (DLW) is the gold standard, unbiased reference technique for assessing total energy expenditure in free-living individuals [27, 37, 38, 184].

In a 24-Hour dietary recall, the respondents are asked to remember and record what they ate and drank in the past 24 hours. A well-trained reviewer is usually involved to probe the respondents with questions to help them remember forgotten consumed foods, beverages, and snacks with portion sizes, preparation methods, and any other related information. Currently, the U.S. National Health

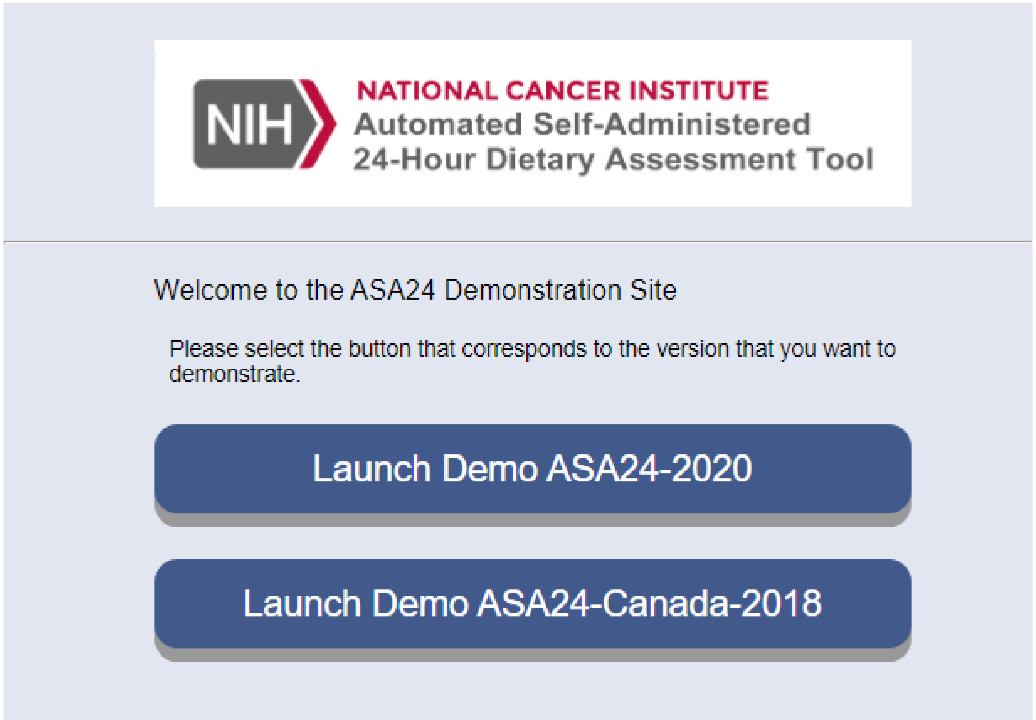

(a)

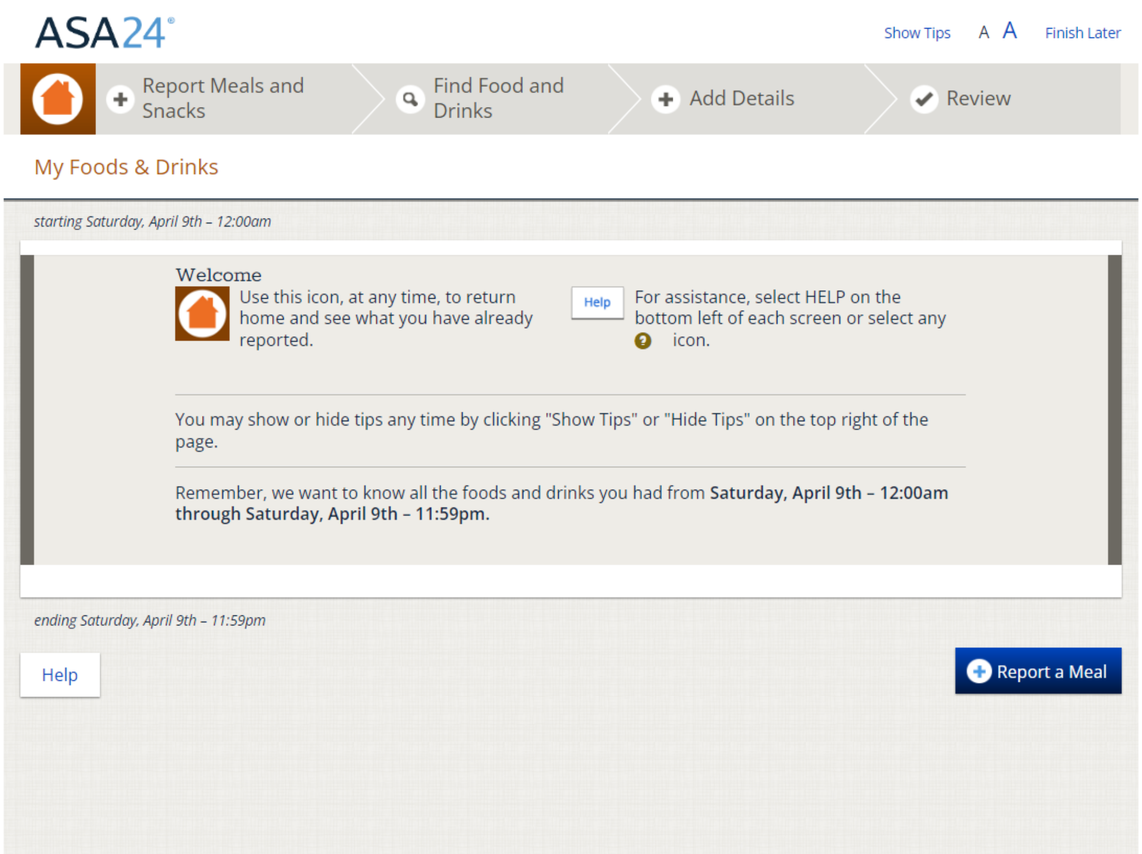

(b)

Figure 1.2: Automated, self-administered 24-hour dietary recall (ASA24) [1,2]. (a) A demonstration site for the ASA24 system. (b) The user is reminded to record detailed information about what they ate the last day.

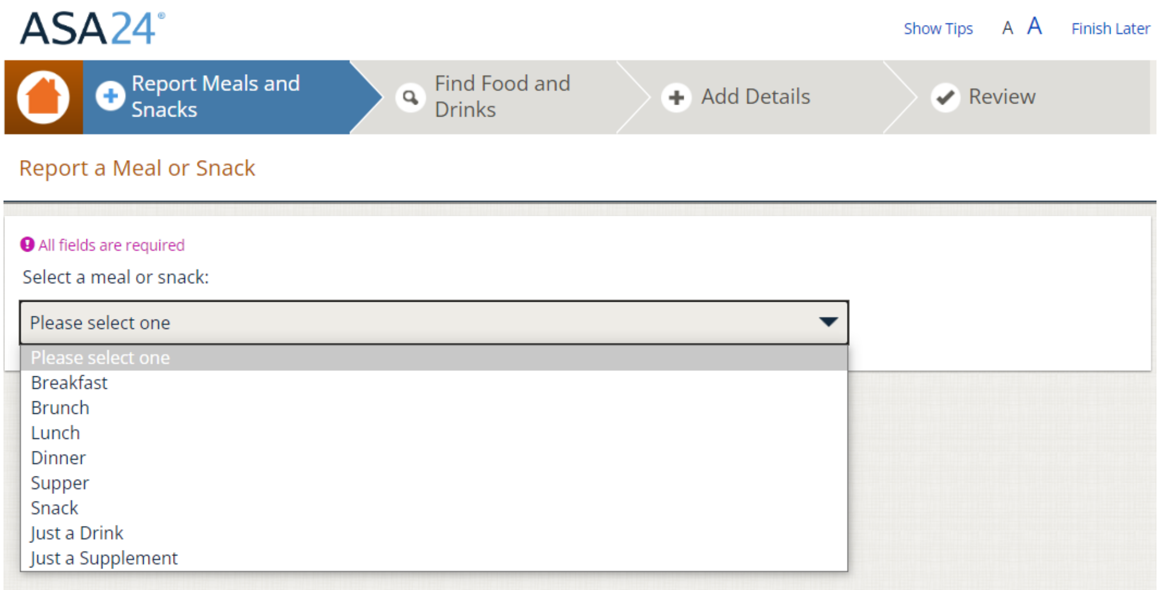

(a)

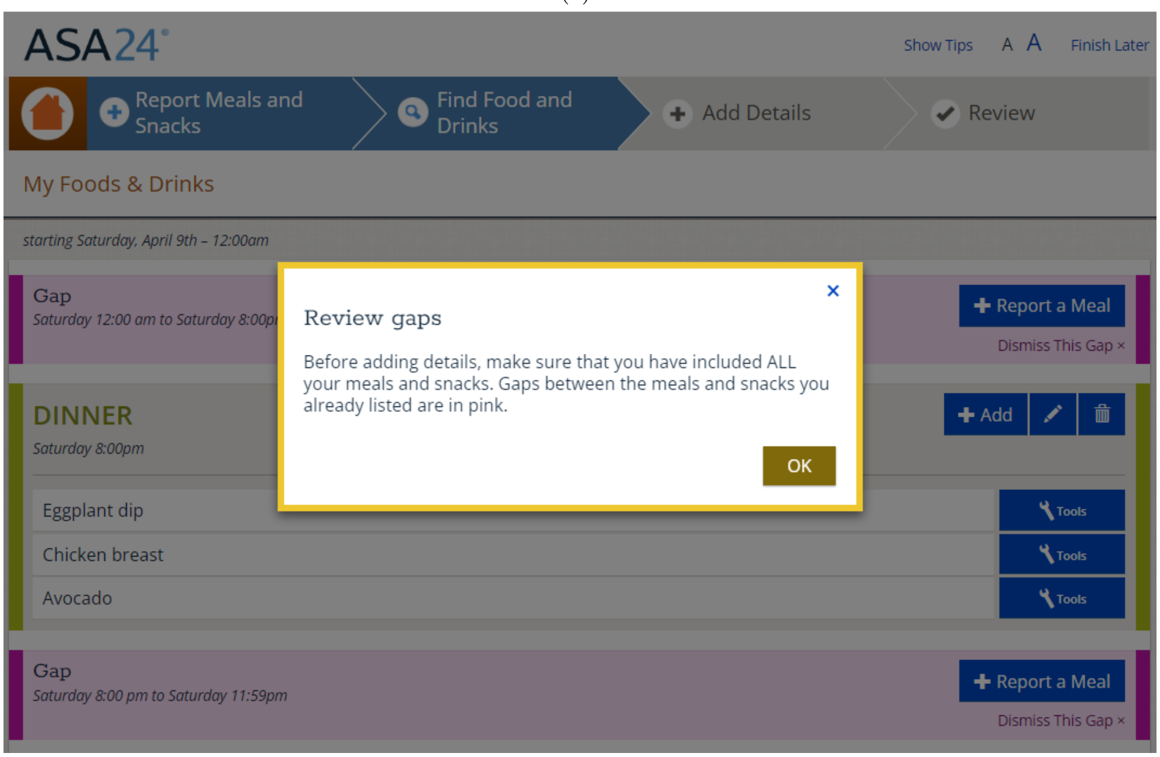

(b)

Figure 1.3: Automated, self-administered 24-hour dietary recall (ASA24) [1,2]. (a) The user selects a meal type and then adds details. (b) The ASA24 alerts the user to make sure that they entered all meals and snacks with all details.

and Nutrition Examination Survey (NHANES) uses a five-pass 24-hour dietary recall. In this method respondents first fill out an initial quick list to record consumed foods and beverages. Second, they go through a list of usually forgotten to report foods to help them remember. Third, they provide time and occasion at which foods were consumed. Fourth, they are asked for more details including portions sizes and time among eating occasions. Fifth, they are again asked to provide any other information that was not already reported. A duration of 30 to 45 minutes is typically used to complete this process. An Internet-based, automated, self-administered 24-hour dietary recall (ASA24) was developed in an effort to automate the 24-hours recall process. The system was developed by the National Cancer Institute under contract with Westat, a social science research company [1, 2, 189]. Fig. 1.2 and 1.3 show snapshots of the ASA24 user interface.

Evaluation of data validity of the 24-hour dietary recalls for energy and protein intake generally reveal under-reporting in the range of 3% to 34% when compared to the recovery bio-markers of DLW and urinary nitrogen [110]. Urinary nitrogen is a bio-marker for measuring protein intake for weight stable individuals [26, 78]. Dietary recall and diary systems tend to use databases for easier, faster, and more accurate retrieval of nutritional and caloric information about the foods and beverages entered by respondents. They may also offer low-cost, low-burden alternatives to the traditional interviewer-led 24-h recalls. However, under-reporting for energy was still found to be around 25% when using the online system compared to that measured by DLW [65]. Moreover, respondents still need basic skills of using this technology and need to spend time answering online questions; this might not fit the needs of some populations such as the elderly and children [58, 102].

A food frequency questionnaire (FFQ) consists of a defined list of foods and beverages ranging from a simple list (e.g., 20 items) to a comprehensive list (e.g., 200 items) [51]. An FFQ captures habitual dietary intake by asking respondents about their usual frequency of consumption of each food or beverage item over a specified time period in the past, over the last year, for example. Respondents answer all questions depending on their memories. The questions also ask about the portion size of each item to estimate an average intake over time. It is common to customize this tool to fit the needs of specific patient categories such as FFQ for children [188], old women [134], or elderly [180]. Fig. 1.4 and 1.5 show an example of an FFQ form that is available online on [3].

The aforementioned classical dietary assessment tools are burdensome and lack objectivity and accuracy [34]. Manual self-monitoring of eating events and quantities leads to the loss of respondents' interest in keeping up with recording their eating behavior. Even the recent approach of

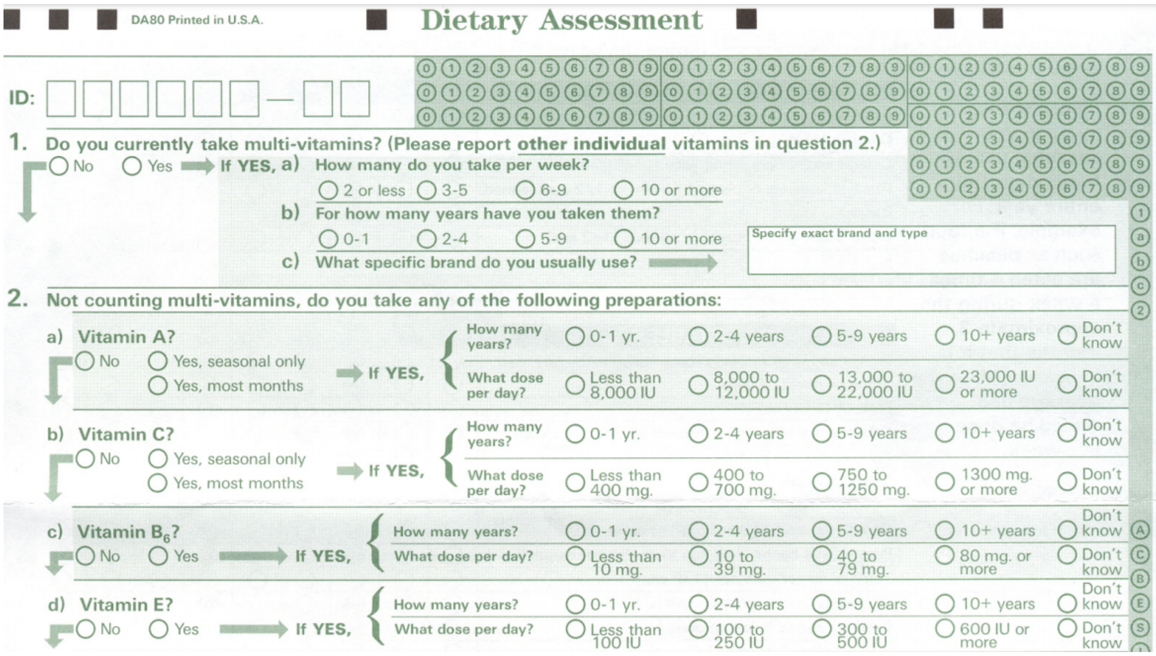
DA80 Printed in U.S.A.

Dietary Assessment

ID: □□□□□□—□□

1. Do you currently take multi-vitamins? (Please report other individual vitamins in question 2.)

○ No ○ Yes → If YES, a) How many do you take per week?
○ 2 or less ○ 3-5 ○ 6-9 ○ 10 or more

b) For how many years have you taken them?
○ 0-1 ○ 2-4 ○ 5-9 ○ 10 or more

c) What specific brand do you usually use? → Specify exact brand and type

2. Not counting multi-vitamins, do you take any of the following preparations:

a) Vitamin A?
○ No ○ Yes, seasonal only ○ Yes, most months → If YES,
How many years? ○ 0-1 yr. ○ 2-4 years ○ 5-9 years ○ 10+ years ○ Don't know
What dose per day? ○ Less than 8,000 IU ○ 8,000 to 12,000 IU ○ 13,000 to 22,000 IU ○ 23,000 IU or more ○ Don't know

b) Vitamin C?
○ No ○ Yes, seasonal only ○ Yes, most months → If YES,
How many years? ○ 0-1 yr. ○ 2-4 years ○ 5-9 years ○ 10+ years ○ Don't know
What dose per day? ○ Less than 400 mg. ○ 400 to 700 mg. ○ 750 to 1250 mg. ○ 1300 mg. or more ○ Don't know

c) Vitamin B_6?
○ No ○ Yes → If YES,
How many years? ○ 0-1 yr. ○ 2-4 years ○ 5-9 years ○ 10+ years ○ Don't know
What dose per day? ○ Less than 10 mg. ○ 10 to 39 mg. ○ 40 to 79 mg. ○ 80 mg. or more ○ Don't know

d) Vitamin E?
○ No ○ Yes → If YES,
How many years? ○ 0-1 yr. ○ 2-4 years ○ 5-9 years ○ 10+ years ○ Don't know
What dose per day? ○ Less than 100 IU ○ 100 to 250 IU ○ 300 to 500 IU ○ 600 IU or more ○ Don't know

(a)

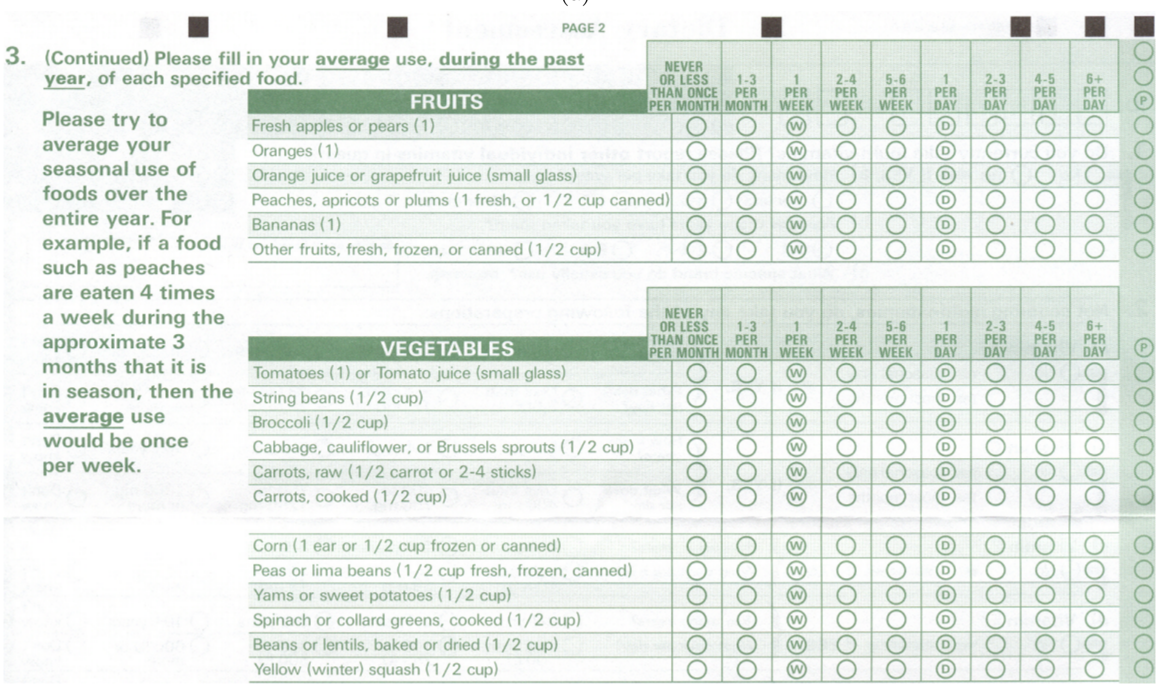
PAGE 2

3. (Continued) Please fill in your average use, during the past year, of each specified food.

Please try to average your seasonal use of foods over the entire year. For example, if a food such as peaches are eaten 4 times a week during the approximate 3 months that it is in season, then the average use would be once per week.

FRUITS	NEVER OR LESS THAN ONCE PER MONTH	1-3 PER MONTH	1 PER WEEK	2-4 PER WEEK	5-6 PER WEEK	1 PER DAY	2-3 PER DAY	4-5 PER DAY	6+ PER DAY
Fresh apples or pears (1)	○	○	W	○	○	D	○	○	○
Oranges (1)	○	○	W	○	○	D	○	○	○
Orange juice or grapefruit juice (small glass)	○	○	W	○	○	D	○	○	○
Peaches, apricots or plums (1 fresh, or 1/2 cup canned)	○	○	W	○	○	D	○	○	○
Bananas (1)	○	○	W	○	○	D	○	○	○
Other fruits, fresh, frozen, or canned (1/2 cup)	○	○	W	○	○	D	○	○	○

VEGETABLES	NEVER OR LESS THAN ONCE PER MONTH	1-3 PER MONTH	1 PER WEEK	2-4 PER WEEK	5-6 PER WEEK	1 PER DAY	2-3 PER DAY	4-5 PER DAY	6+ PER DAY
Tomatoes (1) or Tomato juice (small glass)	○	○	W	○	○	D	○	○	○
String beans (1/2 cup)	○	○	W	○	○	D	○	○	○
Broccoli (1/2 cup)	○	○	W	○	○	D	○	○	○
Cabbage, cauliflower, or Brussels sprouts (1/2 cup)	○	○	W	○	○	D	○	○	○
Carrots, raw (1/2 carrot or 2-4 sticks)	○	○	W	○	○	D	○	○	○
Carrots, cooked (1/2 cup)	○	○	W	○	○	D	○	○	○
Corn (1 ear or 1/2 cup frozen or canned)	○	○	W	○	○	D	○	○	○
Peas or lima beans (1/2 cup fresh, frozen, canned)	○	○	W	○	○	D	○	○	○
Yams or sweet potatoes (1/2 cup)	○	○	W	○	○	D	○	○	○
Spinach or collard greens, cooked (1/2 cup)	○	○	W	○	○	D	○	○	○
Beans or lentils, baked or dried (1/2 cup)	○	○	W	○	○	D	○	○	○
Yellow (winter) squash (1/2 cup)	○	○	W	○	○	D	○	○	○

(b)

Figure 1.4: FFQ example available online on [3]. Respondents are asked to give detailed answers about vitamin supplements (a), fruits and vegetables consumption (b).

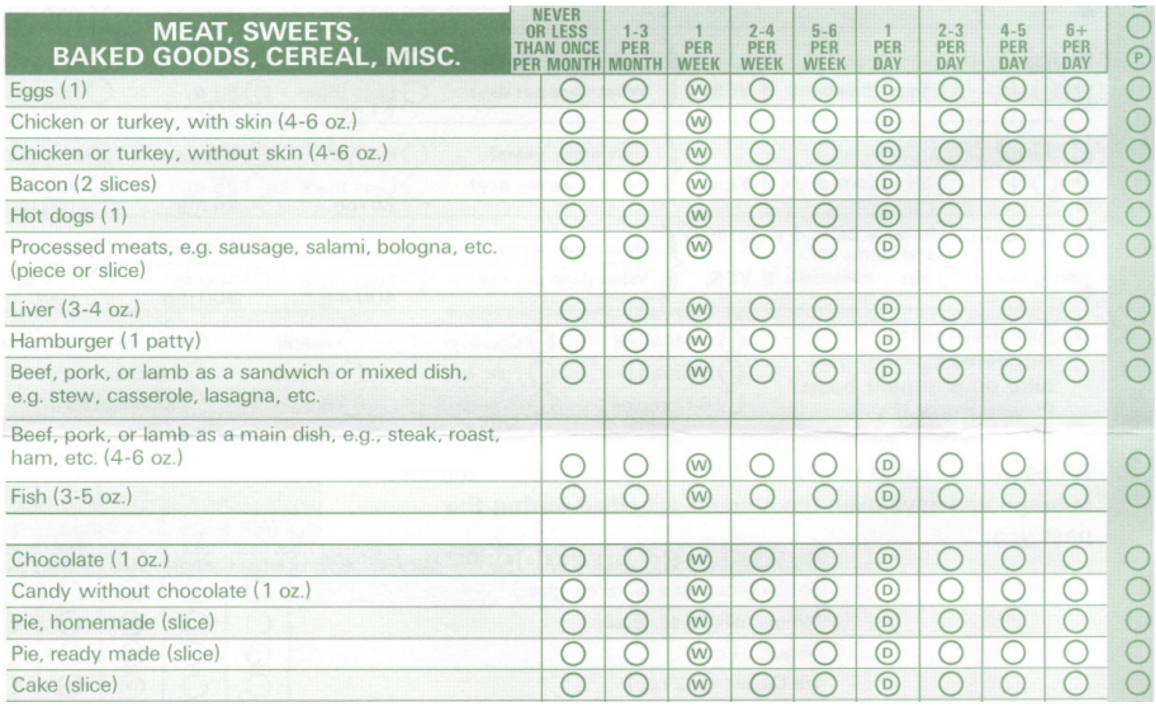

MEAT, SWEETS, BAKED GOODS, CEREAL, MISC.	NEVER OR LESS THAN ONCE PER MONTH	1-3 PER MONTH	1 PER WEEK	2-4 PER WEEK	5-6 PER WEEK	1 PER DAY	2-3 PER DAY	4-5 PER DAY	6+ PER DAY
Eggs (1)			W			D			
Chicken or turkey, with skin (4-6 oz.)			W			D			
Chicken or turkey, without skin (4-6 oz.)			W			D			
Bacon (2 slices)			W			D			
Hot dogs (1)			W			D			
Processed meats, e.g. sausage, salami, bologna, etc. (piece or slice)			W			D			
Liver (3-4 oz.)			W			D			
Hamburger (1 patty)			W			D			
Beef, pork, or lamb as a sandwich or mixed dish, e.g. stew, casserole, lasagna, etc.			W			D			
Beef, pork, or lamb as a main dish, e.g., steak, roast, ham, etc. (4-6 oz.)			W			D			
Fish (3-5 oz.)			W			D			
Chocolate (1 oz.)			W			D			
Candy without chocolate (1 oz.)			W			D			
Pie, homemade (slice)			W			D			
Pie, ready made (slice)			W			D			
Cake (slice)			W			D			

(a)

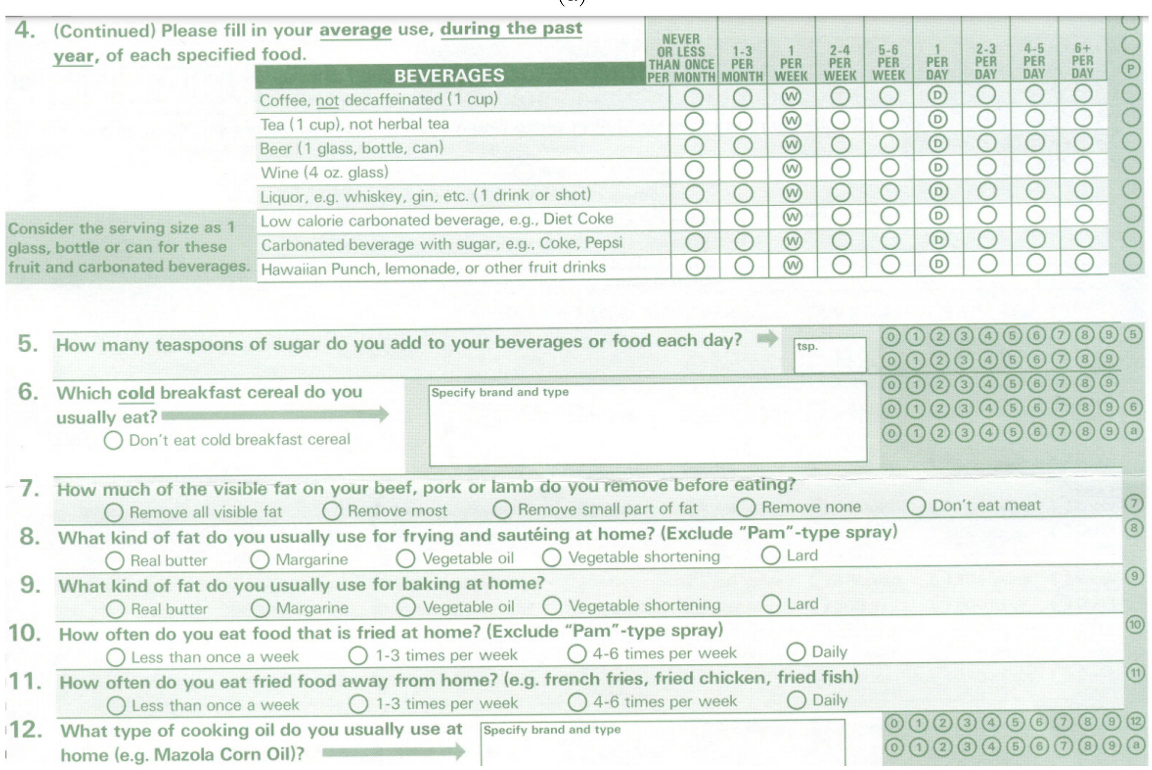

4. (Continued) Please fill in your **average** use, **during the past year**, of each specified food.

BEVERAGES	NEVER OR LESS THAN ONCE PER MONTH	1-3 PER MONTH	1 PER WEEK	2-4 PER WEEK	5-6 PER WEEK	1 PER DAY	2-3 PER DAY	4-5 PER DAY	6+ PER DAY
Coffee, not decaffeinated (1 cup)			W			D			
Tea (1 cup), not herbal tea			W			D			
Beer (1 glass, bottle, can)			W			D			
Wine (4 oz. glass)			W			D			
Liquor, e.g. whiskey, gin, etc. (1 drink or shot)			W			D			
Low calorie carbonated beverage, e.g., Diet Coke			W			D			
Carbonated beverage with sugar, e.g., Coke, Pepsi			W			D			
Hawaiian Punch, lemonade, or other fruit drinks			W			D			

Consider the serving size as 1 glass, bottle or can for these fruit and carbonated beverages.

5. How many teaspoons of sugar do you add to your beverages or food each day? tsp.

6. Which **cold** breakfast cereal do you usually eat? Specify brand and type
- Don't eat cold breakfast cereal

7. How much of the visible fat on your beef, pork or lamb do you remove before eating?
- Remove all visible fat
- Remove most
- Remove small part of fat
- Remove none
- Don't eat meat

8. What kind of fat do you usually use for frying and sautéing at home? (Exclude "Pam"-type spray)
- Real butter
- Margarine
- Vegetable oil
- Vegetable shortening
- Lard

9. What kind of fat do you usually use for baking at home?
- Real butter
- Margarine
- Vegetable oil
- Vegetable shortening
- Lard

10. How often do you eat food that is fried at home? (Exclude "Pam"-type spray)
- Less than once a week
- 1-3 times per week
- 4-6 times per week
- Daily

11. How often do you eat fried food away from home? (e.g. french fries, fried chicken, fried fish)
- Less than once a week
- 1-3 times per week
- 4-6 times per week
- Daily

12. What type of cooking oil do you usually use at home (e.g. Mazola Corn Oil)? Specify brand and type

(b)

Figure 1.5: FFQ example available online on [3]. Respondents are asked to give detailed answers about meat, sweets and baked goods (a), beverages and other miscellaneous dietary questions (b).

using online websites or apps on smartphones still depends on memory and respondents' commitment. Process automation for food intake monitoring is required for data accuracy and long-term usage. Real-time feedback of food consumption creates awareness so that users can stop or limit their eating when alerted by smart automatic dietary monitoring tools.

1.3 Automatic Dietary Assessment Tools

Researchers are investigating different technical modalities to automatically track patients' foods and behaviors to aid dietitians in their treatment. The automation of dietary assessment tools can increase objectivity and accuracy and can promote long-term usage. These methods involve instrumenting people with sensors and miniature electronic devices enabled for in-situ real-time monitoring of activities and signals that indicate the health status of the body. Such data can be used to estimate energy intake and expenditure to help a patient maintain or lose weight.

Information a dietitian would want to obtain include food items, meal type (breakfast, lunch, dinner, snack), time (start/end), nutrition facts (calorie, carbohydrate, fat, sugar, sodium, fiber), portion size, and location (homemade, store-bought, restaurant) [121]. In addition, a dietitian might also want to obtain details about patient's meal microstructure habits such as bite size, eating rate, and chews per swallow [57, 119, 148, 187]. It is hard to obtain microstructure information of eating behavior using classical dietary assessment tools. Such detailed information is valuable, for example, smaller bite size in addition to longer oral processing time was found to significantly decrease food intake [220]. More time spent on oral processing before swallowing could contribute to higher fullness/satiety compared to the same meal and calories when eaten with less oral processing [64]. More oral processing per bite was shown to have a direct effect on reducing energy intake rate and the desired food intake [31, 111, 181]. Several studies showed that faster eating rate is associated with higher energy intake [166, 199]. Some of these dietary information can be automatically detected or classified with various technological modalities that tracks signals generated by the eating action. When a person eats, chewing and swallowing produces sounds and muscular activity that in turn also produces mechanical motion and electrical signals, i.e., electromyography (EMG). Body activities are also involved when a person picks up food and puts it in mouth. For tracking these eating-associated signals, various technological modalities have been developed in the literature including acoustic-based, camera-based, motion-based, or smart environment methods. This section gives an overview of various automatic dietary assessment tools [21, 157, 161].

1.3.1 Acoustic-Based

The acoustic-based techniques use microphones attached to human subjects to listen to sounds produced during eating, i.e., chews and swallows. Analyzing these sounds can provide valuable information such as food texture, oral processing time, eating rate, and intake occasions. Microphones are usually positioned in the ears or on the neck. Fig. 1.6a shows the locations for acoustic-based ADM applications as suggested by [170]. In-ear or behind the ear microphones are usually used to assess chewing sounds as in Fig. 1.6b [143, 197, 217]. It was found that chews can be best detected when a microphone is positioned on the mastoid bone behind the ear [22]. Fig. 1.6c shows an example of using a microphone positioned on the throat to listen to swallows [170,201]. One study to analyze chewing and swallowing sounds was in AutoDietary [23], which used on the neck microphone and achieved 84.9% in food-type recognition. Multiple microphones placed at different locations have been used to detect different eating sounds [137]. In addition to microphones, some studies used different sensors such as an electromyography sensor placed on the throat to detect swallowing activities [15], or pairs of ultrasonic transmitters and receivers to make an ultrasonic doppler sensor that is attached to the neck of a subject as a food recognition wearable sensor [116]. The biggest challenge in the acoustic-based approach is the interference of background environment noise. To overcome this problem, several studies used two microphones: one is for the eating sounds and the other is for the background environment noise cancellation as shown in Fig. 1.6d [147].

Several microphone types were used in the literature for acoustic-based ADM acoustic-based systems such as:

1. piezoelectric bone-conduction microphone EM-L (Temco Inc.),
2. piezoelectric noise-canceling microphone model N4530 (Challenge Electronics),
3. a modified throat microphone XTM70V (iXradio),
4. throat microphone IASUS NT (IASUS Concepts Ltd).

Sazonov *et al.* [170] compared the aforementioned microphone types and concluded that the throat microphone IASUS NT performed the best among the others because of its higher sensitivity to swallowing sounds and its lower susceptibility to ambient noise. Off-the-shelf Bluetooth headsets

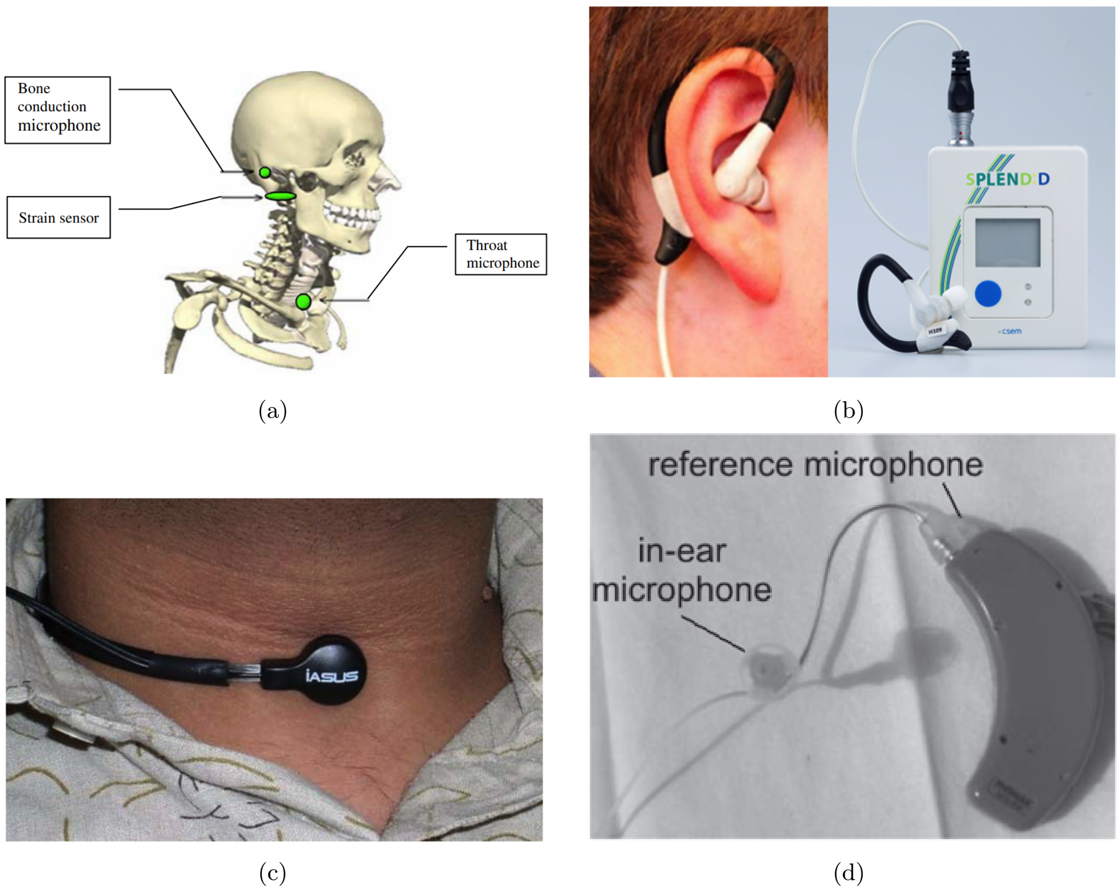

(a) (b) (c) (d)

Figure 1.6: Acoustic-based techniques use wearable microphones for ADM. (a) Microphone locations for ADM applications as suggested by [170]. (b) In-ear microphone for eating detection from [197]. (c) A microphone positioned on the throat to listen to swallows [170]. (d) Two microphones: one is for recording eating sounds and the other is for noise cancellation [147].

have been used to unobtrusively monitor and detect a subject's eating episodes by analyzing the chewing sound [69]. The built-in microphone of a smartwatch was also used to detect ingestion of food and liquid, and to classify among apples, chips, water, speaking, and ambient noise [97].

One of the drawbacks of using acoustic-based techniques for ADM applications is power management. In order to sufficiently preserve important characteristics of the eating sounds, some studies used a sampling frequency of 16 kHz, as per Nyquist–Shannon sampling theorem [140]. This sampling rate creates power management problems for battery powered wearable sensors especially when more microphone channels are used simultaneously as in [137]. It might be bothersome to some users if they have to recharge them more frequently. To solve this problem, Bi *et al.* added a wake-up circuit to their acoustic-based system which stays in sleep state until the wake-up circuit detects a sound that is higher than a preset threshold after which the microcontroller is triggered to wake up and start analyzing the eating sounds [22].

1.3.2 Motion-Based

Motion-based techniques track the mechanical activities associated with eating. These techniques either track the actual mechanical movements or electrical signals produced by the muscular activities. They are mostly implemented in the form of wearable sensors.

1.3.2.1 Chewing

Chewing is the activity of oral processing and breaking down of food into smaller pieces. Muscular activities in the face and skull can be tracked to detect chewing. Frequency of chewing activity is mainly in the range of 0.94 to 2.17 Hz [154] making the sampling rate required for digitizing this signal much lower than that of the acoustic-based systems. Piezoelectric, electromyography (EMG), and accelerometers are the most common used sensors for chewing detection. Produced signals by such sensors can be analyzed to provide useful information such as daily eating schedule, chewing speed, and food type, e.g., liquid or solid [176].

Piezoelectric sensors are attached to skin with medical adhesive or medical tape to detect skin curvature that changes due to chewing activities. Piezoelectric systems generally feature low power consumption, privacy-preserving, and non-intrusive wearable devices. A small piezoelectric strain gauge can be attached to skin below the outer ear closer to the masseter muscle to predict mass and energy intake [212]. However, such application could make a discomfort to users due to

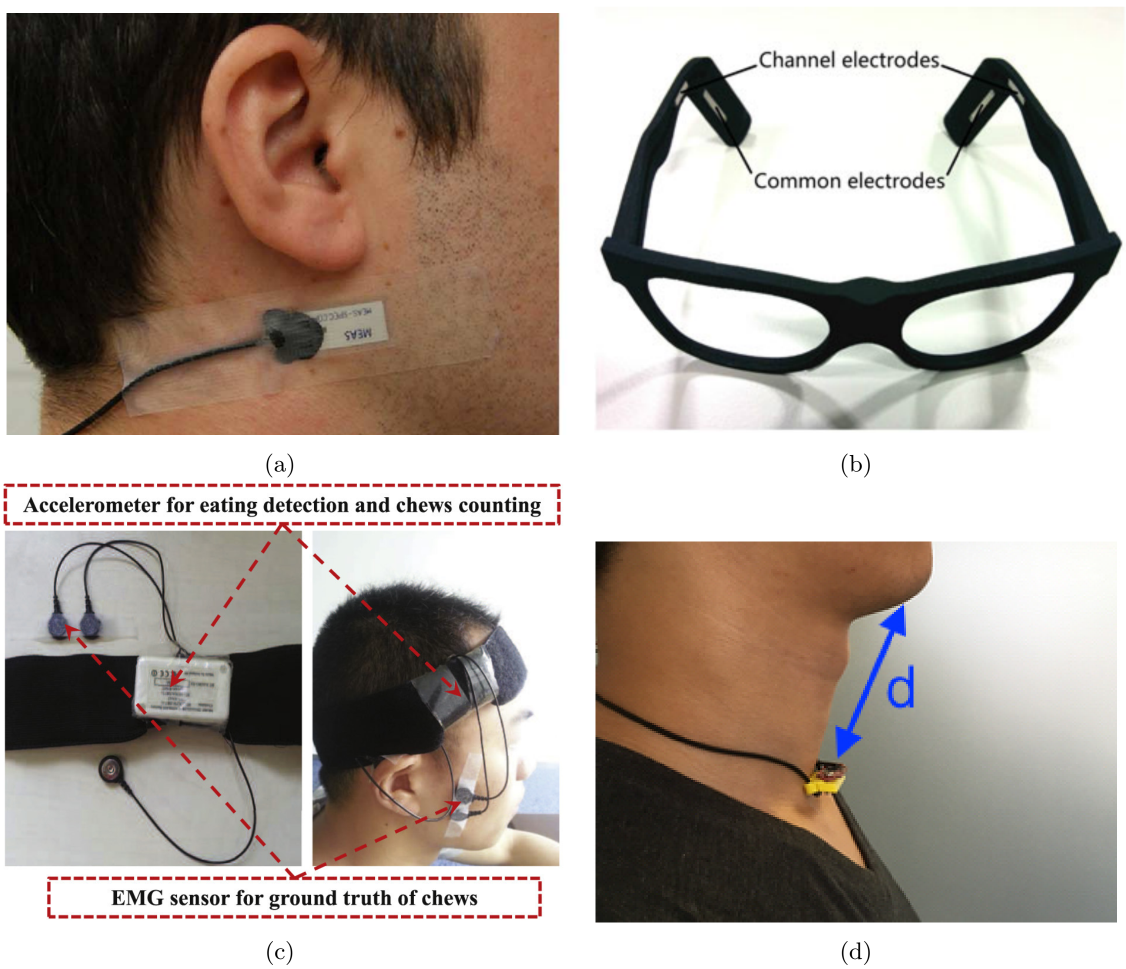

Figure 1.7: Dietary detection systems using signals generated due to chewing activity. (a) A piezo-electric film strain gauge sensor attached below the outer ear [171]. (b) Positions where EMG electrodes can detect a reliable signal [216]. (c) A device containing an accelerometer and an EMG sensor was embedded into a headband [204, 205]. (d) A side view of a proximity sensor on a subject for measuring the distance between a necklace-like wearable sensor and the subject's chin to detect eating episodes [44].

the way they are attached to skin, and it is hard to use these sensors for the detection of liquid consumption [176].

Chung *et al.* embedded two miniature button compression load cells at the hinges of a pair of eyeglasses to measure the cyclic movement of the temporomandibular joint during mastication to classify chewing, talking, and other head movements [45]. Power consumption of foil thin-film strain gauges limits their use in wearable systems due to their low resistance. Alternatively, as shown in Fig. 1.7a, Sazonov and Fontana used a piezoelectric film strain gauge sensor below the outer ear as a low power sensor [171].

Electromyography can be used to measure electrical activity in response to contractions of muscles such as temporalis and masseter muscles. Electrodes of the EMG sensors are either directly attached to skin with a medial adhesive/tape or embedded onto contact points of eyeglasses. To detect eating, Blechert *et al.* attached signal electrodes of EMG sensors behind the right ear on a line between the mastoid and the masseter muscle while positioning the ground electrode on the neck—close to the cervical spine [29]. A diet-aware eyeglasses was designed so that, EMG sensors were embedded onto the eyeglasses temples which are supposed to touch the temporalis muscles for the tracking of chewing activities [84]. When paired with a smartphone via a Bluetooth connection, the glasses can detect intake-related events such as the number of chewing cycles and broad food category. Zhang *et al.* used EMG sensors with small fabric electrodes attached to a 3D printed eyeglasses [218]. Three fabric electrodes were affixed onto elastic suspension to assure electrodes to skull contact. The ground electrode was positioned at the nose and the two signal ones were positioned around the ear. Data were processed off-line to detect the number of chewing cycles and to classify food category (biscuit, banana, jelly baby, toast, and carrot). Later, Zhang and Oliver improved the eyeglasses design by personalization a 3D printed eyeglasses frame to provide enhanced electrodes to skin contact and to reduce noise that is occasionally produced when head moves resulting in detaching the nose pad electrode; electrodes of two EMG sensors were positioned at the temple ends behind ears to monitor activity of temporalis muscles [216]. Fig. 1.7b shows their enhanced 3-D design.

Accelerometers have been used to detect chewing activities as they measure acceleration of movement of a carrying body or structure. An advantage of using accelerometers is that they can be used for the detection of both eating behavior and physical activities at the same time [59, 98]. According to the observation that mastication causes muscles to bulge during chewing, Wang *et* *al.* used a single axis accelerometer attached on the temporalis to detect chewing activities and frequency [204]. A Shimmer 2r sensor — an off the shelf device — was embedded into a headband. This device has a triaxial accelerometer and an EMG sensor, which was used as ground truth. The EMG electrodes were attached on skin over the mastication muscle with a medical tape as shown in Fig. 1.7c. Wang *et al.*, in 2018, improved the system with using three axes of the accelerometer data to further detect and classify the chewing activities and other non-eating activities such as speaking, walking, etc. [205]. Farooq and Sazonov developed a system that encloses 3-axis accelerometer, a Bluetooth module, and a push-button for manual ground truth annotation [60]. The system was attached with heat-shrink tube to the right temple of eyeglasses to address two issues associated with other types of sensors: incorrect sensor placement, which affects signal amplitude, and the discomfort due to direct positioning of sensors on skin.

Chewing can also be detected by different sensors such as a proximity sensor attached to a necklace for tracking the distance from the sensor and a user's chin as shown in Fig. 1.7d [44].

1.3.2.2 Gestures

For dietary related gesture recognition, Amft and Tröster used 9-axis IMU sensor attached to upper and lower jacket arms in addition to other modalities as shown in Fig. 1.8a [16]. They tried different European and American eating-related gestures and their results showed that all those gestures could be recognized using only an IMU located at the lower arm. Dong *et al.* (2009) used an off-the-shelf IMU sensor, namely, InertiaCube3, to track wrist motion relative to the startup orientation based on the gyroscope data, i.e., angular roll, pitch, and yaw [53]. The idea is that a person's wrist rotates and moves in a specific sequence during eating with a hand as illustrated in Fig. 1.8c. Later, Dong *et al.* (2012) built a low cost and smaller prototype of a wrist worn device enclosing a MEMS gyroscope as shown in Fig. 1.8b [54]. The same device was used by Ramos-Garcia *et al.* to recognize five different types of gestures: rest, utensiling, bite, drink, or other, using hidden Markov models that achieved up to 96.5% accuracy [163, 164]. Motivated by the work in [164], Kyritsis *et al.* used a commercially available wristband to detect hand movements associated to eating such as pick up food, upwards, downwards, or no movement [112–114]. Thomaz *et al.* captured continuous data of a 3-axis accelerometer of an off-the-self device (Pebble Watch) to identify arm-to-mouth food intake gestures [192]. Data were being transmitted to a companion smartphone for data storage and retrieval.

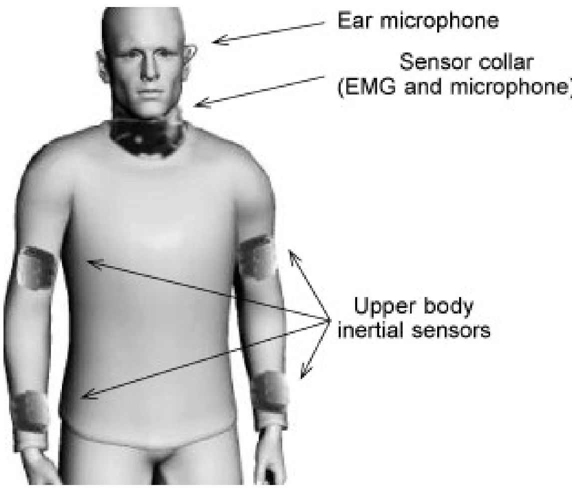

(a)

(b)

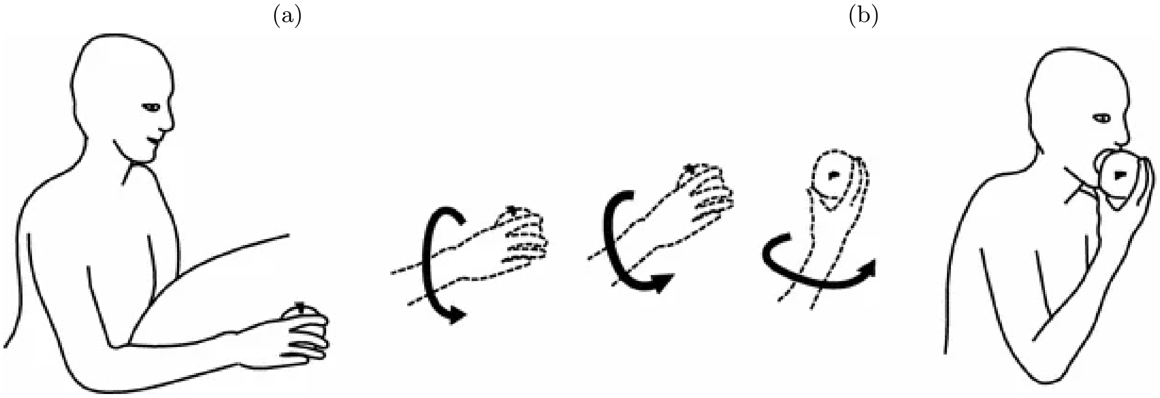

(c)

Figure 1.8: Gestures can be used for automatic detection of dietary monitoring. (a) Four 9-axis IMU sensors were attached to upper and lower jacket arms in addition to two other modalities [16]. (b) A wrist worn prototype enclosing an MEMS gyroscope was presented in [54]. (c) The bite counter uses an inertial measurement units (IMU) to detect wrist rotation which is expected to occur more frequently during eating occasions [54].

Smartphones were used for ADM via tracking of gestures. In the previously mentioned work by Dong *et al.* (2012), users needed to switch ON the device before every meal [54]. Nevertheless, to automate the detection of eating periods in a free-living situations, Dong *et al.* (2013) used an iPhone 4 worn in a watch like configuration to track the wrist motion through continuous recording of the built-in IMU sensors (an accelerometer and gyroscope) and hence track the wrist motion [55]. In addition to automatic tracking of physical activity using built-in IMU, smartphones were used to track other contextual data including GPS for location tracking, and manually recorded information such as food photos, emotion, and food environment [24, 179]

Recently, smartwatches come with variety of built-in sensors that can be used for tracking of physical activities and several body health related signals. Such devices can be used for the monitoring and estimation of both energy intake and expenditure helping users to maintaining healthy lifestyle. Using built-in IMU sensors, smartwatches have been used in the literature for hand gesture tracking for the purpose of ADM. Weiss *et al.* used a smartwatch (accelerometer and gyroscope) and smartphone (accelerometer) to recognize 18 physical activities: six non-hand oriented general activities, seven hand oriented general activities, and five hand oriented eating activities [207]. After comparing different algorithms, the data of smartwatch accelerometer were found to provide the highest accuracy in activity recognition. Stankoski *et al.* used data recorded from smartwatch accelerometer and gyroscope built-in sensors, and implemented deep and classical machine learning algorithms for the detection of eating segments [185]. Their algorithm achieved F1 score 82% in the detection of eating segments.

1.3.3 Image-Based

Image-based techniques use visual information to automatically or manually provide dietary information. Image-based systems can be stationary, portable, or wearable. The main advantage in image-based techniques is that they have been used to detect portion size and food content. Images are taken either actively, where the user needs to manually start photos or video recording, or passively, in which other low power sensors are used to detect eating events/episodes and to automatically trigger the camera functionality [70]. There are common requirements among image-based systems [157]: first, images should be captured at specified angles, second, images of food before eating and the leftover are required for quantifying consumed amount of food, and third, images should include a visual scale reference such as a finger [156], ruler [49], or printed pattern

[125] for quantifying portion size. Image-based techniques can also be affected by other parameters including illumination and the camera itself [156].

Pouladzadeh *et al.* used a smartphone camera to compare recorded photos of food before and after eating to estimate consumption of calorie with the use of nutritional fact tables [156]. Sun *et al.* developed a wearable camera called eButton that can be used for several applications including evaluating diet and physical activity, studying sedentary behavior, assisting the blind and visually impaired people, and other applications [190]. Fig. 1.9a shows how it could be used for diet monitoring. Jia *et al.* developed artificial intelligence (AI)-based algorithm using images collected by free-living individuals with the wearable eButton camera to automatically detect food items in images [93]. They used a convolutional neural network (CNN) classifier, i.e., Clarifai [11], to automatically tag images collected in two data sets. Next, they constructed a dictionary containing possible words that the Clarifai CNN could produce. Using the generated dictionary, their algorithm achieved 86.4% overall testing accuracy for the data set-1 and 74.0% sensitivity and 87.0% specificity for data set-2 when considering food and drink detection. O'Loughlin *et al.* used SenseCam—a wearable camera by Microsoft—to increase the accuracy of manual self-reported 1-day food diary [139]. Each participant wore the camera for one day on the neck and attached it onto the chest with a velcro strap as shown in Fig. 1.9b. They concluded that the camera increased the diary accuracy. A similar study was done to improve dietary assessment accuracy using a micro-camera worn over the ear as shown in Fig. 1.9c [151]. Rachakonda *et al.* developed iLog which is a wearable camera based system attached to eyeglasses [160]. It continuously captures images that are sent to a platform for image processing and automatic classification of food type, and hence estimating how much is too much. The system, moreover, classifies the emotional state and the eating behavior, i.e., normal-eating or stress-eating.

The major problems of using cameras for dietary assessment are power consumption, privacy, storage capacity. Schiboni *et al.* fixed a camera on a cap's visor pointing downwards in an attempt to address the problem of privacy-sensitive image content [172]. A common approach is to let users review all recorded images and keep what they accept to be seen by researchers, or to use an on/off switch to manually control what the camera can record. Signals from a smartwatch built-in sensors such as IMU (accelerometer and gyroscope) were used to classify gestures into either eating or non-eating activities and to trigger the camera on the smartwatch [178]. Controlling the camera functionality in this way manages power consumption and reduces the storage use by recording most

(a)

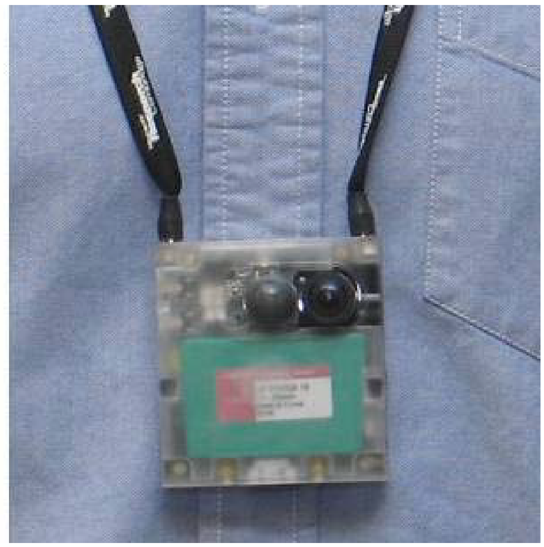

(b)

(c)

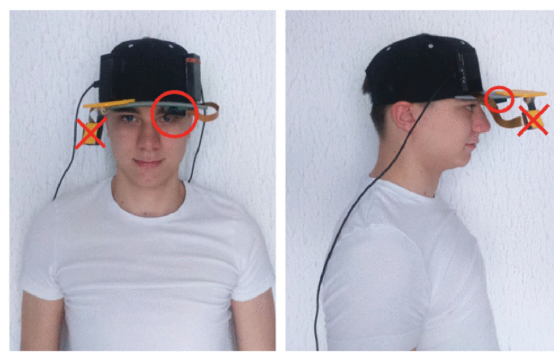

(d)

Figure 1.9: Image-based systems for ADM. (a) eButton wearable camera used for [190]. (b) Sense-Cam (a wearable camera by Microsoft) worn on chest [81]. (c) A micro-camera worn over the ear to improve dietary assessment accuracy [151]. (d) A work around for the privacy problem proposed by [172] who fixed a camera on a cap's visor pointing downwards.

likely food related photos. They developed an improved system, called Annapurna, in which the collected images are transferred into a paired smartphone for further image filtration so that only useful images are kept [177]. They used algorithms for face recognition to remove images containing human faces, color histogram-based to remove solid background images, and edge detector to remove blurry images. The remaining images are transferred to a server that implements AI algorithms for further image filtration and recognition of food containing images. Their process achieved 95% overall recall of meals consumed by participants.

1.3.4 Smart Instruments

Smart home technologies can be used for unobtrusive tracking and monitoring of dietary behavior through instrumenting surrounding environment such as furniture, utensils, or food containers.

The cumulative food intake (CFI) curve has been used to classify the eating behavior of patients [105]. The CFI curve is the weight of food consumed over time modeled in the following quadratic curve

$$w_{\mathrm{q}}(t) = \alpha t^2 + \beta t, \tag{1.1}$$

where β is the initial rate of intake weight at time $t = 0$ sec, and α is the intake weight acceleration that can be used to classify eating rate. A linear eater eats at a constant rate ($\alpha = 0$) while a decelerated eater slows down their eating rate over the course of a meal ($\alpha < 0$) [208, 213]. Healthy people eat at a decelerated CFI curve and hence obese patients and those with an eating disorder are trained to eat at a decelerated rate with the help of modeling their CFI curves [63, 208, 213].

Papapanagiotou *et al.* used a plate scale—called Mandometer—to calculate the cumulative food intake (CFI) curve of a user's eating behavior [144]. Fig. 1.10a shows a plate, which was developed by Mertes *et al.*, embedded with three load cells for measuring picked up food bites and locating which compartment the bite was picked up from to detect type of food [129]. Consumption of beverage, however, is not usually monitored by a plate scale or a smart plate. Mattfeld *et al.* used food trays that carry solid food and beverage containers and four scales embedded into a dining table to detect and measure weight of bites consumed during unrestricted eating; one tray was placed on a scale as shown in Fig. 1.10b [127].

Smart utensils were developed for ADM. Kadomura *et al.* developed a sensor-embedded fork

Figure 1.10: Examples of smart instruments. (a) A three compartment plate embedded with three load cells for measuring bite weight and detecting food type [129]. (b) Food trays placed on scales which are embedded under a dining table [127]. (c) A smart fork embedded with an accelerometer, electrodes, color sensor, and an LED [94]. (d) A smart water bottle embedded with IMU developed by [73].

to study eating behavior of children as shown in Fig. 1.10c [94]. The system uses an accelerometer for motion detection, three electrodes to detect holding, poking, and biting, and a four-channel color sensor and an LED to detect food. Huang *et al.* embedded LEDs as light source and a photodiode as a light detector into a transparent spoon to detect food type [85].

Fluid containers such as water bottles, glass, or cups, have been instrumented with sensors for monitoring fluid intake. Such application can be used for preventing dehydration or overhydration [46]. Sensors used in the literature include IMU to track orientation and movements of a liquid container [52, 73], capacitive or conductive electrodes for sensing liquid level in a container [30, 108], strain gauge to measure container weight [221], and thin metal antennas attached on a plastic bottle to disturb ambient WiFi channel when touched by fingers [68]. An example is shown in Fig. 1.10d.

1.3.5 Multi-Modality Approach

Multi-modality systems were developed to exploit the advantages of some types of sensors and to overcome the drawbacks of others. A practical use of such systems, for example, is the use of an accelerometer and a camera; the accelerometer is used as a low power sensor for the detection of eating events after which the camera is triggered to capture only eating-related images [178]. This practice can conserve power consumption, reduce storage usage by saving only useful images, and preserve privacy. For the detection of chewing, Sazonov *et al.* used a bone conduction microphone placed over the mastoid bone and a foil strain gauge attached with a medical tape on the jaw right below the ear [170]. These two sensors can detect chewing while eating food but are not suitable for the detection of liquid intake. For this reason, they added a throat microphone located over the laryngopharynx as shown in Fig. 1.6a. Fontana *et al.* wirelessly interfaced three different modalities to a smartphone: a piezoresistive jaw motion sensor, an RF transmitter and receiver for hand gesture recognition, and an accelerometer for capturing body acceleration [62]. For physical activity and food intake recognition, Farooq and Sazonov developed a logging system that was attached on the temple of eyeglasses [59]. The system uses a piezoelectric film sensor attached with a medical tape on the skin for chewing detection, and a three axis accelerometer for monitoring body acceleration. A Bluetooth module was used to send data to a smartphone for logging then data were processed off-line on MATLAB. Mirtchouk *et al.* used multi-modality system for eating recognition [131]; they used an earbud with an internal and external microphones to record chewing and to cancel out background ambient noise. In addition, motions were monitored with two smartwatches— one worn on each wrist—and a Google Glass; each of these smart devices has a built-in 9-axis Inertial Measurement Units (IMU).

1.4 Smart Surfaces

One of the challenges in monitoring eating is building instruments that people will wear every day. They have to be comfortable, daily charged, and be able to sense eating-related behaviors. An alternative is to instrument settings where eating occurs, such as a dining table. In this section we discuss technologies that have been explored to build a smart surface.

For this application, a smart surface needs to be able to sense position and weight with enough accuracy to measure intake events, i.e., where, when, and how much food and beverage was lifted from the surface and consumed. Fig. 1.11 graphically illustrates the trend in the literature towards higher accuracy in the detection of weight and position of objects resting on a surface. Some technologies such as touchscreen provide high position resolution but they do not measure weight. On the other hand, the use of a single load cell can provide high weight accuracy but not position of objects resting on a surface. Smart textile technologies can provide good position resolution but not as high weight accuracy as load cells do. The use of a grid of load cells can provide high accuracy of weight measurements and high resolution for accurate detection of position.

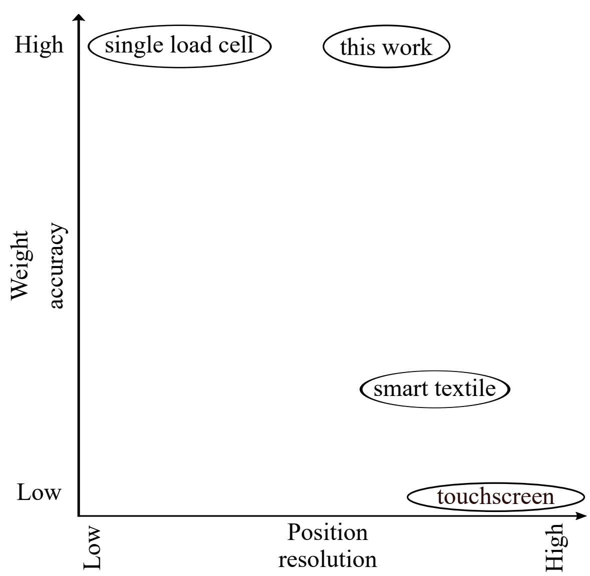

Figure 1.11: Trend in the literature towards higher accuracy for the detection of weight and position of objects resting on a surface.

Table 1.1 lists technologies that were used in the literature for the detection of weight and position of objects resting on a surface. The first technology is a touchscreen built using an infrared camera that is used for locating objects or fingers touching the screen surface [124]. Its high resolution in positioning touching objects is its main strength. A limitation of this technology is that, however, it is not meant to measure weight. The second technology is flexible pressure mapping sensors that consists of a matrix of sensing elements manufactured into a flexible substrate. The material flexibility is the main strength of this technology, but it has a poor accuracy for weight measurements [82, 219]. The third technology is load cells. Load cells provide excellent precision in weight measurements, and are commonly used in body scales, table scales, and similar devices. However, a single load cell (which is how most applications are build) provides no position estimates [127, 144]. The rest of the entries in Table 1.1 describe methods that tried to improve the position estimates provided by load cells. Compared to other methods, the work presented in this dissertation pushes the envelop towards higher accuracy for both position detection of multiple objects resting on a surface and the weight of each object.

Table 1.1: Summary of explored methods that were used for the detection of position and weight of objects when placed on a surface

Ref.	***Technology***	***Position resolution***	***Weight accuracy***	***Application***
[124]	touchscreen	< 1 mm	Cannot measure weight	eating monitoring
[82]	smart textile	1.27 cm	±6.8 g	user interface
[219]	smart textile, force sensors	1 cm	not reported	eating monitoring
[42]	load cells, RFID	30 cm	not reported	eating monitoring
[173]	load cells	2-4 cm (one object only)	±100 g	user interface
[135]	load cells	6.8 cm (one object only)	±39 g	user interface
[77]	load cells	9.4 cm	±3.6 g	eating monitoring
this work	load cells	**5 cm**	**±57 mg**	eating monitoring

Textile or fabric pressure mapping sensors are used to find pressure distribution when a force is imposed over area. Thus visualize the data in a heat map images to identify points with relatively higher pressure compared to neighboring spots. Practical applications of pressure mapping sensors include, for example, electronic skin, plantar pressure imaging, tangible user interface (TUI), and pressure ulcer prevention [76, 117, 118, 150, 219]. These sensors are not meant to measure accurate weights. The reason is that a flexible pressure mapping sensor consists of a grid of sensing elements (sensels) equally spaced from each other. They are embedded into a flexible material such as a fabric, paper, or polymer. When an object is placed on the pressure mapping surface, the force applied by the object footprint is distributed onto some sensels and onto other spots where there are no sensels. This results in an inaccurate weight measurements as the weight can just be partially measured. This problem was reported by Zhou *et al.* who used a textile pressure mapping sensor with 1 cm^2 spatial resolution on a flipped over food tray for dining monitoring application as shown in Fig. 1.13c [219]. In addition, four resistive force sensors were used under corners of the tray to increase the overall weight measurements accuracy. Food weight approximation, however, was far from accurate; it was estimated with an RMS error of 16.62% of the signal span. Flexible pressure sensors lack the repeatability required for accurate weight measurements and is prone to sudden changes as was reported in their study; replacing a glass or cutting on a plate produced random offset [219]. Moreover, some technologies used in flexible pressure sensors exhibit sensitivity that is dependent on applied pressure; starts with high sensitivity at no load and dramatically decreases at larger applied pressures [87, 142]. The sensitivity characteristics S of tactile sensors is generally defined as

$$S = \frac{\triangle X / X_0}{\triangle F}, \tag{1.2}$$

where X is the change in the output signal due to a change in the imposed stimuli or force F [202]. X_0 denotes to the initial output signal at no imposed stimuli or force.

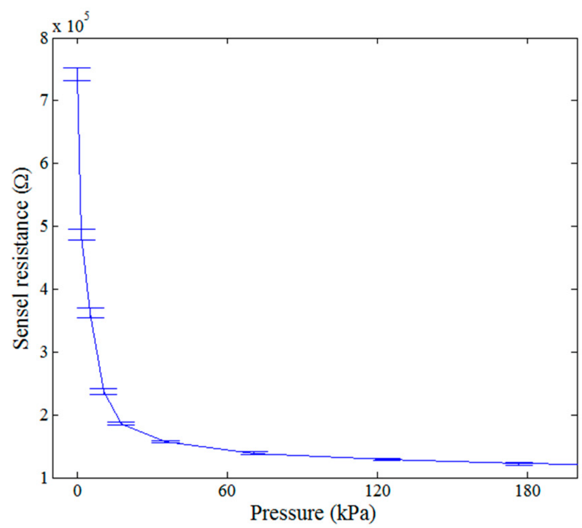

Figure 1.12: Tactile sensors exhibit different sensitivity characteristics for different imposed force; the sensitivity starts high at low applied force and exponentially decreases at under high applied forces [168].

Fig. 1.12 illustrates the sensitivity curve of tactile sensors [168]. This makes a problem in the case of eating monitoring such as when a small bite, e.g., 0.5 g, is picked up from a plate that rests on a flexible pressure mapping surface with the sensitivity characteristics as the one shown in Fig. 1.12. If the pressure imposed by the plate puts the sensels, on which the plate footprint rests, in the low sensitivity region then the weight change made by the pickup of the small bite might likely not be detected. Although new technologies have been developed towards more linear sensitivity behavior, the use of a flexible mapping sensor that uses such technology is still an open research problem for the eating monitoring application [86, 183, 211].

Load cells, in contrast to flexible force sensors, provide better repeatability, accuracy, and linearity, and show almost consistent sensitivity throughout their working range. These properties allow a load cell to reliably and accurately detect a weight change of a thousandth of its rated capacity even when loaded at its full capacity. Load cells are suitable for eating monitoring if they are selected properly with specifications that fit electrically for the range of bite sizes and mechanically for the spatial resolution of the force mapping surface. This will be discussed in more details later in Section 2.2.1.1.

Unrelated to eating monitoring, several related studies tried to track weight and position of objects on a table for several applications. Schmidt *et al.* embedded four load cells under corners of a dining and coffee tables surface to add a user interface feature to the tables to be used as pointing devices [173]. See Fig. 1.13a. This method can be used to estimate the position of a single object on the surface. For position estimate, they reported about an accuracy of about 2% of the surface side lengths, i.e., $135 \times 75\ cm^2$. Similarly, Murao *et al.* used four load cells at the corners of a table, either under tabletop surface or under legs to recognize the actions of adding and removing objects to and from the table, and of four specific activities on the table: typing, moving a computer mouse, writing, and wiping [135]. It was assumed that multiple objects can neither be added nor removed at the same time, but only one object can. Their study revealed that weight error was 39 g and the position error was 6.8 cm.

For dietary monitoring, Chang *et al.* constructed a diet-aware dining table with a tabletop surface that has nine 30x30 cm squares as shown in Fig. 1.13b [42]. A weighing scale and an RFID scanner were embedded under each square to measure weight of food consumed and to detect food item via an RFID manually labeled food containers. This work was an extension of the universal eating monitor by Kissileff *et al.* [103] who used only one weight scale on a dining table. Aforementioned designs that used load cells do not provide footprint information needed for object identification.

In a recent work, a Sensor Interactive Table (SIT), which uses load cells, was developed by Haarman *et al.* [77] for eating monitoring. They built a 1.45 m diameter round-shaped dining table. The table surface consists of 199 hexagon-shaped modules; each module has $76\,\mathrm{cm}^2$ surface area as illustrated in Fig. 1.14. A load cell with 5.0 Kg capacity was embedded under each module. A panel

(a)

(b)

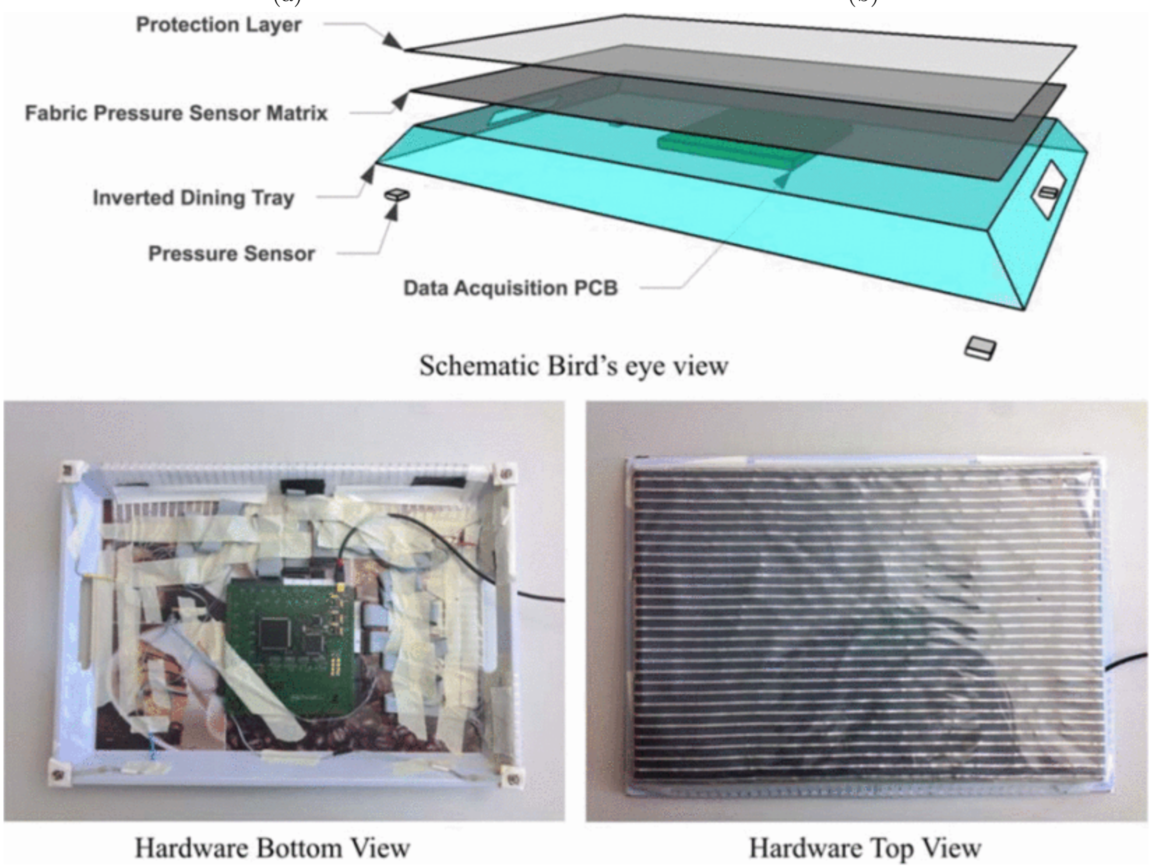

(c)

Figure 1.13: Dining tables that can detect weight and position of objects on a surface. (a) Load cells embedded at the bottom corners of the tabletop of a dining table [173]. (b) Nine scales embedded under a dining table [42]. (c) A flipped over food tray covered with a textile pressure mapping sensor [219].

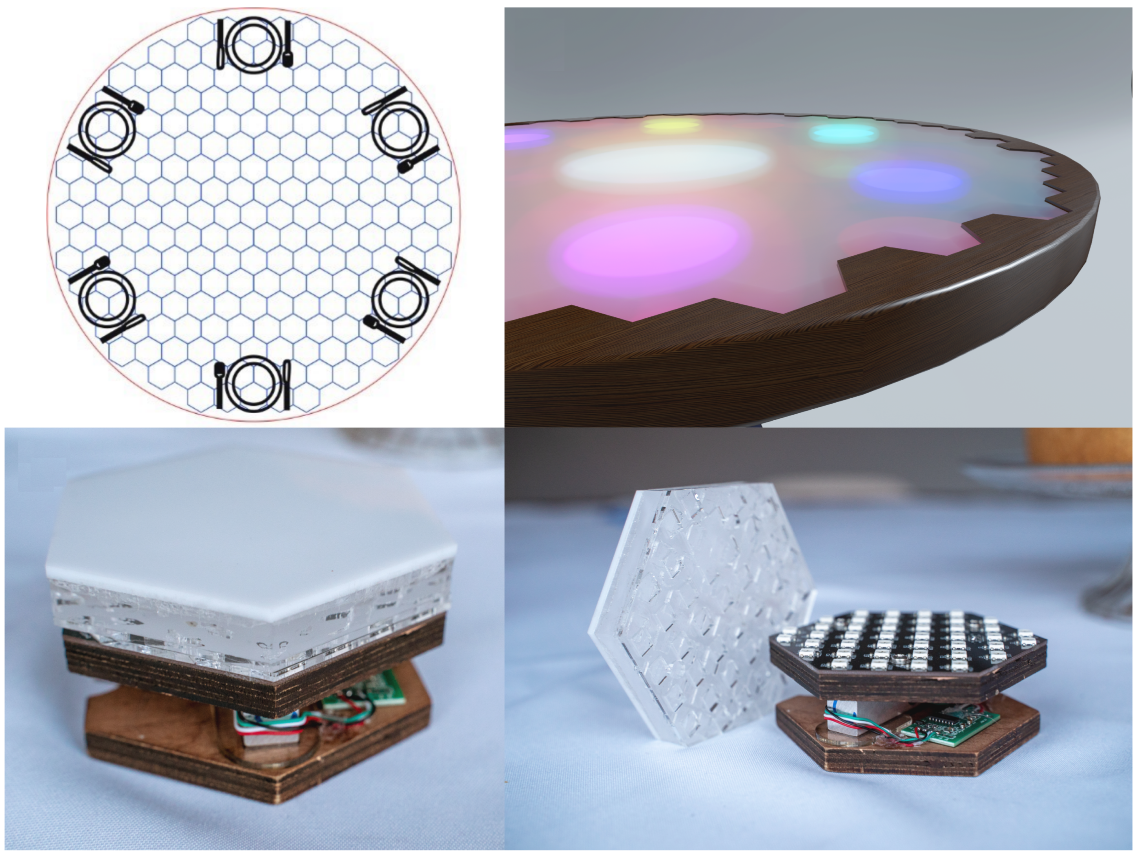

Figure 1.14: The Sensor Interactive Table (SIT), which consists of 199 hexagon-shaped modules each containing a load cell and an RGB LED [77].

of LEDs covered with opaque plexiglass was used on each module to allow interaction with users and possibly to provide feedback about a detected behavior. It was assumed that the minimum bite size is 5 g. Their study, however, show that a single module has weight measurement error of 0.3 to 3.6 g depending on applied load. For dietary monitoring, however, a force mapping surface needs to have more spatial resolution and to be more sensitive than the SIT. That is to correctly capture footprints of food containers to be distinctly classified; footprint area of a cup of water is most likely smaller than that of a single module in the SIT. The minimum bite size, moreover, could be as small as one gram [103]. Therefore, a force mapping surface for dietary monitoring needs to be sensitive enough to accurately measure a fraction of one gram. This dissertation will show how challenging it is to use load cells for a 2D weight sensing surface.

Last, explain that we want to push this envelope further, extending resolution and position accuracy while maintaining weight measurement precision. To do this, we use a much larger number of load cells that most previous works, and manufacture a dense array of load cells. This has a lot of challenges which need to be overcome.

This work aims to push the envelope summarized in Table 1.1 further towards higher spatial resolution while maintaining weight measurement precision. To do this, we use a larger number of sensel density than most previous works, and manufacture a dense array of load cells (384.5 load cells/m^2) that have lower rating capacity (100 g), which allows for higher weight measurement sensitivity (50 mg). This has a number of challenges which need to be overcome. The manufacturing process to be presented in this work paves the way towards even higher sensel density.

1.5 Strain Gauge Load Cells

A strain gauge load cell is a transducer that converts mechanical force into a measurable electrical signal. Each load cell has two main components: frame and an electrical circuit. The frame, which is also called the spring element, is meant to elastically deform due to an applied mechanical force. The frame returns to its normal shape once the force is removed. Strain gauges are firmly bonded to the frame surface to translate that deformation into a change of electrical resistance. A strain gauge, which was invented by Edward E. Simmons and Arthur C. Ruge in 1938, consists of a resistive foil covered with an insulating flexible material. The electrical resistance of this thin foil depends on the deformation curvature. The resistance increases if the frame deformation stretches the strain gauge, and decreases if the deformation compresses the strain gauge.

Load cells are designed in different shapes to fit different applications and weight ranges such as single point beam, ring, S-type, shear beam, bending beam, and many others [133]. Although common shapes of load cells are meant to measure force on one axis, there are other more sophisticated types that measure forces and detect moments in two or three different axes. For each axis, one or more strain gauges are bonded at strategical locations of the load cell frame. Fig. 1.15 shows some examples of load cells used in common scales.

Strain gauges are connected in a Wheatstone bridge circuit to measure small changes in resistance resulting from changes in applied force. Fig. 1.16 shows an excitation voltage is connected across the outer terminals of the Wheatstone bridge. The signal is measured across the middle terminals. One of the Wheatstone bridge resistors is replaced with a strain gauge to form a quarter-bridge. Although this configuration provides strain measurements, it is susceptible to temperature changes; a common problem strain gauges have. Another strain gauge is added to the Wheatstone bridge to cancel out the temperature effect. In this case, the configuration is called half-bridge. Either the resistors R2 and R3 or R1 and R4 are replaced with strain gauges so that the ratio of R2/R3 or R1/R4 stays almost constant regardless of any changes in the temperature. That is because the temperature affects the strain gauges the same way assuming they are the same model and/or have the same characteristics. This configuration does not only alleviate the temperature affect but it could also increase the load cell sensitivity. The sensitivity increases if the two strain gauges are positioned strategically on the load cell frame in such a way that one of them stretches due to the applied force and the other contracts. A full-bridge load cell replaces the four resistors with four strain gauges to get even higher sensitivity and to alleviate temperature effect.

Strain gauge based, single point load cell is a popular type for precision weighing scales. An aperture is cut in the load cell frame with two holes wider than the aperture as shown in Fig. 1.17. The load cell is mounted from one end to a rigid structure and the force to measure is applied onto the other end. The aperture along with the two holes control the deformation caused by the applied force so that the deformation of the body concentrates at the tops and bottoms of the two holes where four strain gauges are bonded. This design helps the single point load cell to gear off-center loading into its measuring axis. In addition, concentrating the deformation at four points increases its sensitivity to detecting small changes in the applied force, which is also amplified by the long beam. The strain gauges are connected in a full-bridge configuration. When a force is applied two

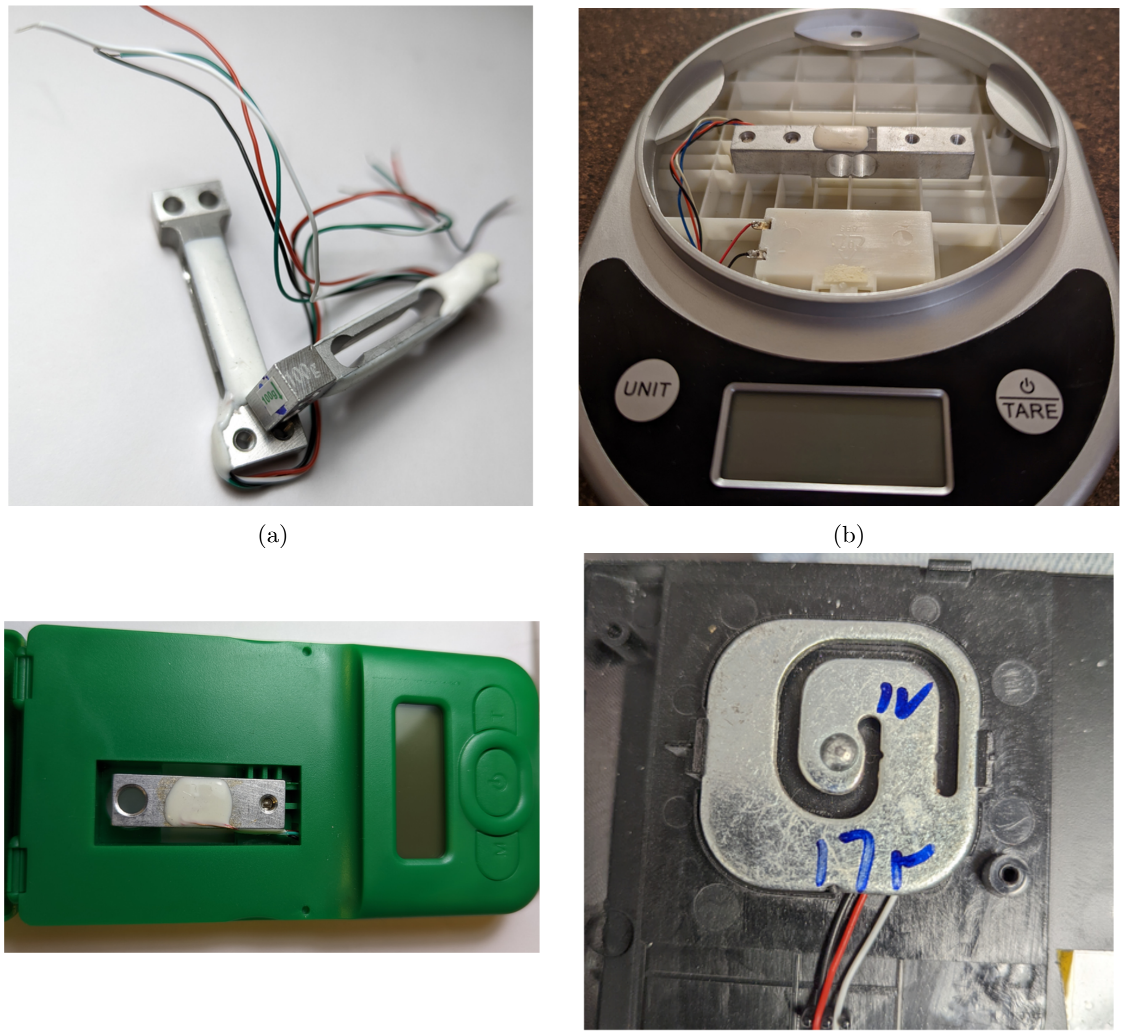

(a) (b) (c) (d)

Figure 1.15: Examples of load cells used for weighing applications. (a) A 100 g capacity single point load cells. (b) Kitchen scale. (c) Pocket scale. (d) Body scale.

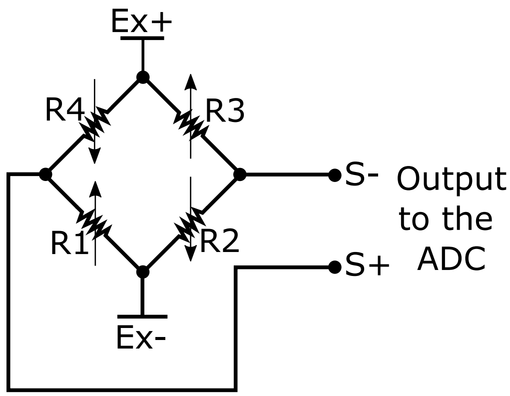

Figure 1.16: Wheatstone bridge is used to measure electrical resistance. An excitation voltage is applied across the outer points of a Wheatstone bridge. Output signal is measured across the internal middle points.

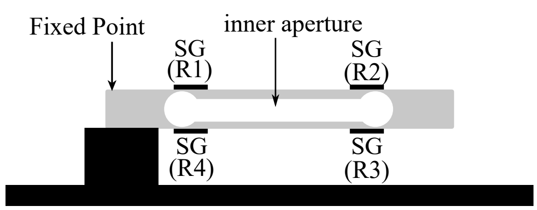

Figure 1.17: A side view of a single point load cell showing four starin gauges R1-R4, and two holes at the end of its inner aperture.

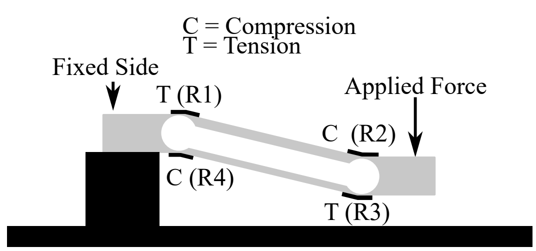

Figure 1.18: When a force is applied on a single point load cell the deformation concentrates at the four points where the strain gauges SG (R1) to SG (R4) are bonded. The strain gauges SG (R1) and SG (R3) measure tension while SG (R2) and SG (R4) measure compression.

resistors — R2 and R4 — measure compression, and the two others — R1 and R3 — measure tension as depicted in Fig. 1.18.

The output signal is in millivolts range. A typical load cell would produce 2mV/V output signal at full capacity. This means when it is fully loaded at its rated capacity and the load cell is excited with 10V, for example, the output signal would be 20mV. This small signal needs amplification.

A load cell can be calibrated using a known calibration weight ($calibration\_weight$) that is equal to the rated capacity of the load cell. The calibration is required to provide meaningful values in units of weights such as grams or pounds. A raw measurement is taken from the amplifier or the ADC when no load is applied to the load cell. This measurement is the zero-offset ($zero\_offset$) or the tare value. Next, the calibration weight is placed on the load cell and another raw measurement is taken. This raw measurement is called full-load ($full\_load$). The calibration value ($calibration\_value$) is hence computed as follows

$$calibration\_value = \frac{full\_load - zero\_offset}{calibration\_weight}. \tag{1.3}$$

Having the calibration value, a raw measurement (raw) can be converted into a meaningful measurement ($weight$) in grams as follows

$$weight = \frac{raw - zero\_offset}{calibration\_value}. \tag{1.4}$$

1.6 Novelty

The novelty of the research presented in this work lies in the construction and testing of a new table instrument to monitor eating. Compared to other research on table instruments, the new table has much higher spatial resolution and thus is capable of better spatial localization and weight measurements of objects on its surface. Compared to wearable sensors, which need recharging and wearing, instrumented house furniture can be always left plugged into the power mains and to the Internet. A mature version of this instrument would automatically differentiate eating episodes from other uses and activities that are usually taking place on dining tables, enabling for more accurate detection of eating events.

Chapter 2 describes the challenges in hardware design. It explains the problem of vertical deviation among tops of the surface tiles of a grid of load cells and the technique that was used to overcome this problem. It describes the electronic circuits used for reading load cells and the mechanical design of the 2D weight sensing surface along with the enclosing wooden box. System performance is evaluated for weight accuracy and repeatability, and the overall performance of the 2D weight surface to provide spatial information of objects resting on the surface.

Chapter 3 describes pilot experiments that involves recording 11 human subjects eating a meal on the custom-built dining table. Each subject ate individually and was video recorded for ground truth. Data generated by the dining table were synced with videos and labeled manually. These data were used for developing and evaluating a rule-based algorithm. Results are presented in this chapter.

Chapter 4 compares the tool developed in this work against other ones developed in related previous works. Data was collected for a total of 32 subjects on our tool for comparative evaluation. Because our instrument produces image of weights, i.e., 2D data, while other methods use 1D weight measurements, we prepared the dataset according to the requirements of the other methods. For example, the summation of all grid cells was used as the input of the algorithm developed by Mattfeld *et al.* [127] who used 1D weighing scale on which a food tray was placed. We used four metrics to evaluate bite detection performance: precision, recall, accuracy, and F1-score.

Chapter 2

Hardware Development

This chapter shows a technique to construct a 2D weight sensing surface with a grid of load cells for eating monitoring application. Nevertheless, this technique can be used to build such surface for different applications as well. It starts by stating the problem description and the challenge in using a grid of load cells to make a 2D weight sensing surface. Next it describes the design of a single grid cell. This is followed by a description of the modifications required to construct the grid. Afterward, it describes the inversion process used to achieve vertical alignment among tops of tiles. Evaluation method of the grid performance and accuracy is then explained. Finally, results are presented and discussed.

2.1 The Problem of Deviation Among Tops of Tiles

The purpose of the 2D weight sensing surface surface is to detect location and to measure weight of an object setting on the surface. An accurate spatial information of an object footprint provides location and weight, and could help distinguish multiple objects from each other when having objects with different footprints. The main challenge is that an object needs to distribute its weight across all cells on which it rests. However, a single load cell deflects only a fraction of a millimeter across its entire range (from no load to rated capacity). Thus, the tops of load cells must be precisely aligned across the entire grid. Fig. 2.1 illustrates this challenge. If one cell is higher than its neighbors, then the object footprint would rest on only that high cell. Additionally, each single load cell uses an overload protector that prevents physical deflection beyond a maximum

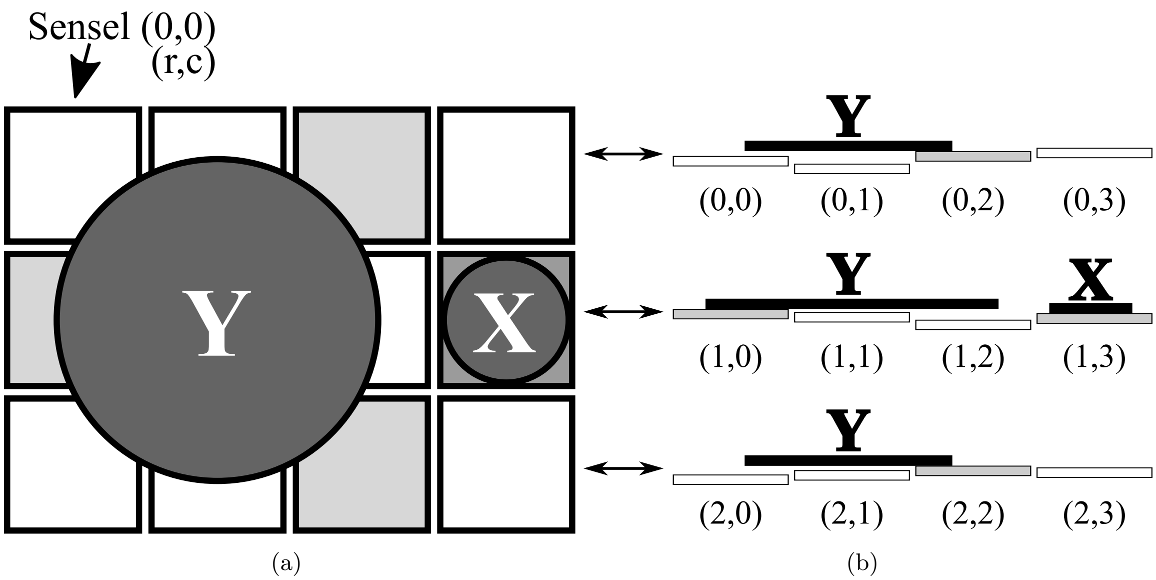

Figure 2.1: Problem of vertical deviation among cells. (a) Horizontal view of a grid of cells. Unlike object X which is measured by one cell (1,3), object Y should rest on nine cells. Due to deviations among the tops of the cells, object Y rests only on the highest three cells. (b) Cross-sectional view of object Y resting on only three cells {(0,2), (1,0), and (2,2)}, which are vertically higher than their neighbors. This problem prevents obtaining correct spatial information. It can also cause inaccurate weight measurements if at least one load cell of the highest three was stopped by its overload protector, which would transfer some amount of the weight to the structure on which the load cell is mounted.

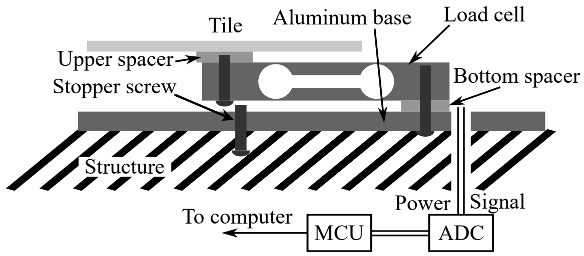

Figure 2.2: Design for one cell. A tile is attached to the top of a load cell that is affixed on a metal base. A stopper screw is used to protect the load cell against over loading. Wires of the load cell are connected to a PCB that provides power, reads data, and sends them to a computer.

range to prevent damage to the load cell. Since the entire deflection range is only a fraction of a millimeter, it is possible for an object to transfer some amount of its weight onto the structure on which the load cell is mounted, preventing weight from being shared amongst neighboring cells, and thus yielding inaccurate weight measurements.

2.2 Methods

This section describes the design of a single cell, which includes components to help with vertical alignment with neighboring cells. Next, it describes the structure and electronics holding a 7×11 grid of cells. This is followed by a description of the inversion process used to achieve vertical alignment.

2.2.1 A Single Grid Cell

One grid cell consists of mechanical and electronic parts. Fig. 2.2 shows a tile mounted on a single point load cell that is mounted on a base. A washer is used between the base and the load cell to provide space for the load cell to flex. Another washer is placed between the tile and the load cell. A stopper screw is used to protect the load cell against overloading. The load cell is connected to a circuit that has an analog to digital converter (ADC). A microcontroller (MCU) reads data from the ADC and sends them to a computer. A square piece of standard glass is used as a tile with 2.28 mm thickness and 47 ± 1 mm side length. We chose glass for its flatness and stiffness.

For a load cell we selected the QL-56 mini (Hanzhong Quanyuan Electronic Co., Ltd, China). It has 100 g loading capacity, $47 \times 12 \times 6$ mm dimensions, and costs less than \$5 USD. The load cell has a rated capacity of 100 g and can safely handle up to 150 g without causing permanent deformation to its frame. Its rated output is 0.7±0.1 mV/V. It comes with four 10 cm long wires which are connected to a PCB that supplies a regulated five volts excitation voltage. We used an HX711 24-bit sigma-delta ADC (Avia Semiconductor, Xiamen, Ltd., Xiamen, China). It has an on-chip oscillator and accepts an external oscillator clock that allows multiple HX711 chips to be synced to each other. The ADC is used with the following configuration: 10 samples per second, 128 gain, and 5 V reference.

2.2.1.1 More Details About Load Cell Selection

This section is just a documentation of lessons learned during the selection of a load cell. Readers who intend to replicate this work for a different application may find this section helpful as it shows the assumptions based on which the design decisions were made.

A force mapping sensor for dietary monitoring application is expected to detect the range of weight changes due to individual intake events, both food and liquid bites. Previous studies give us an idea about this range. Mattfeld *et al.* recorded 20,542 food bites with 8.9 g average weight and 3.3 g standard deviation [127]. The same study recorded 3,559 liquid bites with 30.7 g average weight and 13.7 g standard deviation. It is also possible for a bite to be as small as one gram [103].

It is assumed that three flat-bottomed food containers will be used on the 2D weight sensing surface: a cup, plate, and bowl. Diameter of these container footprints are 6.5 cm, 19 cm, and 10 cm, respectively. Based on the food content and the footprint area, the cup of beverage is expected to apply the highest force per unit area, while the plate is expected to apply the lowest. Based on the assumed footprints of the food containers and the range of their total weights, a load cell can be selected.

To select a load cell for a 2D weight sensing surface, three factors need to be specified: the minimum change of weight a grid cell needs to detect, dimension of the grid cell (spatial resolution), and the maximum possible load applied per grid cell. For our application case, we used the aforementioned order of the three factors to be from highest priority to lowest. This order can change from an application case to another. That is because selection of a suitable load cell for an application is a trade off process. A trade off has to be made between a load cell sensitivity and its maximum loading capacity; a load cell with a rated capacity usually has less sensitivity compared to another load cell with substantially lower rated capacity. A weight of ten grams, for example, is likely considered noise and hard to detect with a 200 kg rated capacity load cell. Another trade off might exist between the spatial resolution and the sensitivity; low profile single point load cells are usually long so that the force applied by a small weight is multiplied by the load cell length to cause a mechanical deflection that can be detected by its strain gauges.

The load cell QL-56 mini (Hanzhong Quanyuan Electronic Co.,Ltd, China) was selected based on our aforementioned priorities after testing different load cells. This load cell has 100 g loading capacity, 47L x 12W x 6H mm dimensions, and costs less than 5 USD. Based on its length, we chose a grid cell dimension of 51 x 51 mm including one millimeter spacing among grid cells. These specifications work well for the other two factors. Because weight of a food container is shared among all load cells on which it rests, the minimum weight a load cell needs to detect is the weight of the smallest bite (i.e., one gram) divided by the maximum number of load cells under the container with the largest footprint area (i.e., the plate). The plate can be placed on 20 tiles maximum. Therefore, the minimum weight a load cell needs to detect is 1/20 g, which can be detected by this load cell. The maximum possible load applied per grid cell is the maximum weight of the container that is expected to apply the highest force per unit area divided by the minimum number of load cells on which the container rests. The cup of beverage is expected to be that container, and is assumed to contain 300 g maximum total weight. Its flat-bottomed footprint can rest on as few as four load cells. Therefore, the maximum possible load applied per grid cell is 75 g, which is lower than the capacity of our selected load cell.

For building the 2D weight sensing surface with an individual grid cell size of 51 x 51 mm, which is slightly larger than the longest dimension of an individual load cell, we decided to build seven rows by 11 columns grid that makes a surface area almost similar to a dining tray.

For performance evaluation and to check the detection ability of the load cell, we used the signal to noise ratio

$$SNR = \frac{\Delta w}{\sigma}, \tag{2.1}$$

where Δw is the change of weight of interest to be detected in grams. The noise σ is the standard deviation of a window of stable measurements while the load cell is under load. Using the signal shown in Fig. 2.3, for example, the SNR is 22.7; the weight of interest to be detected is the 50 mg calibration weight, and the standard deviation is 0.0022 g for the measurements in the time window 206 to 208 seconds excluding the measurements during the transition due to the pick up of the 50 mg weight. Such high SNR indicates that the assumed minimum weight reduction per grid cell (i.e.,

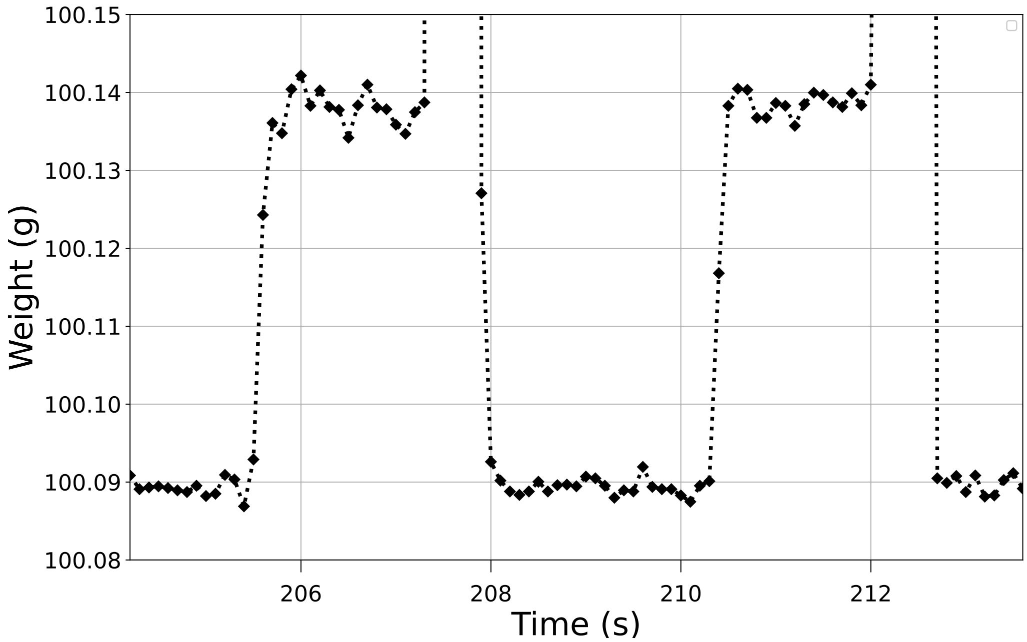

Figure 2.3: Response of the QL-56 mini load cell when a 50 mg calibration weight is placed and then picked up while the load cell is loaded with full capacity (100 g).

1/20 g) can be detected by the QL-56 mini load cell.

2.2.2 Grid Design

Based on the size of our load cell, we chose a grid cell dimension of 51 $\times$ 51 mm to allow 1 mm spacing between adjacent cells. The electronic system layout, shown in Fig. 2.4, consists of 77 cell boards (7 $\times$ 11 grid), a central control unit, and seven row distribution boards that connect all cell boards to the central control unit. Cell boards need to be located close to their load cells because the signal generated by the load cell is small; a change of 50 mg weight would result in about 1.75 uV change in the output signal of the QL-56 mini load cell when excited at 5 V. A sync clock is used to sync all the ADC chips together so data are read simultaneously in parallel. A distribution board for each of the seven rows provides boosted sync clock signal, and power to 11 cell boards. The central control unit generates the sync clock and reads all the ADCs in parallel. We used the development board EK-TM4C1294XL (Texas Instruments) to read data and send them to a computer over an Ethernet connection.

A metal sheet was used to provide a stiff base on which the load cells are mounted. The base is 6061 Aluminum alloy with dimensions of 700 mm length, 500 mm width, and 6.4 mm thickness.

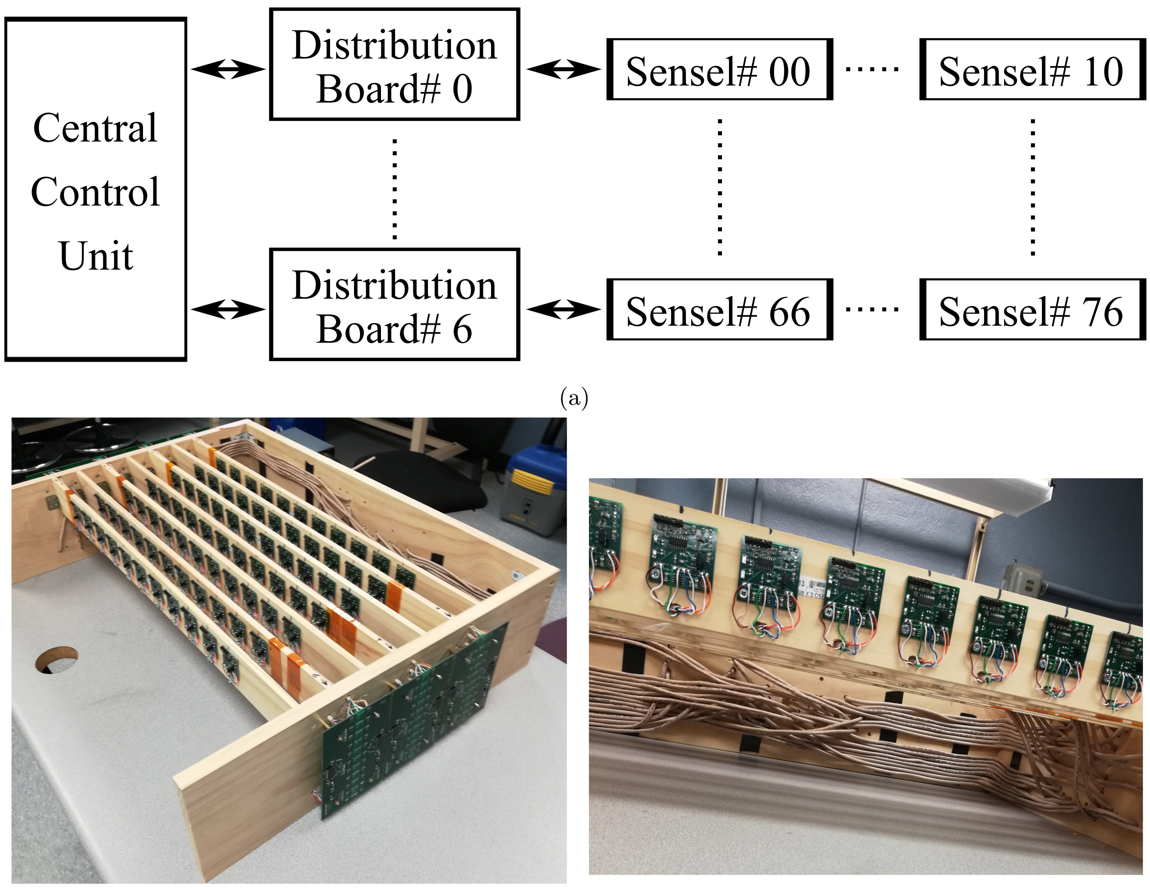

(a) (b) (c)

Figure 2.4: Electronic scanning system. (a) A central control unit provides power and synchronization signal to seven distribution boards that boost and distribute this signal along with power to 77 cell boards. The central control unit reads the 77 cell boards in parallel. (b) PCBs attached to pine wood structure which will be placed under the base of the grid of load cells. Seven distribution boards are attached on the sides. (c) Cell boards are attached on horizontal ribs so that each board is aligned under its load cell.

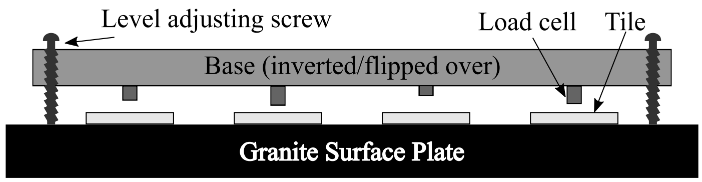

Figure 2.5: A cross sectional view of an inverted metal base on which load cells are mounted. The base vertically rests on a granite surface. Gaps with different heights appear between load cells and their tiles, which are placed on the granite surface. While inverted, these gaps are filled with epoxy to cancel out the height deviations. The surface formed by the tiles should take the flatness of the granite surface after the epoxy is cured and the base is flipped back to normal.

There are four holes on the base for each load cell: one threaded hole for the overloading protection stopper screw, one through-hole for wires to be connected into a cell board under the base, and two through-holes for mounting the load cell. The base and the washers were manufactured with a CNC machine.

2.2.3 The Inversion Process

After all load cells are mounted on the base, we used inversion to attach the tiles to the upper washers using epoxy. The total deflection (from no load to full capacity) of the QL-56 mini load cell is 75.5±9.5 um. Hence, vertical alignment of less than 0.1 mm is required. Fig. 2.5 illustrates our inversion technique. There are four steps: prepare a flat surface reference, make a stencil, prepare tiles, dispense epoxy.

A laboratory grade granite surface was used as a reference for high accuracy flatness. Aluminum angle corners were affixed at edges of two sides of the granite surface to create a corner for retaining the base orientation and position during the inversion. A stencil for maintaining tile orientation during the inversion was made using a laser cutter. We used a 1.87 mm thickness acrylic and cut a grid of 7×11 squares with 49 mm side length for each square, and 2 mm spacing among squares. Next, the stencil was placed on the granite and the base is flipped over the stencil and pushed toward the aluminum angles. At this point the base was resting on the granite surface such that the distance between the granite surface and the upper washers allowed the stencil to move freely; the base has six level adjusting screws (shown in Fig. 2.5) near its long edges to control its vertical level and its distance to the granite surface. The stencil was aligned under the base so that the center of each square is under its corresponding upper washer. Next, the base was removed, and the stencil was taped on the granite surface as shown in Figure 2.6a.

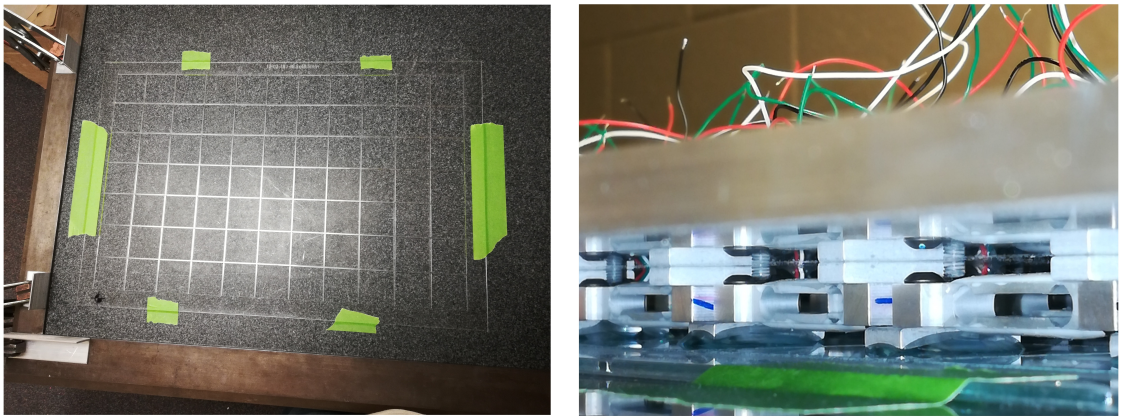

(a) (b)

Figure 2.6: The inversion process. (a) An acrylic stencil is placed on a granite surface to keep orientation and position of tiles. Aluminum corners are affixed at the granite edges to save orientation and position of the base so that upper washers of load cells will align to the center of their tiles, which will be held by the acrylic stencil, during the inversion. (b) The base is flipped over and left resting on the granite surface. Upper washers are dipped into epoxy blobs, which were dispensed at the centers of the tiles.

The squares of glass tiles were cleaned with glass cleaner and put in the stencil square openings. It is important to make sure there is a small gap around each glass tile, so it moves freely without getting stuck in the stencil. After all glass squares were put in the stencil openings, the base was flipped over again on the granite surface and pushed to its aligned position. Next, the level adjusting screws were adjusted such that the gaps among glass tiles and their corresponding upper washers were all about 1 mm. All the six level adjusting screws were used to reduce the effect of the base deflection due to its weight and the weight of its assembled components. The base was removed again for the epoxy to be applied on the glass tiles.

DEVCON 14260, dual-cartridge, 50 ml epoxy adhesive was used with a manual dispenser and a mixing nozzle tip. This epoxy has eight minutes working time which was sufficient to put a blob of the epoxy on the center of each tile before it sets. The size of the blob was small but sufficient to surround the upper washer and make a strong tile to washer bond. Once epoxy was dispensed on all tiles, the base was flipped over and pushed in an angle towards the aluminum angle corners then was left to rest on the granite surface so that each upper washer dips into an epoxy blob as shown in Fig. 2.6b. The base was left overnight for the epoxy to cure.

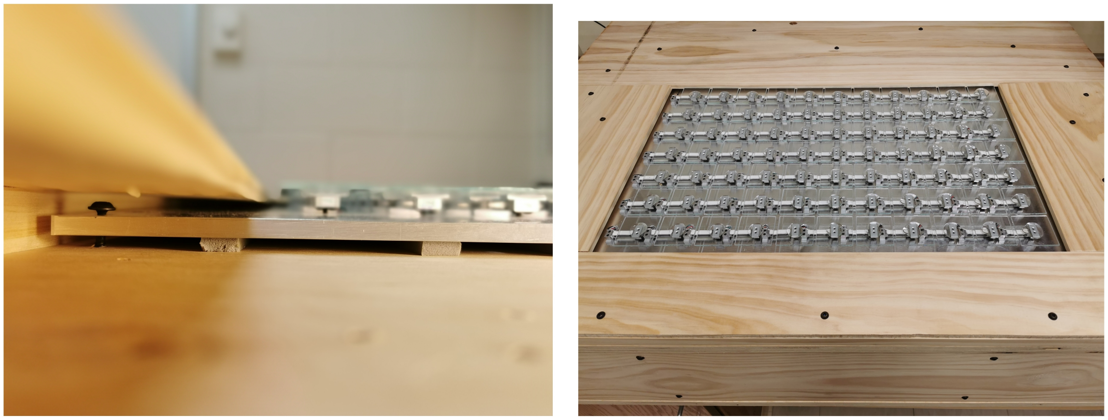

(a) (b)

Figure 2.7: The table. (a) Side view shows strips of window seal foam used as a compliant material to form a cushion under the base for protection against any curvature the plywood might have. (b) The final sensor grid.

2.2.4 The Table

Plywood was added on top of the structure that contains the electronic scanning system shown in Fig. 2.4. Holes were drilled on the plywood for wires of load cells and for the overload protection stopper screws so they could be accessed for tuning. Strips of window seal foam were used on top of the plywood as a compliant material to form a cushion for the base to protect it against any curvature the plywood might have, as shown on Fig. 2.7a. The base was affixed on the plywood with four screws located at the base corners such that screws were only halfway fastened to keep the horizontal position and orientation of the base. The mounting screws were not fully fastened to avoid causing any force that would otherwise make the base to bend and hence change the grid flatness after the inversion. Next, wires of the load cells were soldered to the cell boards. Then the instrument was turned on, and overloading protection stopper screws were tuned using calibration weights to keep load cells under the maximum safe rating. The structure was completed in a box shape with pine wood boards on the sides, and a plywood board at the bottom. Finally, empty space around the grid was filled with pine wood which was made with a wood planer to make the table surface about one millimeter higher than the active sensing area. Fig. 2.7b shows the final appearance of the device.

The table surface was covered with a laminate to hide the surface and to protect it from food spills. The laminate is made of two layers of plastic foil separated by a paper towel, which

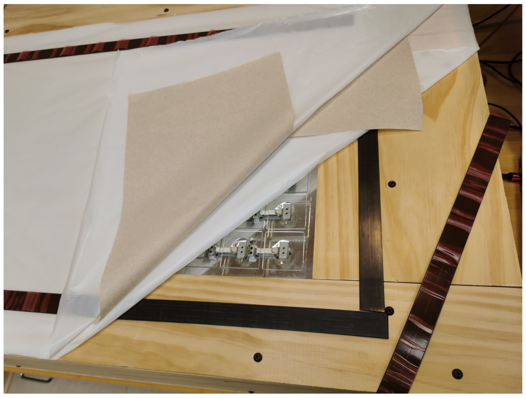

(a)

(b)

1.354	8.170	-0.000	0.000	-0.003	0.000	-0.004	-0.002	0.000	-0.005	-0.003
34.827	36.400	11.542	-0.003	-0.001	-0.004	0.003	-0.002	21.239	47.409	-0.001
24.010	44.439	3.525	-0.005	-0.001	0.001	-0.000	-0.000	21.167	30.095	0.001
-0.004	-0.004	0.002	0.002	17.297	22.650	31.075	1.161	-0.001	0.001	-0.002
0.001	-0.001	-0.004	10.199	28.636	36.410	41.218	7.834	0.009	-0.000	-0.003
-0.007	-0.002	-0.002	5.668	31.370	36.441	32.737	7.951	-0.003	-0.001	0.001
-0.003	-0.000	0.001	-0.005	12.204	16.977	9.496	-0.003	-0.003	0.001	-0.003

(<=0g) **(>=100g)**

(c)

Figure 2.8: (a) A laminate made of paper towel sandwiched in plastic foil was used to protect and hide the active area. Magnetic tape holds the laminate in place. (b) Example dishware with calibration weights. (c) Sensed footprints of objects, where the total weights are 164.3, 349.3, and 119.9 g for bowl, plate, and cup, respectfully.

alleviates friction between the two plastic foil layers to reduce the cross talk among adjacent tiles. The laminate was kept in place with magnet tapes around the active sensing area as shown in Fig. 2.8a. All cells were calibrated with a 100 g weight before collecting data. Fig. 2.8b shows a photo of three pieces of dishware (plate, bowl, cup) placed on the device, with known calibration weights. Fig. 2.8c shows the sensed footprints of these objects. Note the weight of each object is shared among multiple neighboring cells.

2.2.5 Summary of Challenges

Table 2.1 lists a number of design and manufacturing challenges and the workaround we used to overcome each challenge.

The clock distribution problem could be inspired by CCD (camera) and monitor (display) synchronization of thousands to millions of elements. The purpose is to sync all ADCs so that they all provide data at the same time. This helps in obtaining a fixed frame rate and insures new measurements for every frame.

Table 2.1: Summary of challenges and solutions.

Step	***Challenge***	***Solution***
ADC	very small signal from load cells	put sensel boards as close as possible to their load cells, and use parallel topology for the distribution of the sync and data clock signals.
clock distribution	ringing and ground loops	use four layer PCBs, use terminating resistors, and match the characteristic impedance of routes and cables.
load cells	overload protection	use of stopper screws and manually tune each screw using a calibration weight
surface tiles	vertical deviation among adjacent tiles	the inversion method

2.2.6 System Validation

Hardware performance was evaluated by testing single grid cells and multiple grid cells. Table 2.2 summarizes all the tests performed along with the purpose of each test, the number of different positions across the surface grid, and the number of times the test was repeated at each position.

The first group of tests were performed to evaluate performance of single cells. All grid cells were,first, tested for weight measurement accuracy when loaded with five different calibration weights: 1 g, 5 g, 20 g, 50 g, and 100 g. Next, repeatability was evaluated on ten randomly selected cells for detecting a weight change of 50 mg while each cell is loaded with 100 g calibration weight. This test was repeated 30 times on each of the ten cells. This test was followed by testing the time each of the ten cells take to converge to stable measurements.

The second group of tests were conducted on multiple cells. The first test was done by placing a flat-bottomed object at the middle of a 2×2 tiles (10×10 cm^2 area) to evaluate the outcome of the inversion process at reducing the vertical deviation among the tops of adjacent tiles. This test was done at 58 different positions across the grid surface. The second test was meant to evaluate the accuracy of weight measurements when the weight of a flat-bottomed object is distributed among 4×4 tiles (20×20 cm^2 area). This test was repeated at 28 different positions. Finally, the grid was evaluated for the reliability at detecting the minimum expected bite size, i.e., 0.5 g, when picked up form a plate containing a total weight of 560 g.

Table 2.2: Summary of measurement tests.

Area tested	***Purpose of testing***	***Positions***	***Repetitions***
single cell	accuracy across different weights	76	1
single cell	repeatability for detecting 50 mg while loaded with 100 g	10	30
single cell	convergence to stable measurements	10	2
2×2 cells	deviation among tile tops	58	1
4×4 cells	accuracy in weight measurement when distributed across multiple tiles	28	1
$\geq$ 4×4 cells	Ability to detect a weight change of 0.5 g on a plate containing 560 g of total weight	6	25

2.3 Results

In this section, we show results of a number of tests that were conducted to evaluate the design performance. All sensels were calibrated with 100 g calibration weight before collecting data. Table 2.2 summarizes the tests performed. The first three tests evaluated measurement accuracy on single cells, in terms of accuracy, repeatability, and time to converge. The second three tests evaluated measurement accuracy across multiple cells, to evaluate height deviations amongst the tops of adjacent tiles, uniformity of weight distribution across cells, and efficacy to measure small weight changes resembling intake events. The following sections provide more details on each of these tests.

2.3.1 Single Cells

The first group of tests were conducted on single grid cells. For the first test, different calibration weights (1 g, 5 g, 20 g, 50 g, and 100 g) were placed on each sensel to evaluate the accuracy at different loads. Fig. 2.9 shows a plot of reference weights vs residuals, where the standard error increases with applied load. Most of the sensels, however, have less than 0.1 g of standard error when loaded with a 100 g calibration weight. This load is actually more than the

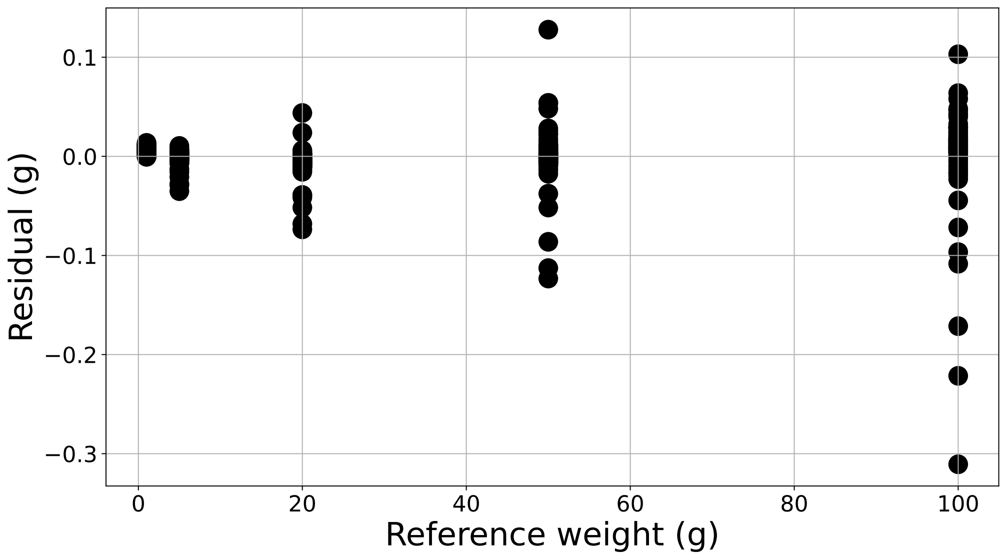

Figure 2.9: Residual plot shows that the standard error increases with applied load. Different calibration weights were used for this test: 1 g, 5 g, 20 g, 50 g, and 100 g.

rated capacity when including the weights of the tile and the upper washer.

For repeatability and reproducibility test, 10 sensels were randomly selected. For each sensel, a calibration weight of 50 mg was placed on and picked up for 30 times while the sensel is loaded with 100 g calibration weight to set the load cell at its rated capacity as shown in Fig. 2.3. Weights were computed as the difference between medians of two windows with size of five samples each before and after the removal of the 50 mg weight. Measurements in the two windows were checked for stability such that the standard deviation of the five samples was less than or equal to 0.05 g. The result is illustrated in Fig. 2.10a, which shows most of the sensels have good repeatability and reproducibility. About 17% of the total number of sensels show less accuracy. We noticed that the sensels with less accuracy have slower settling time than those with good accuracy as shown in Fig 2.10c.

2.3.2 Objects on Multiple Tiles

Two tests were conducted to evaluate the ability of our inversion technique to vertically align the grid of cells. For the first test, a weight of 100 g was placed on the center of a square 50 mm side length piece of standard glass which was placed in the middle of a 2x2 grid of tiles as shown

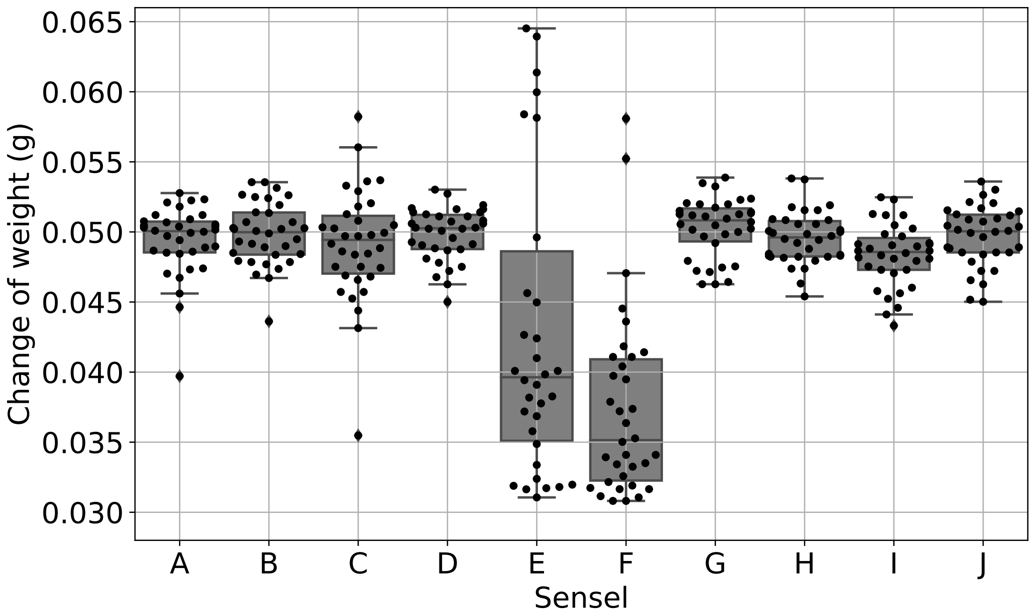

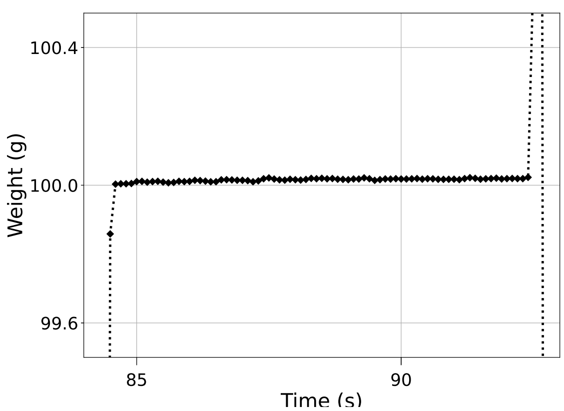

(b)

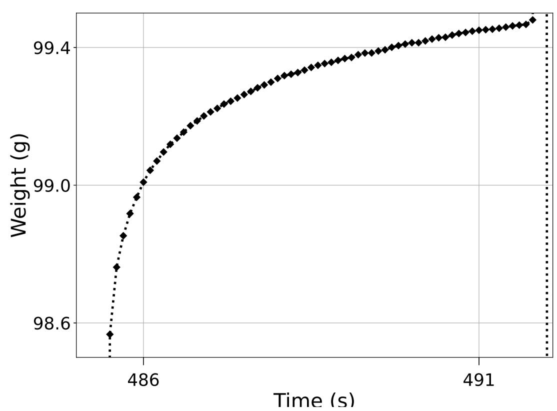

(c)

Figure 2.10: (a) Reproducibility test shows most of the sensels have good accuracy and repeatability for detection of 50 mg of weight change while loaded with 100 g. About 17% of the total number of sensels show less accuracy. (b) An example of a sensel with fast settling time. (c) An example of a sensel with slow settling time.

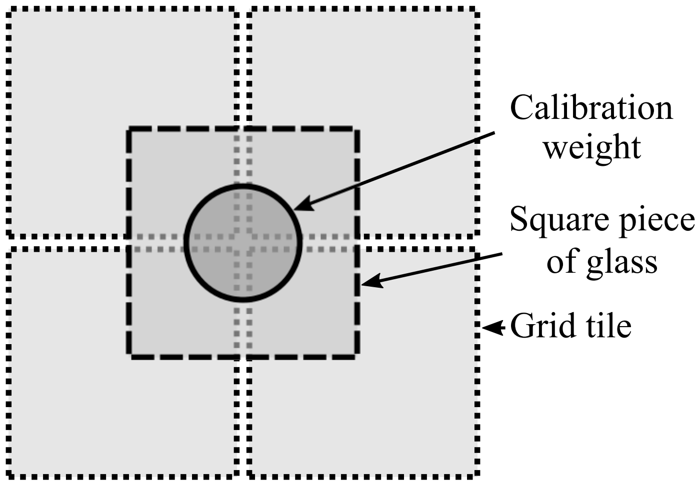

Figure 2.11: A 100 g calibration weight is placed on a 50 x 50 mm square piece of glass which is placed in the middle of a 2x2 grid of tiles. The glass weighs 12.85 g, so total weight is 112.85 g.

in Fig. 2.11. The square piece of glass weighs 12.85 g, so the expected total weight measured by the 2x2 grid is 112.85 g. If weight is distributed perfectly, then each of the four tiles would measure 28.21 g.

To measure the uniformity of distribution, we calculate the standard deviation from the mean (28.21 g) measured at each tile. This test was repeated 58 times all at different positions. Fig. 2.12 illustrates the measured values at one position where the measured total weight is 112.88 g which is 0.03 g in excess. The average distributed weight per tile is 28.22 g with 3.93 g standard deviation. The average total weight at the 58 different positions was 112.81 g with a standard deviation of 0.15 g. At each of the 58 positions, we calculated the standard deviation from the local average distributed weight per tile. The average standard deviation for all 58 positions is 5.5 g. From the perspective of flatness of the grid surface, we found that there is an approximately 4.2±0.5 um deviation observed in this test assuming that 75.5±9.5 um is the average full mechanical deflection of the QL-56 mini load cell — from no load to full load at the rated capacity. See Appendix A.1 for more details of how the deflection distance of the QL-56 mini load cell was measured.

For the second test, a circular piece of standard glass resembling a plate contour was placed as carefully as possible in the center of a 4x4 grid of tiles. The glass was glued to bottom of a paper plate. Together the plate and glass weigh 260 g. To obtain weight measurements, the entire table surface was scanned, and every tile measuring $\geq$ 0.5 g was included, all other tiles were excluded. The total weight was then calculated as the sum of included tiles. The standard deviation of weight

-0.001	**0.001**	**0.004**	**0.005**	**-0.001**	**0.000**	**0.002**	**-0.001**	**0.001**	**0.003**	**0.002**
-0.004	**0.002**	**0.002**	**-0.004**	**0.002**	**-0.000**	**0.001**	**-0.000**	**0.001**	**0.002**	**0.000**
-0.002	**-0.001**	**-0.001**	**28.113**	**33.696**	**-0.001**	**-0.004**	**0.003**	**-0.001**	**0.002**	**0.001**
-0.004	**0.002**	**-0.000**	**26.536**	**24.534**	**-0.002**	**-0.002**	**0.001**	**0.001**	**0.001**	**0.004**
-0.002	**0.002**	**-0.001**	**-0.001**	**0.000**	**-0.000**	**0.002**	**0.001**	**-0.002**	**-0.001**	**-0.001**
-0.002	**0.000**	**-0.000**	**0.002**	**-0.002**	**-0.003**	**0.001**	**-0.001**	**-0.000**	**0.001**	**-0.002**
0.001	**-0.001**	**0.001**	**0.003**	**0.001**	**-0.003**	**0.002**	**-0.000**	**0.000**	**0.000**	**-0.001**

(<=0g) **(>=100g)**

Figure 2.12: A 100 g calibration weight was manually placed in the center of a 50 mm side length piece of glass (weighing an additional 12.85 g) which was placed in the middle of a 2X2 grid. The total measured weight is 112.88 g and the standard deviation among the footprint tiles is 3.93 g.

was also calculated across the included tiles. The reason for this is that with a circular object, not all tiles in the 4x4 grid necessarily measured any weight, depending on exactly where the plate was positioned. This test was repeated 28 times each at a different position on the table surface. Fig. 2.13 shows an example. One factor that is different between this test and the previous 2x2 grid test is that not every one of the 28 tests measured the exact same number of tiles. We found that the average total weight was 259.92±0.22 g. This weight was distributed among tiles under the plate footprint with 12.44 g on average standard deviation. These numbers indicate 99.97±0.1% accuracy in weight estimate (259.92/260 ± 0.22/260).

To evaluate the ability of detection of small weight changes, a 0.5 g calibration weight was repeatedly placed on and picked up from the paper plate that was attached to the circle-shaped

0.000	-0.001	0.000	0.001	0.003	0.000	0.001	-0.000	-0.002	-0.001	-0.000
-0.005	-0.005	0.004	-0.003	19.382	26.532	3.291	-0.000	0.002	-0.000	-0.000
-0.000	0.002	-0.001	14.198	34.408	32.476	16.975	-0.004	0.000	-0.001	0.002
-0.003	-0.000	0.001	11.148	35.920	14.279	15.758	-0.003	-0.001	0.002	-0.001
0.000	0.000	-0.003	3.154	18.302	8.259	5.520	-0.001	0.002	-0.001	0.000
-0.000	-0.004	-0.003	0.005	-0.001	0.001	-0.000	0.002	-0.001	0.002	-0.000
-0.002	0.001	-0.002	0.005	0.000	-0.000	-0.005	-0.001	-0.005	0.006	0.000

(<=0g) **(>=100g)**

Figure 2.13: A flat-bottomed plate placed on 4x4 grid. The plate consists of a paper plate affixed on a circle-shaped piece of glass with 19 cm diameter. The actual total weight is 260 g while the measured total weight is 259.6 g and the standard deviation among the footprint tiles is 12.44 g.

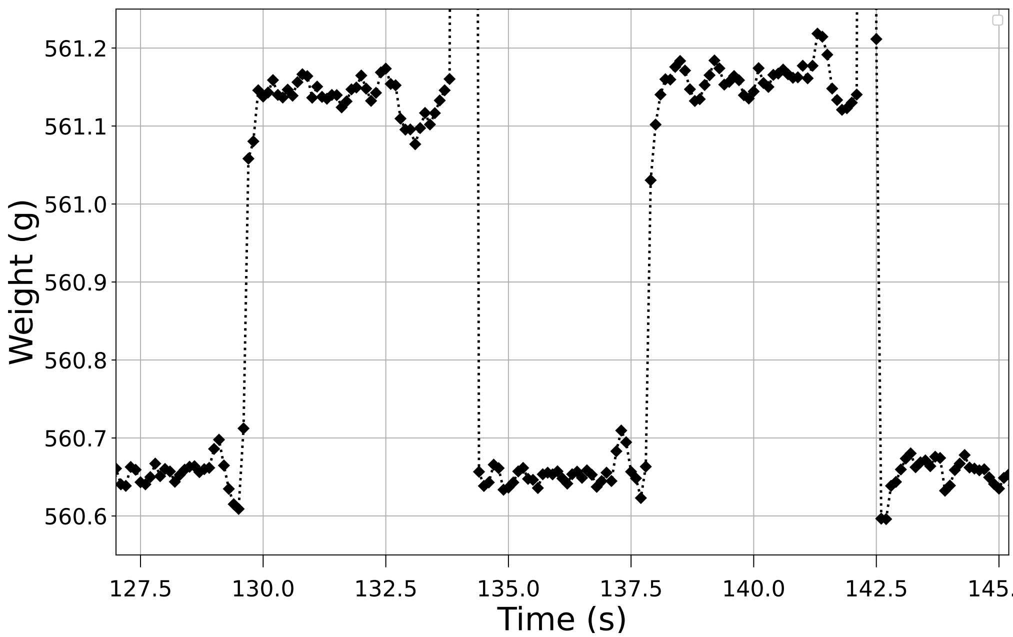

Figure 2.14: A 0.5 g calibration weight is dropped on and picked up from a plate that has a total weight of 560 g.

piece of glass. The 0.5 g calibration weight is smaller than the assumed minimum weight to be detected (i.e., one gram). Another calibration weight of 300 g was put on the paper plate to mimic an amount of food. The total weight was around 560 g. Fig. 2.14 shows the signal produced when the 0.5 g calibration weight was placed on the plate and picked up from it. The SNR was 40.2, which indicates the ability of this design to detect if a peanut was removed from the plate.

2.4 Discussion

This chapter described a novel method to build a force mapping surface using a grid of load cells. Tiles were attached to the tops of load cells to form a 2D weight sensing surface surface that can measure the weights and locations of objects placed upon it. The challenge in building this device is that load cells deflect only a fraction of a millimeter from zero to full load, and thus the tops of surface tiles must be precisely aligned vertically. This chapter described an inversion technique to minimize the deviations among the tops of tiles. Although a dining table application was presented for eating monitoring applications, this technique could be used to build this type of surface for other applications as well.

The results show high accuracy for weight detection, i.e., 99.97±0.1%. Such excellent accuracy agrees with the conclusion in [219] that rigid force sensors should be used to produce accurate weight measurements. Unlike the work in [135], which used four load cells at the corners of a table, this work has an accurate detection of position and weight because of the grid design that can be customized by using more load cells per unit area.

Even weight distribution among multiple tiles is difficult to achieve for a number of reasons: first, tops of tiles need to be perfectly flat, and aligned vertically; second, bottom of an object needs to be solid and perfectly flat; third, object center of mass needs to exactly be at the center; fourth, all load cells in a grid need to translate a change in mechanical deflection into an identical change in their output electrical voltage signal. The fourth point implies two conditions: mechanical and electrical. Mechanically, all load cells need to have exactly the same deflection distance from no load to the full load at the rated capacity. If an object is placed on the force mapping surface, the resulting mechanical deflection must be perfectly consistent among all load cells on which the object rests. Electrically, all load cells must produce the exact same voltage signal as a response to a specific change in the applied load. For these reasons, sensels under footprints show different measurements as shown in Fig. 2.8c. Nevertheless, the inversion technique helped in producing spatial information that represents shapes of object footprints. If higher resolution for spatial information is required for an application then smaller dimension load cells with higher sensitivity should be used.

The cost of the hardware system is dependent to the size of the active sensing area. The hardware presented in this dissertation is for 7×11 grid of load cells. While the total cost of building the hardware was about $5,000, the cost is expected to decrease if the design is mass-produced.

Chapter 3

Pilot Experiment

This chapter describes a pilot experiment after building the hardware and obtaining results showing that the instrument is capable of the detection of small weight changes on the dishware placed on it. This chapter describes an algorithm to track weight profiles of three food containers placed on the dining table. It also describes data collection of a pilot study that involved recruiting 11 human subjects who were video recorded during eating a meal on the custom-built dining table.

3.1 Consumption Event Detection

The detection process starts by computing the zero offset (tare) value for each cell. Then for each frame, all measurements are converted into meaningful values in grams to produce an image of weights. Each image frame is processed to segment food containers using geometric information of their footprints. The sum of weights under each food container is saved in a weight profile array. The weight profile for each food container is fed into an algorithm to detect eating events.

3.1.1 Geometrical Descriptor Segmentation

Each frame of load cell measurements is segmented to identify the locations of food containers using geometric knowledge of their footprints. For the pilot experiment, we used the plate, bowl and cup shown in Fig. 2.8b. Each was modeled by a template containing a circular shape of the expected size. The plate is searched for first, followed by the bowl, with the cup last. The group of cells identified for each object are combined to obtain the current total weight of the container.

The weight of each container over time is analyzed for consumption events. Note that this analysis occurs in parallel and thus actions involving consumption from multiple containers can be detected simultaneously.

The output of this segmentation are three groups of cells representing footprints of food containers. The sum of each group is the weight of the corresponding container. Each container has a weight profile array that represents the total weight of that container at every sampled frame. This signal is fed into a bite detection algorithm.

3.1.1.1 Detailed Segmentation Algorithm

For every frame, the image of weights is converted into a binary image using 0.5 g as a threshold. The binary image is searched for cells surrounded by true-valued neighbors. A true-valued cell with eight true-valued neighbors is likely to be under the plate. This cell is considered for sub-cell resolution search. The center of the plate is moved inside this cell with 10 cm sub-cell resolution step size. At every move, the complete grid is searched for any whole or partial cell exists inside the diameter of the plate. The search stops at the position at which a maximum number of cells touching the plate footprint was found. This number is expected to be in the range between the minimum and maximum possible number of cells that can fit inside circle area of the plate. If this criteria is not met then another true-valued cell with eight true-valued neighbors is searched for again and the sub-cell resolution search is repeated. The process is repeated for the bowl and cup after finding the position of the plate considering lower numbers of true-valued neighbors of a true-valued cell.

A number of steps are followed to test if a true-valued cell is touching container footprint. First, cells are excluded if the distance between their centers and the center of container (CC) is greater than the container radius (CR) plus half the cell diagonal (CD), which is 36.06 mm for the size of our grid tile. Second, a cell is considered inside the container footprint area if the distance between CC and the cell center or any of its four corners is less than $CR + CD$. Third, if a cell was not excluded by the first step and was not included by the second step then it might be touching the container footprint from a side of the cell tile. The cell side is determined by the angle value between CC and the cell center using arc tangent. If the angle is, for example, between 45° and 135° from the perspective of the cell then it is likely touching the container footprint from the upper side of the cell tile. In this case, the upper side is searched with a sub-cell resolution. The cell is included if any point on the side makes a distance that is less than $CR + CD$.

3.1.2 Bite Detection Algorithm

Consumption events are detected by identifying periods of time before and after food or beverage is removed from the table and calculating the respective change in weight of the container. At each time step, the stability of container weight is calculated by analyzing a window of the most recent five total weight measurements. If the standard deviation of these weights is above 0.5 g, it is assumed the subject is interacting with the table or container and thus a stable weight is not available. A basic event can be detected as the difference in weight between two successive stable periods. If the weight decrease is > 0.5 g and < 40 g, then a consumption event is detected (threshold values selected based upon 20,542 bites analyzed in [127]). The type of consumption (food or beverage) is determined based upon which container was used (e.g., the cup is assumed to contain beverage). If the weight increases, i.e., something has been added to a container, then the previous three stable weights are analyzed as a sequence. For example, this can happen when a subject picks up a mass of food, ingests a portion of it, and returns the remainder to the container. If the difference between the first and third stable periods is >0.5 g and <40 g, then a consumption event is detected. If the decrease is between 1 g and 6 g and can be associated with an increase in the same range, it is assumed that a utensil was lifted from the container and then returned to it. Filtering these events helps reduce false positive detections of consumption.

The bite detection algorithm (Algorithm 1) uses two main inputs: Weight Profile array (WP) and Frame Number (FN). Other input variables are also output that hold states and historical statistics of previous frames. These variables are Moving STandard Deviation (MSTD), CHange OCcurred (CHOC), Utensil PLaced (UPL), Mass Bite Picked Up (MBPU), and DeTected WeighT (DTWT). At every frame, the algorithm is executed for every food container.

The algorithm extracts two quantities from the WP; the moving standard deviation (MSTD), and the WeighT DiFference (WTDF). The MSTD is compared against two hard-coded thresholds to detect whether or not measurements are stable. While the measurements of the current container are unstable, i.e., MSTD is greater than a threshold for change (STD_TH4Ch), the variable CHOC is updated with the latest frame number. Once measurements are stable, i.e., MSTD is less than a threshold for stability (STD_TH4Stb) and if CHOC holds a non-zero value, WTDF is computed as the Last Stable Weight (LSW) subtracted from the Weight After CHange (WACH). The LSW is the

Algorithm 1: Bite Detection

```
Input: WP, FN, MSTD, CHOC, UPL, MBPU, DTWT
Output: MSTD, CHOC, UPL, MBPU, DTWT
MSTD[FN] = std({WP[FN-0], ... ,WP[FN-4]})
if MSTD[FN] > STD_TH4Ch then
    CHOC = FN
end
if CHOC > 0 and MSTD[FN] < STD_TH4Stb then
    if UPL > 0 and MSUPD() then
        WTDF = WACH() - LSW()
        if WTDF < -MWD then
            if UPL-MWU<=|WTDF|<=UPL+MWU then
                UPL = false
                CHOC = 0
                return
            end
        end
    end
    if MSBPD() then
        WTDF = WACH() - LSW()
        CHOC = 0
        if -MWD < WTDF < MWD then
            return
        end
        if WTDF > 0 then
            if WTDF >= MBT then
                if MBPU > 0 then
                    MFC = DTWT[MBPU] + WTDF
                    if MFC < -MWD then
                        DTWT[MBPU] = MFC
                        MBPU = 0
                    else
                        MBPU = 0
                    end
                end
            else
                if minWoU < WTDF < maxWoU then
                    UPL = WTDF
                end
            end
        else
            DTWT[FN] = WTDF
            UPL = false
            if WTDF <= -MBT then
                MBPU = FN
            end
        end
    end
end
```

median of the last stable window that is searched for backwards in the WP. The WACH is either median or average of a stable window that takes place after measurements stabilize. If WTDF is considered noise if it is smaller than Minimum Weight to be Detected (MWD). The WTDF is then used in two main conditional tests.

In the first conditional test, the algorithm checks for utensil pick up if previously placed on the current food container (i.e., UPL > 0) and if Measurements are Stable for Utensil Pick up Detection (MSUPD). UPL is cleared if WTDF is similar to that of the utensil previously placed (stored in UPL) on the current container within a Margin of Weight of Utensil ($\pm$MWU). This test reduces false positives.

The second conditional test classifies events based on whether WTDF is an addition or reduction after the Measurements become Stable for Bite Pick up Detection (MSBPD). If MBPU was previously detected and WTDF is a weight addition that is greater than Mass Bite Threshold (MBT) then DTWT—indexed by MBPU—is updated with the actual amount of Mass Food Consumed (MFC), otherwise this event is ignored. If DTWT is a weight reduction then it is a bite detection; FN is saved in MBPU if DTWT was a mass bite (i.e., WTDF>MBT).

3.1.3 Parameters Tuning

The threshold for change (STD_TH4Ch) and the threshold for stability (STD_TH4Stb) are dependent on the characteristics of the load cells used; they were set to 0.5 g and 0.15 g, respectively, based on the load cell used in this work. The window size was set to two samples when computing MSUPD and WACH for utensil pick up detection. For all other computations, window size was set to five samples. MBT was set to 40 g. MWD and MWU were set to 0.5 g. Minimum and maximum weights of utensils, i.e., minWoU and maxWoU, are dependent on the type of utensils used. They were set to one and six grams, respectively. Fig. 3.1 shows a zoomed in signal when a bite was detected.

3.2 Eating experiment

Eleven human subjects were video recorded for ground truth while eating a meal on this dining table. This study was approved by the Institutional Review Board (IRB) at Clemson University (Clemson IRB number: IRB2021-0462) and all subjects signed a written informed consent.

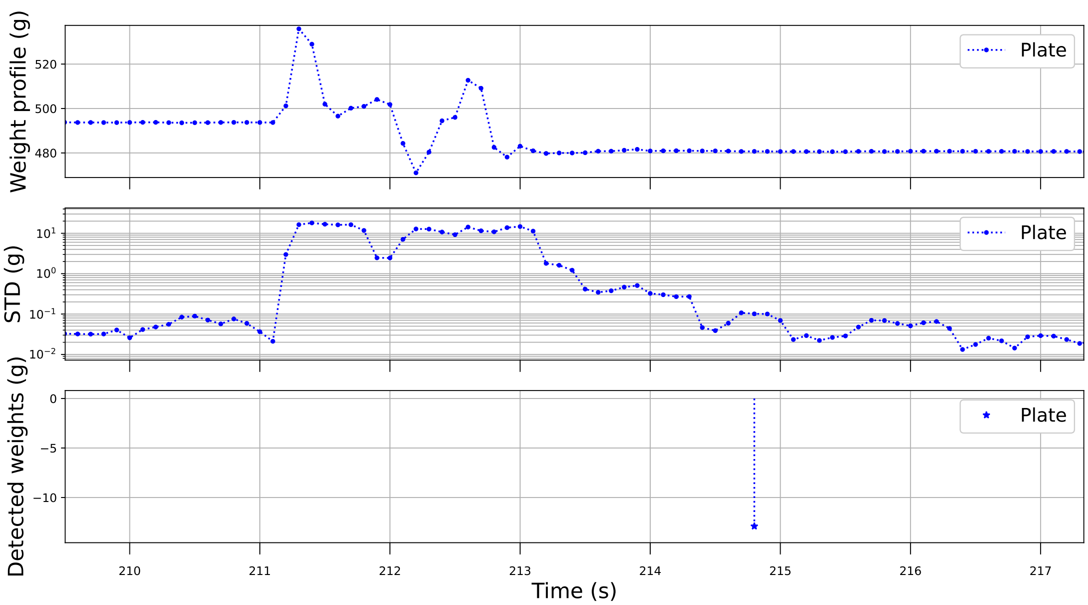

Figure 3.1: A moving window with size of five samples on the weight profile signal is used to detect stable periods. When a user interacts with a food container sitting on the grid surface, the standard deviation of the moving window goes higher than 0.5 g, e.g., t=211.2, indicating instability and an end of a stable period. After a bite is picked up, the standard deviation starts to decrease until it goes below 0.15 g, e.g., t=114.4, indicating the beginning of a stable period. If this stability continues for five samples, e.g., t=114.8, the algorithm computes the weight difference between the medians of this stable period and the previous one. The algorithm issues a detection moment if the weight difference is larger than 0.5 g.

(a) (b)

Figure 3.2: The laboratory where the experiments were conducted. (a) A front room where each participant first sign consents and where the researcher waits until the participant is done eating their meal. (b) A back room has the custom-built dining table and a desk on which the participant prepares and heat their food using the microwave shown.

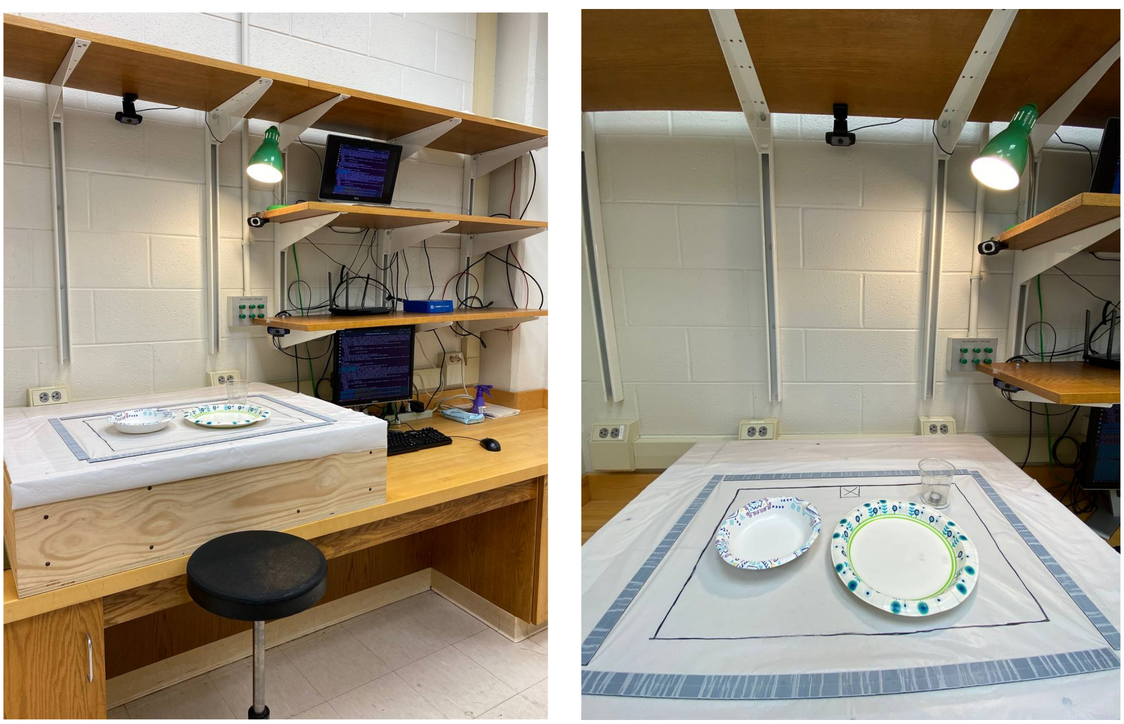

(a) (b)

Figure 3.3: The laboratory where the experiments were conducted. (a) The custom-built dining table is sitting on a bench. Three webcams are mounted to video record participants at different angles. A router connects the dining table to computers. (b) This is how it looks like to participants when they sit for eating a meal.

IRB permission, consent forms, and recruitment fliers are shown in Appendix B.1. All recordings took place in laboratory conditions. Subjects were 20 to 30 years old of age, and their average body mass index (BMI) was 25±5 kg/m^2.

Each subject was given a new disposable paper plate, paper bowl, plastic cup, and plastic utensils (fork, knife, and spoon). The paper plate and bowl, and the plastic cup were placed on flat-bottomed bases. Subjects were instructed not to remove the plate and the bowl but can move them away or closer to them. Food options consisted of frozen meals and refrigerated salad sold in sealed boxes commercially available in grocery stores and supermarkets. This was easier for laboratory conditions, supply, and COVID-19 conditions. Subjects chose to eat Alfredo pasta with chicken and broccoli, chicken fried rice, Caesar salad with chicken, and Santa Fe style salad with chicken. Subjects prepared their own salads and heated food in a microwave oven in the lab. Water was given to all subjects as a beverage.

Fig. 3.2 and 3.3 show the laboratory environment where the participants were recorded. When a participant arrives, they get into a from room where they sit on a desk to read and sign consents. The researcher waits in this room while the participant eats. Another room in the back has the custom-built dining table and a desk on which the participant prepares and heat food using a microwave. Three webcams are mounted at different positions and angles to video record participants.

Accuracy in the detection of consumption events was measured using methods adapted from [54]. The actual time of consumption (ground truth) was defined as the moment when food (solid food or drink) was put in mouth. Therefore, for the evaluation of consumption event detection, data were labeled using the recorded videos. A true positive occurs whenever our algorithm detects an event in the window from the previous ground truth to the next ground truth event. This window is necessary because food pickup occurs before ingestion; thus, the table detects the event prior to actual consumption. A false positive occurs whenever our algorithm detects an event not associated with a ground truth event within the window of time from the previous detection.

3.3 Procedures to Follow by Researcher and Subjects

Here are the steps followed while recording participants to eating on the dining table. The aim of documenting these steps is to make it easier for future researchers to conduct the same experiments for data collection. See Appendix A.3 for how videos and data were recorded on a Linux machine.

Lab needs to be prepared for cleaned for healthy eating environment. Supplies provided for these experiments include paper plate and bowl, plastic cup, wrapped plastic utensils, napkins, plastic foil to cover the dining table, and velcro fasteners for the plastic cup. Water was purchased in bulk and kept refrigerated in the lab. Foods were ordered based on participants' preferences. For the experiments conducted in this research, food options consisted of frozen meals and refrigerated salad sold in sealed boxes commercially available in grocery stores and supermarkets. This was easier for laboratory conditions, supply, and COVID-19 conditions. A microwave was provided in the lab for preparing frozen foods.

3.3.1 For the Researcher

3.3.1.1 Planning for an Experiment

- When a participant emails the researcher informing an interest to participating in the study, they should be replied back to set an appointment for the experiment and to ask them what type of frozen food and refrigerated salad they would like to eat.
- The foods requested by participants need to be ready before experiments and must be kept in an appropriate storage either in a freezer for frozen foods or a refrigerator for fresh salad.

3.3.1.2 Before a participant comes

- Make sure face mask and gloves are on.
- Sanitize all surfaces and touchable objects.
- Make laptops ready for recording.
- Check functionality and readiness of the dining table.
- Make sure cameras have correct numbers on computers. This is for consistency in numbering cameras which are mounted at different angles and positions.
- Prepare Velcro for the cup base.
- Frozen food is in a freezer and salad is in a refrigerator.

- Place plate, cup, and bowl bases on the dining table surface to explain to participants how food containers are assumed to be placed on the surface. Food containers need to be removed before starting the actual meal recording and replaced to the surface after at least 5 sec of the beginning of recording. This beginning of the data with no objects placed on the surface are used to set a zero reference for each grid cell.

3.3.1.3 After a participant arrives

- Take consents.
- Ask participant for their weight and height.
- Show participant how to eat on the table and what to avoid doing while eating (avoid touching sensing area, researcher will refill the water cup, do not lean on the sensing area)
- Tell participants to not take food containers off the dining table surface during or after eating.

3.3.1.4 After a participant leaves

- Throw away used dishware.
- Sanitize surfaces and all touchable objects.
- Change the table plastic foil cover.
- Check calibration.
- Prepare for next participants by checking supplies, e.g., water, dishware, cups, napkins, and wrapped utensils, etc.

3.3.2 For the Participant

3.3.2.1 Once a participant arrives

- Sign consent.
- Provide weight and height.
- Reheat food using the in-lab microwave.
- Go through steps of how to empty food into dishware.

- See how to grab the plastic cup.
- Stick a Velcro to the center of outer bottom of a new plastic cup. Place this cup into its base and gently twist it to make sure velcro fasteners stick to each other.
- Use a new pack of plastic utensils.
- Empty food into new food containers (a plate and a bowl) while these new containers are on a different table. This is done to avoid spillage on the smart dining table.
- Inform the researcher that food is ready so that the researcher can start recording data and video.
- When informed, take food containers one at a time and place them into their bases on the smart dining table.
- Ask the researcher to fill in the water cup.
- Inform the researcher before start eating.
- Start eating.

3.3.2.2 During eating

- Ask the researcher for water refill.
- Put unused utensils on the side outside the sensitive area. Do not place utensils on the active area.

3.3.2.3 After eating

- Inform the researcher that you are done.
- Do not take dishware off the smart dining table until the researcher tells you to do so.

3.4 Results

Fig. 3.4b shows a plate, cup, and bowl resting on the table surface. Fig. 3.4b shows a visualization of the segmentation output for a single frame. The total weight of sensel measurements

(a)

-0.00	0.05	0.02	0.09	-0.02	0.00	0.00	0.00	-0.06	232.08	232.08
-0.01	306.08	306.08	-0.03	0.09	-0.05	-0.09	-0.11	-0.03	232.08	232.08
-0.09	306.08	306.08	306.08	-0.02	532.41	532.41	532.41	0.04	0.08	-0.10
0.09	306.08	306.08	0.46	532.41	532.41	532.41	532.41	0.11	0.08	-0.20
0.04	0.13	0.07	-0.00	532.41	532.41	532.41	532.41	532.41	-0.02	-0.11
0.04	0.02	-0.06	-0.06	532.41	532.41	532.41	532.41	-0.08	-0.32	-0.27
0.04	0.03	0.04	0.03	0.00	532.41	532.41	0.49	-0.04	-0.08	-0.12

(<=0g) (>=100g)

(b)

Figure 3.4: Visualization of weights of food containers setting on the grid. (a) Food containers sitting on the table surface. (b) A visualization of the total weight measurements produced by the segmentation algorithm.

under each food container is summed up for each frame. The image of weights shows 532.41 g on the plate, 232.08 g on the cup, and 306.08 g on the bowl. The total of weights for each food container is tracked over time to form a weight profile that is analyzed to detect eating events, to measure food consumption in unit of weight, and to find multiple statistics of interest such as eating rate, average bite size, and meal duration.

Fig. 3.5a shows the weight profiles of the meal shown in Fig. 3.4. During this meal, a subject ate 259 g of chicken fried rice (Lean Cuisine), 211 g of deluxe caesar salad with chicken (Simply Fresh Salads) and drank 350 ml of water. The complete meal duration was about 16.5 minutes. The top window shows plots of weights of the three containers over time; the plots are colored in blue, magenta, and green for the plate, cup, and bowl, respectively. The weight profiles can be seen decreasing as foods and beverage are being consumed. The bottom window shows the detection events and their weights for each food container. Negative values refer to the weight reduction in the weight profiles. The Y-axes shows weight in grams and the X-axes shows time in seconds for both windows. The bottom window shows 67 detected bites whereas there were 64 actual bites. Thus, the F1 score for this meal was 0.977. An interesting information shown in the top window is the mixing of food intakes; subject 4 switched between the entree food and salad and drank water over nine bites. Unlike subject 4, subject 6, shown in Fig. 3.5b, liked to finish the salad first then switched to eating the entree food , and consumed water over four bites which were less in counts but larger in size than those consumed by subject 4. The cup was refilled with water only once at time 1300 sec for subject 4 and twice at 360 sec and 610 sec for subject 6.

Fig. 3.6 shows examples of a short and long meals. Fig. 3.6a is a short meal in which 34 total actual bites were consumed over 7.2 minutes. In this meal, subject 8 ate larger bites with average bite size of 17 gpb (grams per bite) than subject 9 whose average bite size was 5.4 gpb. Weight profile of subject 9 is shown in Fig. 3.6b. As illustrated by the blue weight profiles, subject 8 has a steeper slope compared to that of subject 9. The meal duration for the latter was 18.3 minutes and the number of actual bites were 103 out of which 99 were correctly detected.

Table 3.1 shows the results of the consumption detection algorithm. Subjects consumed a range of 13-48 bites from the plate, 11-43 bites from the bowl, and 3-11 drinks from the cup. The total number of ground truth intake events was 685 across the 11 subjects. F1-score for per subject was 0.91 to 1.0, and for per container was 0.97 for the plate and bowl, and 0.99 for the cup. The Average F1-score for the 11 subjects is 0.967%. The experiment demonstrates that this instrument

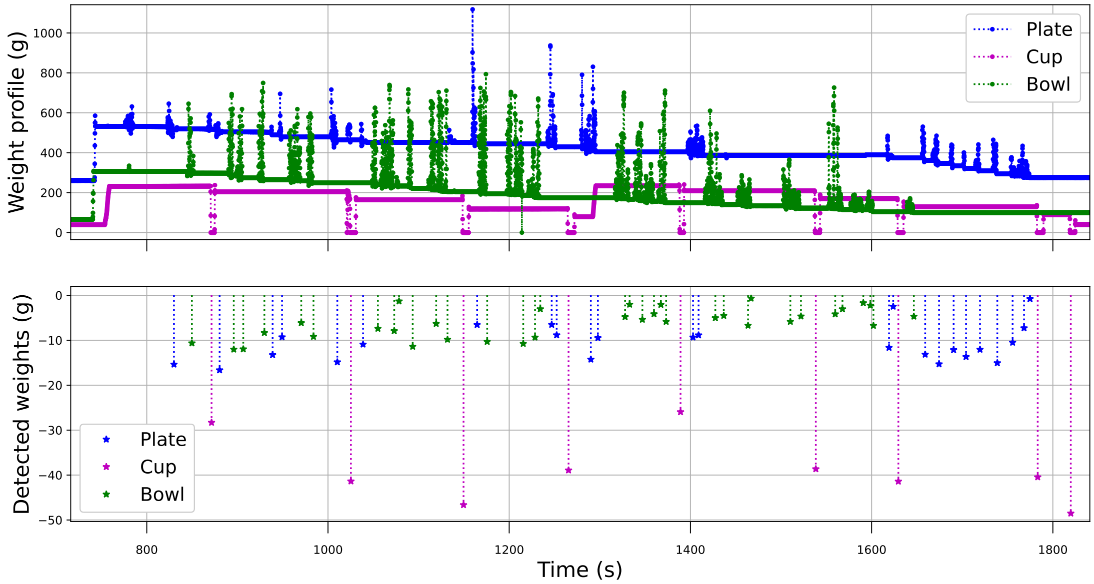

(a)

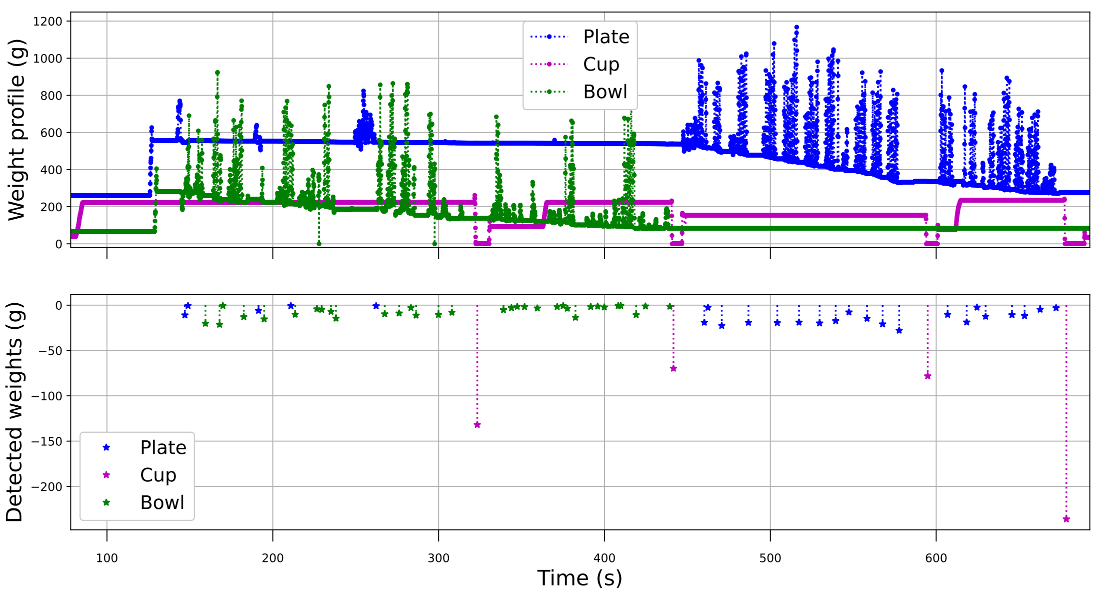

(b)

Figure 3.5: Examples of complete recording of meals. The upper plots depicts the weight profiles of the three food containers: plate, cup, and bowl. The lower plots show the times and weights of detected consumption events where the negative numbers refer to reduction in weight measurements. (a) Subject number 4. (b) Subject number 6. See Table B.1 in Appendix B.2 for food options each subject ate.

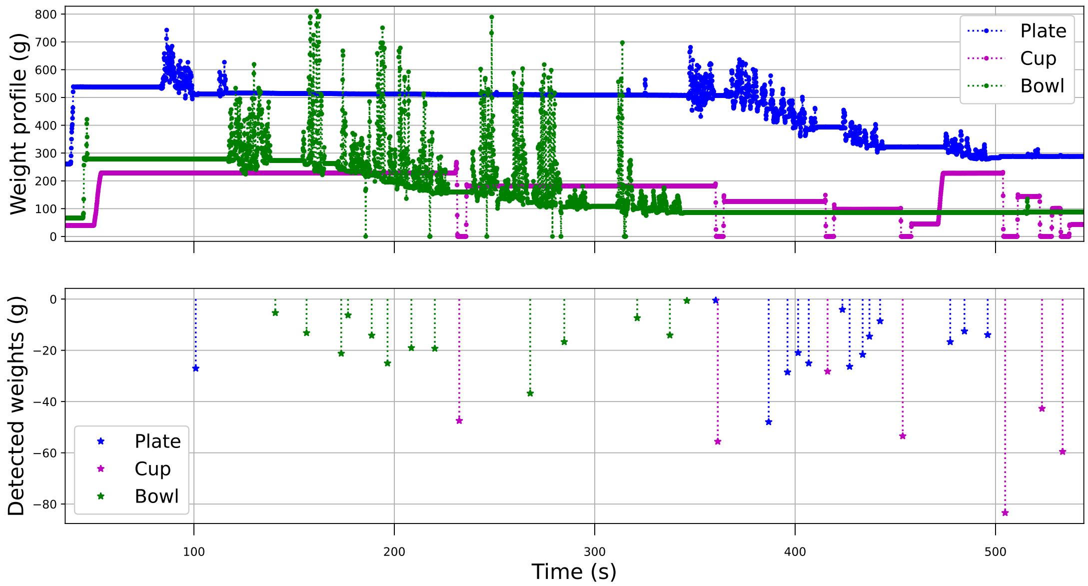

(a)

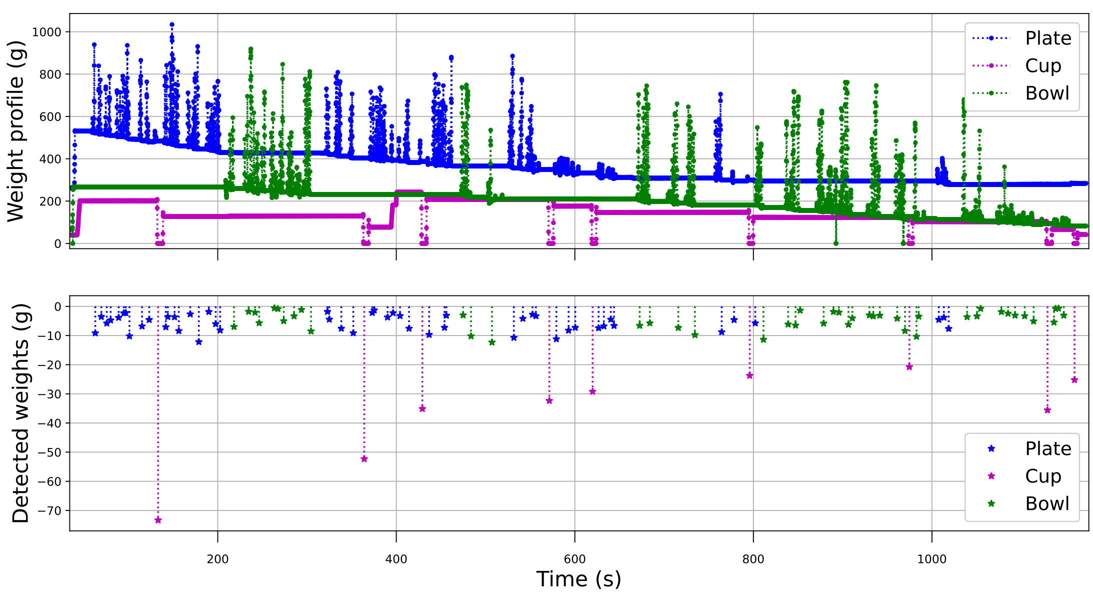

(b)

Figure 3.6: More examples of complete recording of meals. The upper plots depicts the weight profiles of the three food containers: plate, cup, and bowl. The lower plots show the times and weights of detected consumption events where the negative numbers refer to reduction in weight measurements. (a) Subject number 8. (b) Subject number 9. See Table B.1 in Appendix B.2 for food options each subject ate.

Table 3.1: System performance for bite detection of 11 human subjects eating on the dining table,

Subject		***Plate***	***Cup***	***Bowl***	***F1-Score***
1	TP	19	10	27	0.991
	FP	0	0	1	
	FN	0	0	0	
2	TP	19	5	41	1.0
	FP	0	0	0	
	FN	0	0	0	
3	TP	20	9	19	0.990
	FP	1	0	0	
	FN	0	0	0	
4	TP	22	9	33	0.977
	FP	2	0	1	
	FN	0	0	0	
5	TP	35	3	38	0.993
	FP	1	0	0	
	FN	0	0	0	
6	TP	17	4	31	0.912
	FP	6	0	2	
	FN	0	0	2	
7	TP	29	6	31	0.957
	FP	2	1	1	
	FN	1	0	1	
8	TP	13	7	11	0.912
	FP	1	0	2	
	FN	1	0	2	
9	TP	48	9	43	0.971
	FP	1	0	2	
	FN	0	0	3	
11	TP	21	11	28	0.984
	FP	1	0	1	
	FN	0	0	0	
13	TP	23	7	26	0.974
	FP	2	0	0	
	FN	0	0	1	

Figure 3.7: Snapshot of a subject during meal recording.

is capable of detecting and measuring individual consumption events during a meal.

The algorithm can, moreover, compute other interesting dietary assessments for the same 11 subjects as listed in Table 3.2. The data produced by the 2D grid of load cells can be used to find the eating rate for each food container. The table shows the eating rates which are computed as the number of seconds used for consuming food from a specific container divided by the number of bites picked up from the same container. Higher values of this measure, i.e., slow eating rate, can help reaching satiation with a reduced amount of energy intake as suggested by multiple studies [181]. Another useful measure our method can find is the bite size; smaller bite size and longer oral processing were found to help reduce energy intake [220]. The table shows the total consumption and the average bite size in grams for the food consumed from each container. Moreover, for each subject, the table shows the meal duration in minutes and the food to drink ratio, where the food is the sum of foods from the plate and bowl.

Table 3.2: Other dietary assessments computed by the smart dining table. Subjects 1-9, 11, 13

Subject		***Eating rate (spb)***	***total consumption (g)***	***Average bite size (g)***	***Food to drink ratio***	***Duration (min)***
1	Plate	38.6	245.6	12.9	0.94	12.7
	Cup	75.6	491.8	49.2		
	Bowl	16.1	214.4	7.7		
2	Plate	18.3	243.7	12.8	2.15	10.4
	Cup	124.4	223.7	44.7		
	Bowl	14.2	236.2	5.8		
3	Plate	24.3	291.8	13.9	1.20	12.3
	Cup	79.1	372.5	41.4		
	Bowl	37.8	154.7	8.1		
4	Plate	40.2	258.5	10.8	1.34	16.5
	Cup	107.6	350.3	38.9		
	Bowl	24	210.7	6.2		
5	Plate	9.6	289.2	8	2.17	13.5
	Cup	135	224.4	74.8		
	Bowl	12.2	196.9	5.2		
6	Plate	21.7	293	12.7	0.99	8.6
	Cup	93.8	515.9	129		
	Bowl	9.1	218.6	6.6		
7	Plate	22.4	272.7	8.8	2.62	11.5
	Cup	92.1	157.1	22.4		
	Bowl	20	139.2	4.3		
8	Plate	29.6	268.6	19.2	1.26	7.2
	Cup	45.9	370.5	52.9		
	Bowl	17.3	199.3	15.3		
9	Plate	19.9	278.1	5.7	1.48	18.3
	Cup	116.2	327.6	36.4		
	Bowl	21.1	205.6	4.6		
11	Plate	20.7	306.3	13.9	0.87	10.2
	Cup	56.7	582.6	53		
	Bowl	20	201.6	7		
13	Plate	18.5	262.5	10.5	0.86	8.1
	Cup	67.3	508.9	72.7		
	Bowl	15.7	173.8	6.7		

Fig. 3.7 shows a snapshot from a video recording of a subject eating a meal. The subject ate a cheese sandwich (220g) and green salad (217.9g). The subject picked up the sandwich from the plate at multiple moments. At some of these moments, there were partial bites. A partial bite is the consumption of part of a mass food such as a pizza, burger, or sandwich. During partial bites, a subject consumes multiple bites before returning the remaining of a mass food into the food container and hence there is no interaction of the table. As a result, the F1 score of the detection algorithm for the whole meal was 90%. The ground truth moments of the sandwich consumption were 17 out of which only 10 were correctly detected. On the other hand, all the ground truth moments of the salad (44 GT bites) and water (3 GT bites) consumption were detected correctly because there were interactions with the table for every salad or drink bite event.

3.5 Discussion

This chapter described pilot experiments involving 11 human subjects eating on the custom -built dining table. Each frame was segmented using geometric information of the food container footprints. The sum of cells under the segmented footprints was tracked over time to analyze weight profiles of each food container. A rule-based algorithm was developed to automatically detect consumption events using the weight profile of each food container.

The results agree with the suggestion in [127] for the use of 2D images of weights for better tracking of food containers placed on a dining table for eating monitoring. In that study, a tray holding multiple food containers was placed on a 1D weighing scale. When a person picked up food from one container then switched to another container or interacted with the tray, weight measurements could not stabilize. This problem significantly decreased accuracy in detecting consumption events. Mertes *et al.* reported the same problem when a plate with three compartments was embedded with three load cells to measure the weights of bites and to predict the compartment from which they were taken [129]. They found that measurements did not stabilize quickly enough when a subject picked up food from one compartment then took the next bite from a different compartment. Our novel 2D device overcomes these limitations.

There are a number of reasons for FNs. The algorithm fails to detect bites smaller than 0.5 g which is the defined threshold to filter out noise. Small bites are common at the end of meals when subjects try to pick up small food residues from food containers. The algorithm also fails in detecting bite pickups when a subject eats too fast preventing food containers to stabilize between bite pickup events although these cases are rare because the sampling rate is fast enough to capture most of the bite events. Such case of a FN happens due to the window size of the moving standard deviation. Reducing this size increases FPs, and increasing it slows down the detection and increase FNs. FPs can be triggered when moving food containers over the surface; this happens when the weight difference of a food container at different locations is larger than 0.5 g. FPs can also be triggered on a food container When food containers touch each other while a subject eats from one of them, a FP can be triggered on the other container.

This device can provide the following statistics for studying eating behavior: total amount consumed (grams), duration of eating episode (minutes), eating rate (grams or bites per second), bite size (grams per bolus), food-to-beverage ratio (percentage), and behavior count (food intake and beverage intake counts). These types of measurements can assist with the study of anorectic drugs by quantifying their impact [104]. They can also objectively quantify the effect of behavior manipulations such as slowing eating [88, 208] or taking smaller sized bites. The measurements can be made with no extra effort on the part of the user other than they eat at the instrumented table, thus promoting regular daily use [83, 157]. The automation provided by the device reduces cognitive load for tracking eating behavior which is also important for promoting regular daily use [206].

Chapter 4

Comparison of Detection Methods

This chapter compares the performance of the new tool developed in this study against others in the literature. Methods are briefly reviewed along with the hardware used to collect the data. An objective process for comparing these tools will be described. The goal of this chapter is to evaluate the improvement on the detection of eating events afforded by our new tool.

4.1 Related works

Several previous works have experimented on the detection of individual consumption events using table scales. A table scale contains one load cell and measures all the weight placed on top of it. Typically, the table scale is set on top of a table surface, and then a tray is placed on top of the table scale to hold dishware. Foods and beverages are placed into the dishware. The weight on the table scale is measured over time and can be analyzed to detect when individual consumption events occur. Table 4.1 lists three state-of-the-art methods described in the literature that have achieved the best performance on this problem. The following provides a brief description of each method.

Table 4.1: List of bite-detection methods to be compared

Author	***Algorithm***	***Instrument***
Mattfeld *et al.* 2016 [127]	rule-based	a dining table embedded with weighing scales
Mertes *et al.* 2019 [129]	random forest classifier	a three compartment smart plate embedded with three load cells
Papapanagiotou *et al.* 2018 [144]	context-free grammar (CFG)	the Mandometer, version 5
This work	rule-based	7×11 grid of load cells embedded under the surface of a custom-built dining table

Mattfeld *et al.* embedded a weighing scale onto a dining table to continuously measure the weight of a food tray that carries food and beverage [127]. They developed a rule based algorithm to detect bite events and size. Because there is only one weight profile for the whole tray, they used defined thresholds to differentiate among different types of bite events. They defined that a single bite — shown in Fig. 4.1a— needs to be in the range $3\sigma_{\text{noise}}$ to 30 g, where σ_{noise} is the scale noise (0.29 g) and was experimentally determined. It is also required that a single bite must not be followed by an increase beyond the scale noise, i.e., $w_b - w_c \leq 3 * \sigma_{\text{noise}}$ g, in weight profile after a preceding unstable period; this was considered to reduce FPs that would result when a subject picks up a napkin or utensil and returns it back to the tray. Fig. 4.1b shows a mass bite which is defined to be a reduction in the range 100 to 300 g followed by an increase where the difference in weight before and after this sequence must be in the range $3\sigma_{\text{noise}}$ to 30 g. A decease in the weight profile in the range of 80 to 550 g followed by an increase is assumed to be a bite of drink which needs to be in the range of $3\sigma_{\text{noise}}$ to 80 g as the resulting difference between before and after this sequence. A bite of drink is depicted in Fig. 4.1c. Fig. 4.1d shows an example of a meal that has the tree types of bites: a drink bite at A-B, mass bites at C-D and E-F, and single bites at G, L, and M.

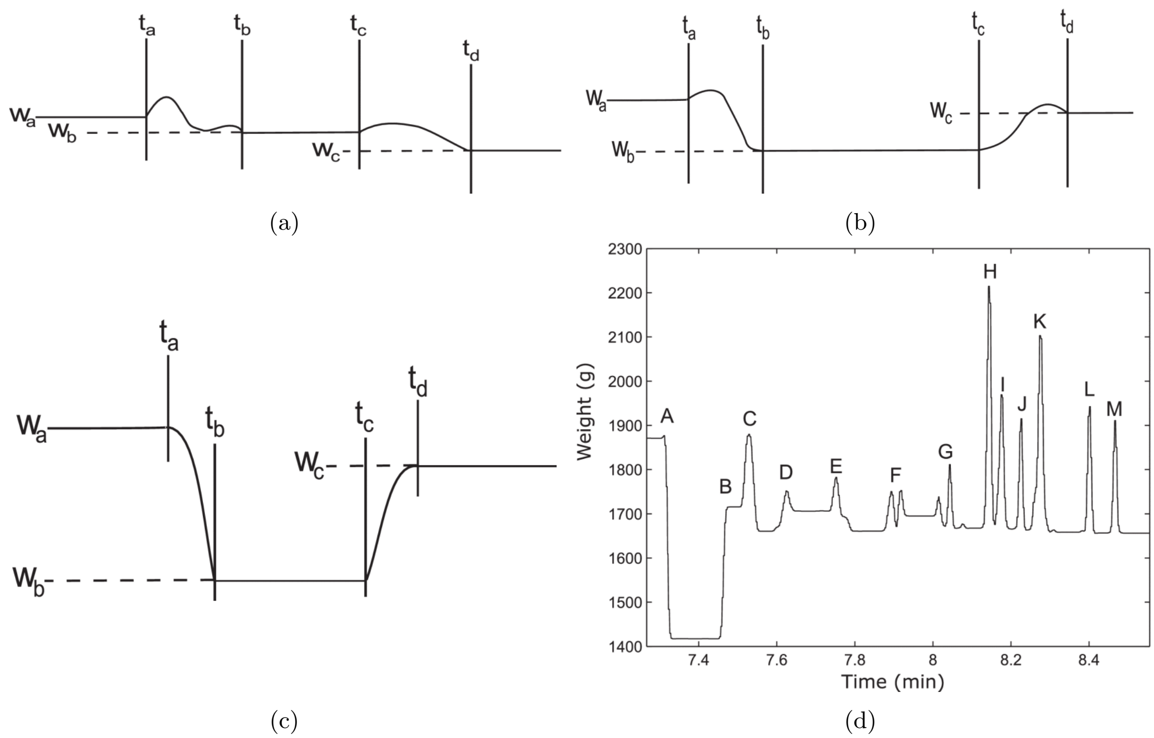

Figure 4.1: Rule-based algorithm developed by [127]. (a) A single bite needs to be in the range $3 * \sigma_{\text{noise}} \leq w_a - w_b \leq 30$ g, where σ_{noise} is the scale noise (0.29 g). This single bite event must not be followed by an increase beyond the scale noise, i.e., $w_b - w_c \leq 3 * \sigma_{\text{noise}}$ g. (b) and (c) A sequence of weight decrease followed by an increase indicates either a mass or a drink bite. A mass bite is assumed to have a reduction in the range 100 to 300 g whereas a drink bite is assumed to have a reduction in the range 80 to 550 g. A resulting difference $W_a - W_c$ is expected to be in the range $3 * \sigma_{\text{noise}}$ to 30 g for a mass bite, and in the range $3\sigma_{\text{noise}}$ to 80 g to a drink bite. (d) A weight profile for a meal showing the three bite types: A-B is a drink bite; C-D and E-F are mass bites; and single bites at G, L, and M.

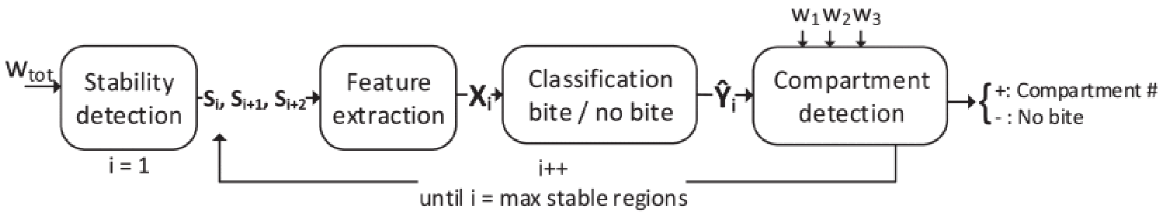

Figure 4.2: The detection pipeline by [129]. Stable periods are identified by processing the weight signal to make feature vectors that combines information of three consecutive stable periods. Identification of compartments from which a bite was picked up, is detected after a positive classification of a bite event by the random forest model.

Mertes *et al.* used three load cells embedded under a three compartments plate to detect bite size and what compartment a bite was picked up from [128, 129]. Measurements from the three load cells are summed up in a weight profile for bite detection. Bite detection is centered around the weight difference between two consecutive stable periods. Stability is detected when the standard deviation of a moving window goes below 3 g. One second window size was used. A random forest classifier was trained with feature vectors $\boldsymbol{X_i}$ which combine information about three consecutive stable regions

$$\boldsymbol{X_i} = [(W_i - W_{i+1}), (W_i - W_{i+2}), (T2_i - T1_{i+1}), (T2_i - T1_{i+2})] \tag{4.1}$$

where W_i is the mean weight value of a stable period, and $T1_i$ and $T2_i$ are the respective start and stop moments of a stable period, respectively. Thus, feature vectors give the model ability to look ahead to detect single bites or partial bites that involves returning remaining of a mass bite. Fig. 4.2 shows the detection pipeline in their study.

Papapanagiotou *et al.* used context-free grammar (CFG) to model meals as strings [144]. They used a plate scale—called the Mandometer— to calculate the cumulative food intake (CFI) curve of a user's eating behavior [145, 146]. The actual weight profile signal of the plate is pre-processed to remove jitter, i.e., any sudden, non-persisting change that is ≤ 1 g. Next, plate weight is subtracted from the total weight, and negative values are set to zero. This is followed by characterizing regions as either stable or unstable using the weighing scale margin of error. After pre-processing, the signal is segmented into three types of intervals as terminal symbols for the CFG: rising (r), decreasing (d), and bite (b) intervals. The amount of weight decrease makes the difference between the d and b intervals; b-interval is assigned to regions with 20 g weight reduction whereas

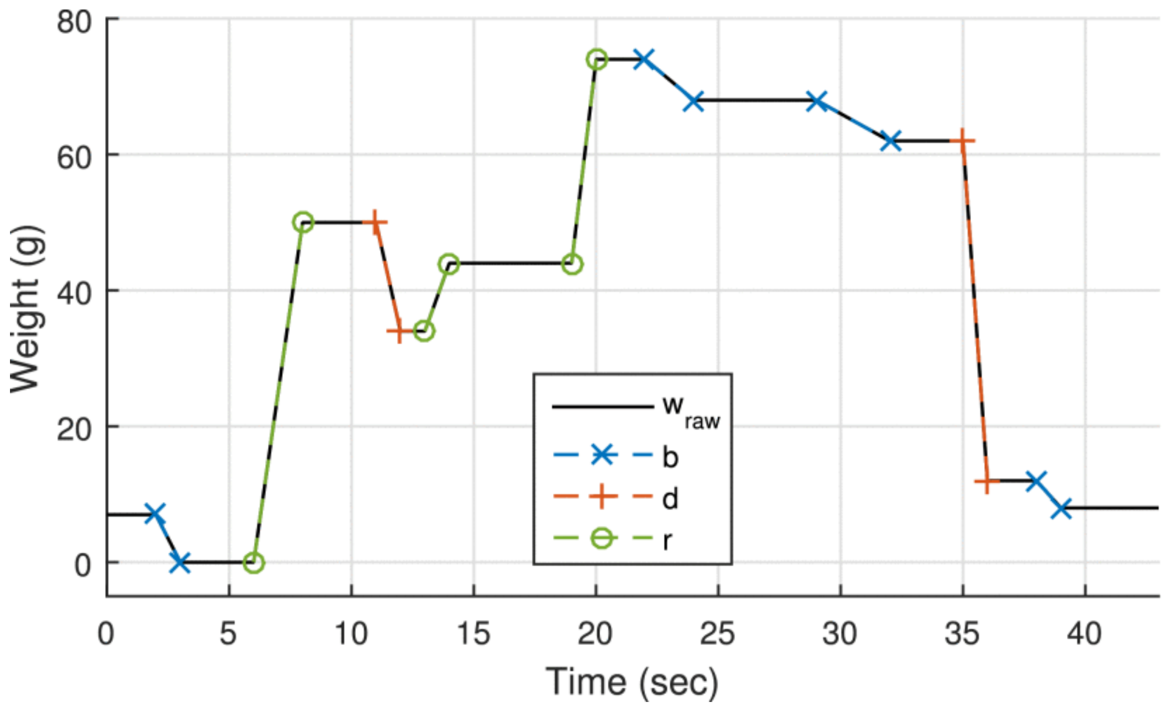

Figure 4.3: An artificial weight profile for eating a meal on on a weighing scale [144]. Weight reductions that are $\leq$ 20g are plotted with dashed blue line marked with (x) whereas weight reductions of $>$ 20g are plotted in orange dashed lines marked with (+). Dashed light green line marked with (O) shows the moments of risings in weight.

d-intervals are assigned to regions with higher weight reductions. Fig. 4.3 shows an artificial weight profile for eating a meal on a weighing scale.

4.2 Dataset

More data were collected for more validation of the algorithm developed in this work and for the performance comparison of the algorithms discussed above which are summarized in Table 4.1. Table 4.2 describes the dataset. The total number of human subjects recorded is 32; nine females and 23 males. The total number of ground truth (GT) moments is 1,836, and the total meal duration is 376 minutes.

Table 4.2: Dataset description

	minimum	***average (±STD)***	***maximum***
BMI (kg/m^2)	16.5	25.6 (±6)	47.8
age (years)	20	25.9 (±5.5)	40
meal duration (minutes)	5.2	11.7 (±4.2)	23.6
ground truth moments	29	57.4 (±19.4)	103

4.3 Data Preparation

Measurements for all grid cells were converted into grams and were summed up for every frame to make one dimension weight measurements because other methods run on only one dimension weight profiles. Ground truth moments were aggregated for all food containers. This was done to evaluate the algorithms developed by Mattfeld *et al.* [127] and Papapanagiotou *et al.* [144]. We are thankful to the first authors of these two works who agreed to help in the evaluation process for the comparison. The author of [127] provided source code which we ran with one modification, namely the sampling rate was set to 10 Hz. The author of [144] was contacted and agreed to run our data through their code; they provided back to us the results of when intake events were detected.

The algorithm of [144] was evaluated by the first author. Their algorithm requires ground truth labels for bite size, artifacts, and weight and moments of food additions. Because this information is not available in our dataset, the evaluation was done using the best training values from their dataset. The following pre-processing steps were applied on each recording before applying the algorithm: application of morphological image opening operator on the graph of the signal, using a structure element of 21 samples (about 2 seconds); application of morphological image closing operator on the graph of the signal, using a structure element of 21 samples (about 2 seconds); re-sampling from 10 to 1 Hz (using MATLAB's resample()); lastly, weight measurements were rounded to nearest integers to get to 1 g of weight measurement accuracy.

We re-implemented the method proposed in [129] to evaluate its performance for bite detection on our dataset. Data preparation was done by converting all recordings into feature vectors $\boldsymbol{X_i}$ as in Equation 4.1. Every feature vector is constructed using three consecutive stable weight periods, and it consists of four values: the difference in average weight measurements between the first and the second stable periods ($W_i - W_{i+1}$); the difference in average weight measurements between the first and the third stable periods ($W_i - W_{i+2}$); the difference in time between the end of the first stable period and the beginning of the second stable period ($T2_i - T1_{i+1}$); and the difference in time between the end of the first stable period and the beginning of the third stable period ($T2_i - T1_{i+2}$). One second moving window was used to compute the moving standard deviation. A stable period starts when the standard deviation of the moving window goes below a threshold of 0.5 g, and it ends when the standard deviation goes above this threshold. This threshold was found to give better results on our dataset than the threshold value used in [129], i.e., 3 g. There were 3,151 feature vectors in our dataset. Feature vectors $\boldsymbol{X_i}$ were labeled with actual eating events; a vector is labeled with a true bite if an actual bite was consumed at any moment in the time window $T2_i$ to $T2_{i+1}$. The random forest was implemented with the same settings used by [129]. We used the random forest classifier from the python library scikit-learn. Leave one subject out cross validation method was used for training and evaluation.

4.4 Results

This section shows the results of comparing the different state-of-the-art methods for bite detection. In addition, it shows further evaluation for the method developed in this work. The bite detection results were evaluated using the same method explained in Section 3.2.

4.4.1 Comparison

For the evaluation purpose, detection of eating events are categorized into true positives (TP), false positives (FP), and false negatives (FN). A true positive occurs whenever an algorithm under test detects an eating event that is associated to a ground truth in the evaluation period. An evaluation period is defined as the time window that has a labeled ground truth event and is bounded by a previous and a next ground truth events. Note that the first evaluation period starts ten seconds before the first ground truth event and ends at the second ground truth event. The last evaluation period ends ten seconds after the last ground truth event and starts from the second last ground truth event. A false positive occurs whenever an algorithm detects an event not associated with a ground truth event within an evaluation period. A false negative occurs whenever an algorithm fails to detect an actual eating event within an evaluation period.

In classification context and to compare our detection method against the three other state-of-the-art methods, we use four metrics: precision, recall, accuracy, and F1-score. Precision is the fraction of the number of correctly detected events (TP) divided by the total number of all detected events (TP + FP). Therefore, precision is computed as

$$Precision = \frac{TP}{TP + FP}. \tag{4.2}$$

Recall is the fraction of the number of correctly detected events (TP) divided by the total number of all actual true events (TP + FN). Recall is computed as

$$Recall = \frac{TP}{TP + FN}. \tag{4.3}$$

Accuracy is the fraction of the number of correctly detected events (TP) divided by the total number of all detected and undetected events (TP + FP + FN). Therefore, accuracy is computed as

$$Accuracy = \frac{TP}{TP + FP + FN}. \tag{4.4}$$

F1-score is the harmonic mean of precision and recall. F1-score is computed as

$$F1\text{-}score = 2 \cdot \frac{precision \cdot recall}{precision + recall} = \frac{2 \cdot TP}{2 \cdot TP + FP + FN}. \tag{4.5}$$

Table 4.3 summarizes the results of the comparison. All numbers are averages with the standard deviation being enclosed inside parenthesis. The highest numbers are in bold. The F1-score of our method was considerably higher than all other methods, by 10-18%. Recall was 13-21% higher, and accuracy was 8-28% higher. The only metric where one of the other methods performed better was that the precision of [127] was 1% higher than ours (98% vs 97%). However, that method had much lower recall and accuracy. This combination indicates their method was far too conservative triggering event detections; most detections triggered were correct, but many actual events were missed. Overall, these results demonstrate that the use of a grid of load cells as a 2D weighing surface improves the detection performance.

Table 4.3: Results of comparing bite-detection methods.

Author	***Precision***	***Recall***	***Accuracy***	***F1-Score***
Mattfeld *et al.* 2016 [127]	**0.98 (±0.03)**	0.78 (±0.43)	0.77 (±0.38)	0.86 (±0.01)
Mertes *et al.* 2019 [129]	0.84 (±0.05)	0.84 (±0.05)	0.84 (±0.05)	0.84 (±0.05)
Papapanagiotou *et al.* 2018 [144]	0.83 (±0.25)	0.76 (±0.49)	0.64 (±0.23)	0.78 (±0.01)
This work	0.97 (±0.04)	**0.97 (±0.03)**	**0.92 (±0.06)**	**0.96 (±0.03)**

4.4.2 Further Evaluation of the Method Developed in this Work

In addition to the results shown in Table 3.1, Tables 4.4 and 4.5 show the results of bite detection of the rest of 32 recorded subjects. The overall average F1-score is 0.96. Subjects 10 and 12 ate cheese sandwich and biscuit, respectively. The algorithm failed to detect partial bites because there were no interaction with the table after each partial bite. When a subject picks up a food mass such as a burger or a piece of pizza, the food might be consumed over multiple partial bites before returning the food to its food container. As a result, there might be no interaction with the table, and hence the algorithm fails to detect actually consumed bites.

The use of 1D data — as the case of other methods we are comparing against — cannot provide accurate information for each food container resting on a weighing surface. Our instrument, on the other hand, can accurately provide such information on dietary assessments as shown in Tables 4.6 and 4.7 that show other detailed dietary assessments for subjects 10, 12, 14-32. Dietary assessments for subjects 1-9, 11, and 13 are shown in Chapter 3 in Table 3.2. Dietary information shown in these two tables include: eating rate in average number of seconds between consecutive bites for each food container; cumulative total weight of food consumed from each food container; average bite size picked up from each food container; ratio of weight of consumed food (plate and bowl) to the weight of consumed drink (cup); and the duration of complete meal.

4.5 Discussion

In this chapter we conducted a performance comparison of our method against the three state-of-the-art methods for bite detection using weight measurements of food containers [127, 129, 144]. A brief background explanation was provided for each of the three methods. More human subjects, total of 32, were recorded for the purpose of this comparison and for more evaluation of the method developed in this dissertation. While our method uses 2D data produced by our tool, the other methods use only 1D data. As a result, the 2D data were converted into 1D by summing up all measurements of the grid of load cells for every frame or sample moment into one weight measurement. This value represents the weight of all food containers. Tracking this value for all frames over the course of a meal makes up a weight profile for every human subject. The dataset was prepared based on the requirements of each method.

Using four metrics, the results show that our method scored the highest for recall, accuracy, and F1-score. This result suggests that the 2D instrument has better accuracy detecting intake events than 1D instruments. In addition, a 2D instrument can provide dietary assessments and eating behavior statistics that other methods cannot provide when using 1D data.

A future work might try more complex algorithms or implement the methods, which we compare against, using the 2D data. Specifically, we use the output of the segmentation such that weight profile of each food container is fed into different algorithms for another way of comparison.

A limitation of the work discussed in this chapter is the restricted eating. In an unrestricted eating, more activities are expected, and subjects might behave in an unexpected way; subjects can eat, for example, with utensils then suddenly use hands. They remove containers from the table surface making the signal disappear. They might remove food from one container to mix it with

Table 4.4: Evaluation of bite detection of the method developed in this work for subjects 10, 12, 14-21.

Subject		***Plate***	***Cup***	***Bowl***	***F1-Score***
10	TP	7	3	44	0.90
	FP	1	0	1	
	FN	10	0	0	
12	TP	10	5	47	0.96
	FP	0	0	0	
	FN	4	0	1	
14	TP	15	5	28	0.92
	FP	5	0	1	
	FN	0	0	2	
15	TP	20	7	19	0.90
	FP	5	0	1	
	FN	0	0	4	
16	TP	12	2	17	0.97
	FP	2	0	0	
	FN	0	0	0	
17	TP	27	4	22	0.99
	FP	0	0	1	
	FN	0	0	0	
18	TP	10	5	14	0.94
	FP	4	0	0	
	FN	0	0	0	
19	TP	43	7	41	0.99
	FP	0	0	0	
	FN	0	0	2	
20	TP	12	7	16	0.95
	FP	2	0	2	
	FN	0	0	0	
21	TP	18	5	14	0.99
	FP	0	0	0	
	FN	0	0	1	

Table 4.5: Evaluation of bite detection of the method developed in this work for subjects 22-32.

Subject		***Plate***	***Cup***	***Bowl***	***F1-Score***
22	TP	18	6	22	0.97
	FP	1	0	0	
	FN	0	0	2	
23	TP	30	1	58	0.97
	FP	3	0	1	
	FN	0	0	1	
24	TP	9	4	23	0.92
	FP	5	0	1	
	FN	0	0	0	
25	TP	20	5	33	0.89
	FP	12	0	0	
	FN	0	0	2	
26	TP	20	11	47	0.98
	FP	1	0	0	
	FN	0	0	2	
27	TP	15	6	11	0.97
	FP	0	1	0	
	FN	0	1	0	
28	TP	51	3	37	0.99
	FP	1	0	0	
	FN	1	0	2	
29	TP	29	2	21	0.99
	FP	1	0	0	
	FN	0	0	0	
30	TP	29	3	20	0.97
	FP	1	0	2	
	FN	0	0	0	
31	TP	34	5	15	0.97
	FP	2	0	0	
	FN	1	0	0	
32	TP	19	2	20	0.96
	FP	3	0	0	
	FN	0	0	0	

Table 4.6: Other dietary assessments computed by the smart dining table for subjects 10, 12, 14-21

Subject		***Eating rate (spb)***	***total consumption (g)***	***Average bite size (g)***	***Food to drink ratio***	***Duration (min)***
10	Plate	109	220.8	27.6	1.37	15.9
	Cup	297.3	320.6	106.9		
	Bowl	18.8	217.9	4.8		
12	Plate	130	272.7	27.3	1.01	23.6
	Cup	173.6	472.4	94.5		
	Bowl	25.6	206	4.4		
14	Plate	33.4	248.8	12.4	1.80	12.2
	Cup	150.2	238.8	47.8		
	Bowl	23.1	180.7	6.2		
15	Plate	25.5	394.8	15.8	1.38	10.4
	Cup	84	359.5	51.4		
	Bowl	26.1	100	5		
16	Plate	45.3	225.7	16.1	2.87	11.1
	Cup	119	119.5	99.8		
	Bowl	15.3	117.5	6.9		
17	Plate	6	203.3	7.5	0.96	8.4
	Cup	90.8	344	86		
	Bowl	20.7	127.7	5.6		
18	Plate	40.3	347.2	24.8	1.27	9.7
	Cup	86.4	345.3	69.1		
	Bowl	24.3	92.3	6.6		
19	Plate	13.7	342.8	8	0.43	19.8
	Cup	157.4	201.8	28.8		
	Bowl	14.5	179.3	4.4		
20	Plate	39.1	212	15.1	1.07	9.6
	Cup	84.6	360.4	51.5		
	Bowl	20.1	171.9	9.6		
21	Plate	32.1	306.6	17	2.83	9.8
	Cup	109.8	141.2	28.2		
	Bowl	41	92.3	6.6		

Table 4.7: Other dietary assessments computed by the smart dining table for subjects 22-32

Subject		***Eating rate (spb)***	***total consumption (g)***	***Average bite size (g)***	***Food to drink ratio***	***Duration (min)***
22	Plate	17.4	234	12.3	1.70	5.2
	Cup	53.7	198.4	33.1		
	Bowl	9.9	102.3	4.6		
23	Plate	21.2	313.6	9.5	10.62	11.6
	Cup	20	78.4	78.4		
	Bowl	11.7	519	8.8		
24	Plate	29.9	215.9	15.4	2.00	6.8
	Cup	48.2	192.7	48.2		
	Bowl	7.1	170.1	7.1		
25	Plate	19.6	355.2	11.1	1.43	10.3
	Cup	121.8	396.5	79.3		
	Bowl	12.8	212.9	6.5		
26	Plate	11.3	314.2	15	1.93	15.4
	Cup	84.1	360.2	32.7		
	Bowl	17.4	379.6	8.1		
27	Plate	50.7	235.8	15.7	0.97	15.9
	Cup	121.9	381.2	54.5		
	Bowl	49.3	132.9	12.1		
28	Plate	19.6	423.6	8.1	2.81	16.8
	Cup	226.7	238.9	79.6		
	Bowl	11.5	248.1	6.7		
29	Plate	7	329.6	8.3	2.68	7.3
	Cup	163	205.3	102.7		
	Bowl	21.4	221.1	10.5		
30	Plate	14.7	277.7	9.3	3.46	7.4
	Cup	116.3	118.5	116.3		
	Bowl	20.2	132.3	20.2		
31	Plate	16.9	310.5	8.6	2.53	9.9
	Cup	117.6	188.8	37.8		
	Bowl	39.3	168	11.2		
32	Plate	25	182	8.3	1.64	9.4
	Cup	63	174.6	87.3		
	Bowl	13.3	103.8	5.2		

other food in another container. The dataset used in the work of Mattfeld *et al.* was collected in an unrestricted eating. Their method was able to correctly detect 39% and failed to detect 47% of 24,101 ground truth bites labeled in their dataset [127]. Compared to their dataset, their method achieved 78% recall on our dataset. The restricted eating in a laboratory environment, which is the case in our study, seems to be the reason for this improvement. However, it is also possible that the improvement in other algorithms is a result of using the 2D weighing surface that helps in getting stable measurements and a segmented area for each food container. It is expected to have less stable weight measurements when placing multiple food containers on a food tray that is placed on only one scale; subjects can frequently and quickly pick up two bites by switching from a container to another resulting in continuous unstable weight measurements for multiple bites. Further collection of data in a free living environment is required to test the improvement that could be obtained when using a 2D weighing surface.

Mass bites were also limited in our dataset. we have only two subjects (10 and 12) who ate sandwiches. This is a small sample of partial bites compared to the dataset of [127] in which 14% of 24,101 ground truth bites were partial bites. Detection of partial bites eaten from a mass bite is beyond the capabilities of weighing sensors. Tracking of weight measurements alone is not sufficient for the detection of partial bites and another modality is required to address this problem such as using a bite counter or chewing monitoring device. Multi-modality systems have been used in the literature to take advantage of the strengths of different sensors to complement each other [120,132]. Similarly, a weighing scale can be used to provide accurate weight measurements in addition to a chewing or swallowing sensor to detect when a bite was actually consumed.

Chapter 5

Conclusion

This dissertation presented a custom-built dining table that automatically monitors eating and can report statistics including the amount of consumed bites per unit time, bite size in grams, and total weight consumed over the course of a meal. The work was motivated by the problem of obesity which is a globally growing health problem. To approach the problem of obesity, dietitians need to assess and monitor patient eating behavior. Classic eating dietary tools are subject to bias, depend on patient memory, and lack accuracy. Various automatic eating dietary tools have been developed by researchers for objective, accurate, low cost, and in-situ monitoring.

This work shows a method to embed a grid of load cells under the surface of a dining table that can detect the locations and weights of food containers sitting on the table surface. These containers need to distribute their weights among the load cells on which they rest. The challenge is that a typical load cell deflects for less than 0.1 mm from zero to full load. Thus, the tops of load cells need to be vertically aligned within a few micrometers across the grid to allow for correct spatial information and weight distribution to be measured. To obtain a low vertical deviation among the tops of load cells, we developed a manufacturing technique in which the grid of load cells are inverted or flipped over on a reference flat granite surface. The finished surface was mounted on a wooden box that contains the scanning electronics of the load cells.

The design was tested for accuracy of weight measurements and weight distribution. The results shows that weight measurements were 99.97±0.1% accurate. The average measured standard deviation of weight distribution among 2x2 grid cells was 5.5 g. This is equivalent to approximately 4.2±0.5 um deviation from the perspective of surface flatness.

We conducted an initial pilot study that involves recruiting 11 human subjects to voluntary participate and eat on the dining table after we received an IRB approval. Data were labeled for ground truth using synced videos. Foods include fresh salads and frozen meals for solid foods and water for beverage. We developed an algorithm that, first, segments the images of weights produced by the grid of load cells, second, detects bites picked up from the food containers. Per-subject F1-score ranged from 0.91 to 1.00 for the detection of bite consumption.

More human subjects were recorded for further evaluation of our method which was also compared against three state-of-the-art methods that we found in the literature for bite detection using weight measurements. The dataset contains a total of 32 subjects, 1,836 ground truth moments of labeled eating events, and a total meal duration of 376 minutes. Our method scored 96% F1-score for bite detection. The other methods we compared our method against use 1D weight measurements while our instrument produce 2D data. As a result, we prepared the data based on the requirements of each method. Four metrics were used to evaluate the comparison: precision, recall, accuracy, and F1-score. Our method achieved the highest for recall, accuracy, and F1-score. This result shows that the use of 2D weighing instrument significantly improves the bite detection capability in addition to providing other dietary assessments that are likely impossible to accurately quantify using 1D of weight measurements. The dietary assessments include food to drink ratio, bite rate, and bite size picked up from each food container.

5.1 Future Work and Open Problems

A higher resolution grid can be built using a smaller load cell. Thus, larger weights can be distributed among more load cells and a more representative spatial information of object footprints can be obtained. For eating monitoring application, more sensitive load cells are required when smaller in size load cells are used so that weight reductions due to pick up of small bites can still be sensed when distributed among more load cells.

Adding a smart textile sensor to the top of the surface would complement the high accuracy of weight measurements provided by the load cells with high position resolution provided by the smart textile. It would also be interesting to try a new smart textile technology that has more linear sensitivity behavior [86]. The use of this technology for eating monitoring is still an open question for a research.

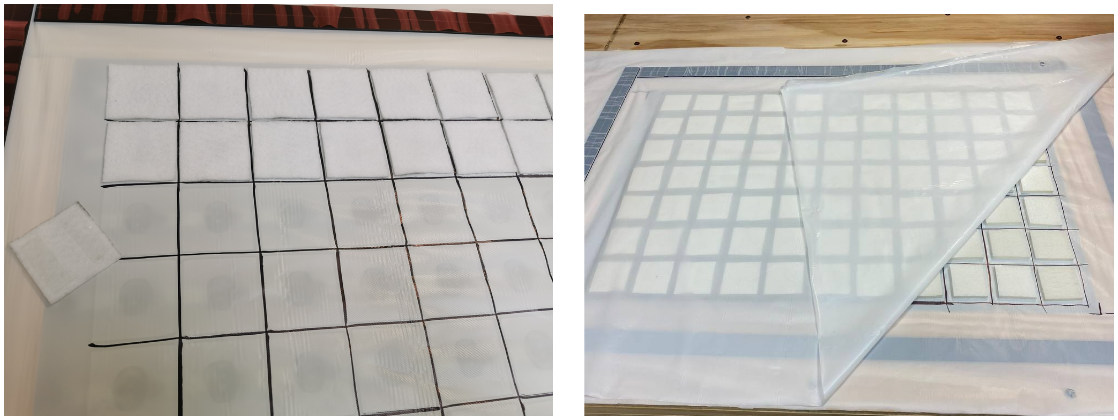

(a) (b)

Figure 5.1: Square pieces of spongy fabric are attached on a plastic foil to enable for the use of regular dishware which have poor bottom flatness. After testing this idea, cross talk was observed on the grid cells surrounding the footprint of a regular flat-bottomed plate.

Another idea that might wroth trying is the use of a spongy laminate to enable the use of regular dishware. Unlike the custom-built, flat-bottomed dishware used in this study, regular and commercially available plates and bowls do not have high flatness bottoms. Thus, a spongy laminate is required to help distribute the weight of objects among all grid cells on which they rest. Moreover, the laminate needs to be flexible enough to prevent any cross talk between adjacent grid cells. In an attempt to use such regular dishware with our dining table, we tried to make a spongy and flexible laminate. Square pieces of a spongy fabric — each was cut with dimension of about 4x4 cm just smaller than the size of our tiles — were used between two layers of flexible plastic foil. The center of each fabric square was aligned to the center of a grid tile. All of these square pieces of fabric were attached with a two-sided tape on one of the flexible plastic foil as shown in Fig. 5.1. We tested this laminate with a regular, commercially available, flat-bottomed plate. The results showed that the laminate helped distribute the weight of the plate on the grid cells on which it rests. However, cross talk was noticed; the laminate was not flexible enough and the weight of the plate was also distributed on adjacent grid cells surrounding the footprint size of the plate. More improvements and modifications on this laminate might be required to make it work.

The algorithm can still be improved to detect and track regular dishware with various footprints. The current image segmentation algorithm expects to see a full area of a circle shaped footprints representing food containers. However, for regular dishware, the image segmentation should expect to see different shapes; regular dishware usually have edges footprints such as the circumference of a circle.

It would be interesting to try carbon fiber for the grid tiles and other mechanical parts to make the structure lighter and more stiff and rigid. Doing so could make the instrument lighter and hence mobile.

Our algorithm can be improved in multiple ways. Even though false footprint segmentation was rarely noticed, i.e., approximately less than ten frames in the whole data set, segmentation can be improved to be smarter and able to track footprints when food containers are removed for some time and then replaced at a different location on the grid. The segmentation algorithm can also be improved to work with more variety of object footprints and sizes for more flexibility. The bite detection algorithm might need to be tested and improved to work with a broader variety of food options and to handle non-eating gestures such as the use of utensils in a way that is smarter than using their weights. Resting and removal of utensils on and from the plate or bowl were sources of FPs and FNs. When a utensil, for example, is left on a plate before the plate is placed on the dining table surface, a FP is detected when the utensil is picked up. An example of a FN is the case when part of a picked up food falls back into a food container making a weight addition that is in the range of the hard-coded weights of the used utensil, i.e., minWoU and maxWoU, as explained in Section 3.1.3. In this case, the algorithm considers this weight addition as if a utensil was rested into the food container. If another utensil was used to pick up a bite that has a weight close to the weight of the utensil then this bite will be ignored. Another source of FNs is the case when eating mass bites (a large amount of food, for example a sandwich, is picked up and a bite is ingested from it). For this case, an integration of other modalities that automatically detect food consumption could complement our approach. One more important improvement of the algorithm is to add the ability for automatic detection of eating episodes to make it an unobtrusive instrument. The dining table should automatically detect when someone is eating on it to start the automatic dietary assessment and to ignore non-eating gestures.

Appendices

Appendix A Instructions of Instrument Usage

A.1 Measuring Deflection Distance of Load Cells

The deflection distance of a single point load cell is defined as the displacement of the point of axial load application in the primary axis between no load and the rated capacity load conditions [12]. Datasheets of some load cells like the one used in this research do not show the deflection distance. In this case, the following procedure can be used to measure the deflection distance. This procedure should be done with a statistically acceptable sample size to generalize for a set of similar load cells. For each load cell:

1. Load cell is mounted firmly on a rigid base. There needs to be a stopper tuning screw right under the force application end.

2. Calibrate the load cell using a calibration weight that is equal to the rated capacity.

3. After calibration is done, place a calibration weight that is a few grams heavier than the rated capacity on the load cell.

4. Using an L-shaped screw driver fasten the stopper screw until the weight measurements start to change then stop and mark the weight measurement and mark the point at which the L-shaped screw driver is pointing.

5. Continue fastening the stopper screw until the weight measurements have reduced the same amount of the rated capacity then stop and mark the spot at which the L-shaped screw drier is pointing.

6. Use an angle ruler to measure the angle between the two points θ.

Assuming the load cell weight measurements is linearly proportional to the deflection distance and the stopper screws are pointed at their contact with the load cells, we can calculate the deflection distance using the measured value θ and the pitch size of the stopper screw α. For example, if $\theta = 55°$ and $\alpha = 0.5$mm then the deflection distance is

$$deflection\ distance = \alpha * \frac{\theta}{360} = 0.5 * \frac{55}{360} = 76.38um$$

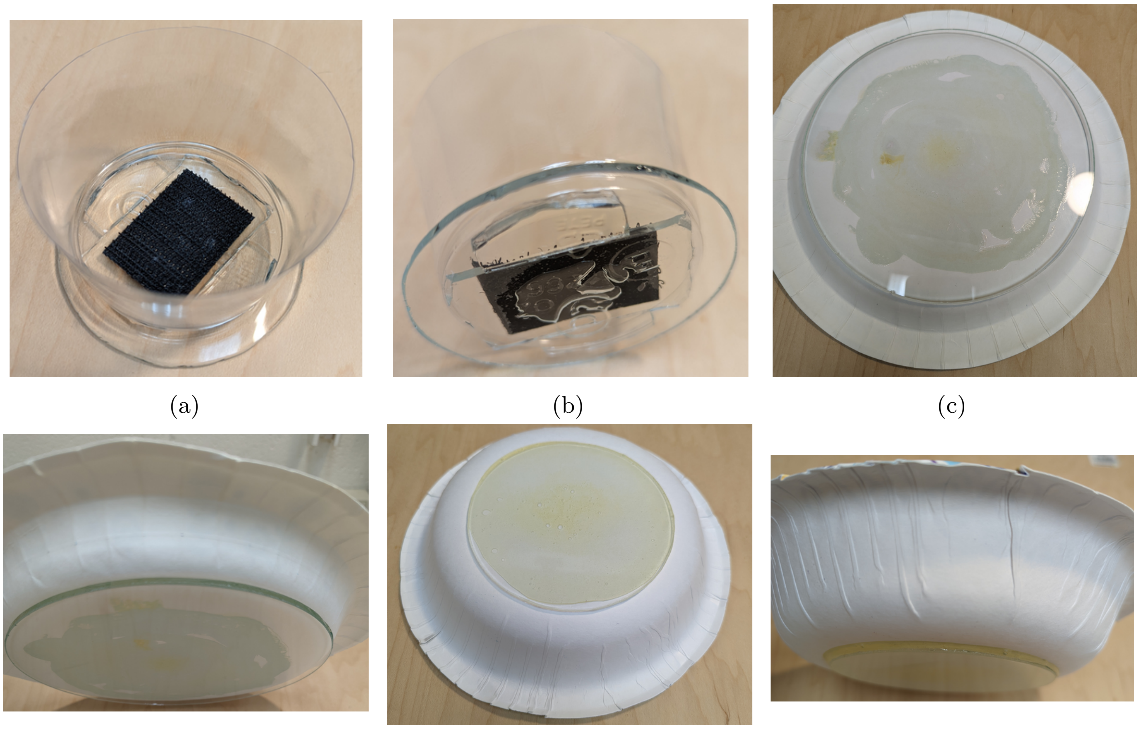

(a) (b) (c)

(d) (e) (f)

Figure A.1: Flat-bottomed bases of food containers. (a) and (b) A plastic cup cut in half and attached to a circle-shaped piece of regular glass with diameter of 6.5 cm. A velcro fastener was attached to the internal bottom of the base of half cup so that it holds to another fastener that is attached to the external bottom of a new plastic cup. (c) and (d) A paper plate attached to a a circle-shaped piece of regular glass with diameter of 19 cm. (e) and (f) A paper bowl attached to a a circle-shaped piece of regular glass with diameter of 10 cm.

A.2 Food Container Bases

Fig. A.1 shows the flat-bottomed bases used during the data recording to meet the the design assumptions that food containers have flat footprints. A paper plate and bowl were attached to circle-shaped pieces of regular glass with diameters of 19 cm, and 10 cm, respectively. A plastic cup was cut in half and attached to a circle-shaped piece of regular glass with diameter of 6.5 cm. A velcro fastener was used to attach a new plastic cup to the flat-bottomed base so that it is used as one piece; this is required because a user is expected to pick up the cup and drink water frequently during a meal.

A.3 Recording Data

Data are sent from the instrument in ASCII format over Ethernet connection using a UDP protocol to port **44335** on the receiving side. Data can be recorded on a Linux system using the following command

```
nc -u -l -k 44335 > data.txt
```

Video files were recorded using ffmpeg as follows

```
ffmpeg -f v4l2 -s 640x480 -input_format mjpeg -i ${camera} -g 5 ${videoName}
```

where ${camera} is a USB webcam located at, for example, /dev/video2, and ${videoName} is a file name with an extension such as video.mp4.

The two commands were included into a bash script file that runs from a terminal on Linux so that the two files can be synchronized with a negligible time difference. This makes the data visualization easier for study and annotation.

A.4 Cleaning

A drop of glass cleaner is dispensed on each tile. Gently rub each tile with a finger. Then wipe each tile with a clean paper towel.

Appendix B Data Collection

B.1 IRB Permission and Consent Forms

The following pages show the IRB permission to conduct experiments by recruiting human subjects and the consent forms which were signed by each subject. Emails and fliers — shown in Fig. B.1 — were used to recruit subjects. Only a free meal was offered for subjects as an incentive.

Division of
RESEARCH
Research Compliance

To: Adam Hoover

Re:

Clemson IRB number:	IRB2021-0462
Expedited Category:	6 & 7
Determination Date:	June 21, 2021
Completion Date:	May 31, 2021
Funding Sponsor:	N/A
Project Title:	Smart Dining Table

The Clemson University Institutional Review Board (IRB) determined that the proposed activities involving human participants meet the criteria for expedited review under 45 CFR 46.110.

Principal Investigator (PI) Responsibilities: The PI assumes the responsibilities for the protection of human subjects as outlined in the Principal Investigator's Responsibilities guidance.

Non-Clemson Affiliated Collaborators: This determination only covers Clemson affiliated researchers on the study. External collaborators will have to consult with their respective institution's IRB office to determine what is required for their role on the project. An IRB Authorization Agreement is required for Clemson's IRB to be the IRB record for the study.

Informed Consent: Study personnel are required to use the approved informed consent document(s) for the study, unless a waiver of consent is granted.

Waiver(s) granted for this study:
☒ None

☐ The IRB granted a waiver of signed consent pursuant to 45 CFR 46.117(c)(1)
- ☐ (i): That the only record linking the subject and the research would be the informed consent form and the principal risk would be potential harm resulting from a breach of confidentiality. Each subject (or legally authorized representative) will be asked whether the subject wants documentation linking the subject with the research, and the subject's wishes will govern.
- ☐ (ii): That the research presents no more than minimal risk of harm to subjects and involves no procedures for which written consent is normally required outside of the research context.
- ☐ (iii): If the subjects or legally authorized representatives are members of a distinct cultural group or community in which signing forms is not the norm, that the research presents no more than minimal risk of harm to subjects and provided there is an appropriate alternative mechanism for documenting that informed consent was obtained.

☐ The IRB granted a waiver of some elements of informed consent pursuant to 45 CFR 46.116(f) because the research involves no more than minimal risk to the subject, the waiver will not adversely affect the rights and welfare of the subjects, and the research could not be practicably carried out without the waiver.

☐ The IRB granted a waiver of consent pursuant to 45 CFR 46.116(f) and 45 CFR 46.408(c)-waiver for parents- because the research involves no more than minimal risk to the subject, the waiver will not adversely affect the rights and welfare of the subjects, and the research could not be practicably carried out without the waiver.

Progress Report: A progress report is required at least 30 days before the scheduled expiration date to extend the approval period.

Modifications: The PI is required to submit all proposed changes (i.e., increase in enrollment; modifications to research methods/instruments, recruitment procedures/documents, incentives, informed consent process/document, data, etc.) to the IRB office using the amendment request form. All changes must be reviewed and approved prior to implementation; except when an immediate change is necessary to eliminate a hazard to the participants, or to provide participants with new information on adverse event or research results considered essential to a participant's decision whether to continue participation.

New Funding: Notify the IRB office If new funding is received for an active study. IRB review of the new award must be completed before new funds can be spent on human research activities, as the new funding source may have additional or different requirements.

Reportable Events: Notify the IRB office immediately if there are any unanticipated problems involving risk to subjects, complications , adverse events and/or any complaints from research participants that may change the level of review from expedited to full board review. Additional information available at https://www.clemson.edu/research/compliance/irb/forms.html.

Study Personnel Changes: An amendment request form is required for all personnel changes. Use the team member form to report changes to the study team. CITI training documentation is required for all team members, including the PI.

CITI Training: All study personnel are required to complete the CITI human subjects training course.

Non-Clemson Affiliated Sites: A site letter is required for all off-campus sites. Refer to the guidance on research site/permission letters for more information. An amendment request form is required to add additional sites to the study.

International Research: Clemson's IRB approval is based on U.S. human subjects protections regulations and Clemson University human subjects protection policies. Researchers should become familiar with all pertinent information about local human subjects protection regulations and requirements when conducting research in countries other than the United States. We encourage you to discuss with your local contacts any possible human subjects research requirements that are specific to your research site, to comply with those requirements and to inform Clemson's IRB office of those requirements so we can better help other researchers prepare for international research in the future.

New IRB Application: A new application is required if the study remains open for more than 5 years after the initial determination.

Closure: Notify the IRB office when the study can be closed or if the PI leaves the university. Closure indicates that research activities with human subjects are no longer ongoing, have stopped and are complete. Human research activities are complete when investigators are no longer obtaining information or biospecimens about a living person through interaction or intervention with the individual, obtaining identifiable private information or identifiable biospecimens about a living person and/or generating identifiable private information or identifiable biospecimens about a living person.

Contact Information: Please contact the IRB office at IRB@clemson.edu or visit our webpage if you have questions.

Clemson University's IRB is committed to facilitating ethical research and protecting the rights of human subjects. All research involving human participants must maintain an ethically appropriate standard, which serves to protect the rights and welfare of the participants. This involves obtaining informed consent and maintaining confidentiality of data.

Institutional Review Board
Office of Research Compliance
Clemson University
https://www.clemson.edu/research/compliance/irb/

IRB Number: IRB00000481
FWA Number: FWA00004497

Information about Being in a Research Study
Clemson University

Tracking Eating Behavior Using a Smart Dining Table

KEY INFORMATION ABOUT THE RESEARCH STUDY

Voluntary Consent: Adam Hoover is inviting you to volunteer for a research study. Dr. Hoover is a Professor in the Department of Electrical and Computer Engineering at Clemson University.

You may choose not to take part and you may choose to stop taking part at any time. You will not be punished in any way if you decide not to be in the study or to stop taking part in the study. If you choose to stop taking part in this study, the information you have already provided will be used in a confidential manner.

Study Purpose: The purpose of this research is to study eating behavior using a smart dining table. The table uses sensors embedded in the table surface to detect dishware and measure its weight. These measurements are used to detect individual bites of food and drinks of liquid to quantify eating behaviors. None of this data is displayed to the person while eating so that it will not affect their natural behaviors. If you participate in this study, you will be asked to eat a meal on the smart dining table.

Activities and Procedures: Your participation in the study will include:

- Self-reporting your height and weight.
- Eating a meal on the smart dining table. The meal will be ordered from an on campus restaurant or cafeteria and will be provided to you at no cost. Please notify the research team of any allergy concerns.
- Being video recorded while eating the meal. This will be used to transcode the times of ingestion events that took place on the dining table.

Participation Time: It will take you about 15 to 30 minutes to be in this study.

Risks and Discomforts: If you have any food allergies or history of an eating disorder that could affect your comfort in eating a meal, please notify the research team. If you experience discomfort during the experiment at any time, please notify the research team and the experiment will be halted.

Possible Benefits: You may not benefit directly for taking part in this study, however the data collected in this study will be used to develop algorithms and validate the accuracy of the smart dining table for future research in eating behaviors.

EXCLUSION/INCLUSION REQUIREMENTS: You must be 18 years or older to participate in this study.

AUDIO/VIDEO RECORDING AND PHOTOGRAPHS: You will be video recorded during eating the meal. This will be used to mark the times of actual ingestion. Videos will be retained indefinitely for potentially updating the manually marked times of actual ingestion. You will be asked to sign a media release form so that the recordings may be shared publicly to further facilitate this research and disseminate its results.

EQUIPMENT AND DEVICES THAT WILL BE USED IN THE RESEARCH STUDY:
You will eat on a dining table that was developed for this research.

PROTECTION OF PRIVACY AND CONFIDENTIALITY

The results of this study may be published in scientific journals, professional publications, or educational presentations.

All sensor data will be deidentified during recording using a unique ID number for each participant. Sensor data recorded by the smart dining table will consist of a grid of weight measurements over time of objects on the table surface. Video will be recorded synchronously and will generally show the head and upper limbs of a participant so that ingestion events (intake of food and beverage) can be seen. The video will be used to mark the actual times of ingestion events in the sensor data (known as “ground truth”). These times will be used to evaluate the accuracy of the smart dining table for automatically detecting ingestion events.

Identifiable information collected during the study could be used for future research studies or distributed to another investigator for future research studies without additional informed consent from the participants or legally authorized representative.

We might be required to share the information we collect from you with the Clemson University Office of Research Compliance and the federal Office for Human Research Protections. If this happens, the information would only be used to find out if we ran this study properly and protected your rights in the study.

CONTACT INFORMATION

If you have any questions or concerns about your rights in this research study, please contact the Clemson University Office of Research Compliance (ORC) at 864-656-0636 or irb@clemson.edu. If you are outside of the Upstate South Carolina area, please use the ORC’s toll-free number, 866-297-3071. The Clemson IRB will not be able to answer some study-specific questions. However, you may contact the Clemson IRB if the research staff cannot be reached or if you wish to speak with someone other than the research staff.

If you have any study related questions or if any problems arise, please contact Adam Hoover at Clemson University at 864-656-3377, ahoover@clemson.edu

CONSENT

By signing this consent form, you indicate that you have read the information written above, are at least 18 years of age, have been allowed to ask any questions, and you are voluntarily choosing to take part in this research.

Participant’s signature: ____________________________________ Date: __________

Print name: ____

A copy of this form will be given to you.

Electrical and Computer Engineering

PHOTO/VIDEO PUBLICATION RELEASE FORM

Smart Dining Table for Automatic Detection of Eating Events

Researcher(s): Prof. Adam Hoover
Contact Information: ahoover@clemson.edu

All persons taking still photographs or videos for Clemson University-related research publications must obtain a signed release form from anyone who is visibly recognizable in the photograph or video. Crowd scenes where no single person is the dominant feature are exempt. This form is intended for use with Clemson University IRB approved research under the above noted IRB protocol.

Participant Consent:

I am 18 years of age or older and hereby grant the researcher designated above from Clemson University permission to photograph, audio record, and/or videotape my voice and likeness and to use my voice and likeness in photograph(s), audio recordings, and/or videotaping as part of the above titled IRB approved research study.

I give permission for the researcher to distribute and/or use any photograph(s), audio recording(s), and/or videotape(s) made as part of this research project in research presentations, publications, for educational uses, or through any other venue as long as my name is not used. All media will become the property of Clemson University. I will make no monetary claim against Clemson University for the use of the photograph(s), audio recording(s), and/or video recording(s).

Printed Name: Date:

Signature: ____

Clemson University Researcher:

Name: Date:

Signature: ____

Spring 2022 **Please participate**

Free Meal

We are looking for volunteers to participate in eating a free meal in Fluor Daniel EIB room 345.

Description of the project: The purpose of this research is to develop hardware and algorithms to detect eating events taking place on a dining table. Your participation will require 15 minutes of your time in a visit to our lab, where you will eat a meal on a custom-built dining table. Food will be ordered from Publix and will be provided to you. You will be video recorded during eating the meal. The QR code below shows an explanation of the research.

To participate: You must be an adult between 18 and 100 years of age. People having anorexia, bulimia or any other eating disorders will be excluded from the study.

If you like to participate you can choose any fresh salad and frozen food that can be found in the local Publix store and that needs to be eaten with standard utensils: a fork, spoon, and knife. Cold, bottled water will be provided as a beverage. Here are examples of the food we previously provided but you can choose different ones.

This research is conducted under the direction of Adam W. Hoover, Department of Engineering, Computing, and Applied Sciences, and has been reviewed and approved by the Institutional Review Board of Clemson University (IRB2021-0462).

To learn more or to participate, please contact Mohammad Mayyan at mmayyan@g.clemson.edu

Figure B.1: The flier used to recruit human subjects to voluntary participate in the study.

B.2 Food Options Subjects Chose to Eat

Table B.1 lists the food and salad each subject ate on the dining table. All foods listed in the second column, i.e., ***Food***, were frozen except for subjects 10 and 12 who ate sandwiches. All salads were refrigerated and ordered from grocery stores. Fig. B.2 shows examples of the fresh salads and frozen foods eaten by participants. Subjects 10 and 12 were excluded from the results shown in Table 3.1.

Table B.1: List of food options participating subjects chose to eat.

Subject	***Food***	***Salad***
1	Lean Cuisine Chicken Fried Rice	Simply Fresh Salads Salad, Deluxe Caesar, with Chicken
2	Lean Cuisine Chicken Fried Rice	Simply Fresh Salads Salad, Deluxe Caesar, with Chicken
3	Lean Cuisine Chicken Fried Rice	Simply Fresh Salads Salad, Deluxe Caesar, with Chicken
4	Lean Cuisine Chicken Fried Rice	Simply Fresh Salads Salad, Deluxe Caesar, with Chicken
5	Lean Cuisine Alfredo Pasta, with Chicken & Broccoli	Simply Fresh Salads Salad, Deluxe Caesar, with Chicken
6	Lean Cuisine Alfredo Pasta, with Chicken & Broccoli	Simply Fresh Salads Salad, Deluxe Caesar, with Chicken
7	Lean Cuisine Alfredo Pasta, with Chicken & Broccoli	Simply Fresh Salads Salad, Deluxe Caesar, with Chicken
8	Lean Cuisine Alfredo Pasta, with Chicken & Broccoli	Simply Fresh Salads Salad, Deluxe Caesar, with Chicken
9	Lean Cuisine Alfredo Pasta, with Chicken & Broccoli	Simply Fresh Salads Salad, Deluxe Caesar, with Chicken
10	Cheese sandwich	Green salad
11	Lean Cuisine Alfredo Pasta, with Chicken & Broccoli	Simply Fresh Salads Salad, Deluxe Caesar, with Chicken

Table B.1 Continued: List of Food Options Participating Subjects Chose to Eat

Subject	*Food*	*Salad*
12	Chick-fil-A® Chicken Biscuit	Simply Fresh Salads Salad with Chicken, Santa Fe Style
13	Lean Cuisine Alfredo Pasta, with Chicken & Broccoli	Simply Fresh Salads Salad, Deluxe Caesar, with Chicken
14	Stouffer's Lasagna with meat and Souce	Publix Deli Grilled Chicken Caesar Salad
15	Amy's Enchilada, Cheese	Publix Deli Turkey Cobb Salad
16	Amy's Enchilada, Roasted Poblano	Publix Deli Turkey Cobb Salad
17	Stouffer's Lasagna with meat and Souce	Publix Deli Turkey Cobb Salad
18	Lean Cuisine Orange Chicken	Publix Deli Grilled Chicken Caesar Salad
19	Lean Cuisine Chicken Fried Rice	Simply Fresh Salads Salad with Fresh Mozzarella, Gourmet Caprese, Loaded with Toppings
20	Amy's Enchilada, Roasted Poblano	Simply Fresh Salads Salad with Fresh Mozzarella, Gourmet Caprese, Loaded with Toppings
21	Lean Cuisine Favorites Fettuccini Alfredo	Publix Deli Grilled Chicken Caesar Salad
22	Amy's Enchilada, Roasted Poblano	Publix Deli Grilled Chicken Caesar Salad
23	Lean Cuisine Favorites FAVORITES Chicken Fettuccini	Boar's Head Bold Chef Salad
24	Amy's Enchilada, Cheese	Simply Fresh Salads Salad with Fresh Mozzarella, Gourmet Caprese, Loaded with Toppings
25	Stouffer's Chicken A La King	Simply Fresh Salads Salad, Deluxe Caesar, with Chicken
26	Stouffer's Escalloped Chicken & Noodles	Publix Deli Grab & Go Salad, Strawberry & Glazed Pecan

Table B.1 Continued: List of Food Options Participating Subjects Chose to Eat

Subject	***Food***	***Salad***
27	Lean Cuisine Favorites FAVORITES Chicken Fettuccini	Publix Deli Grilled Chicken Caesar Salad
28	Boston Market Beef Steak & Pasta	Publix Deli Turkey Cobb Salad
29	Lean Cuisine Favorites Five Cheese Rigatoni	Publix Deli Chef Salad
30	Home made Frittata	Home made green salad
31	Home made rice and chicken	Home made green salad
32	Healthy Choice Simply Steamers Meatball Marinara	Publix Deli Traditional Greek Style Salad

(a)

(b)

(c)

(d)

(e)

(f)

(g)

(h)

(i)

(j)

(k)

(l)

Figure B.2: Examples of food options participants ate on the dining table. (a)-(f) are fresh salads. (g)-(l) are frozen foods.

Appendix C Schematics and PCBs

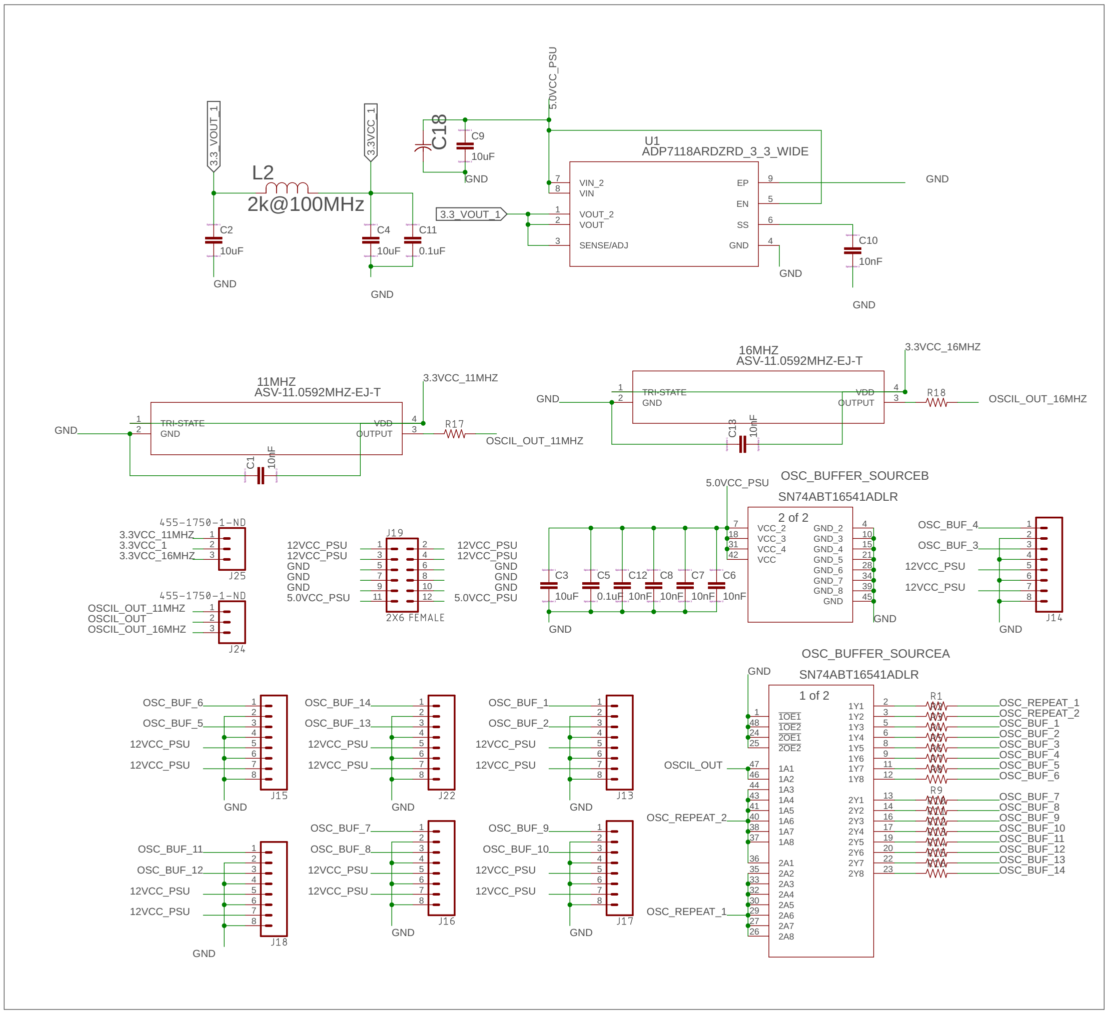

Figure C.1: Sync clock .

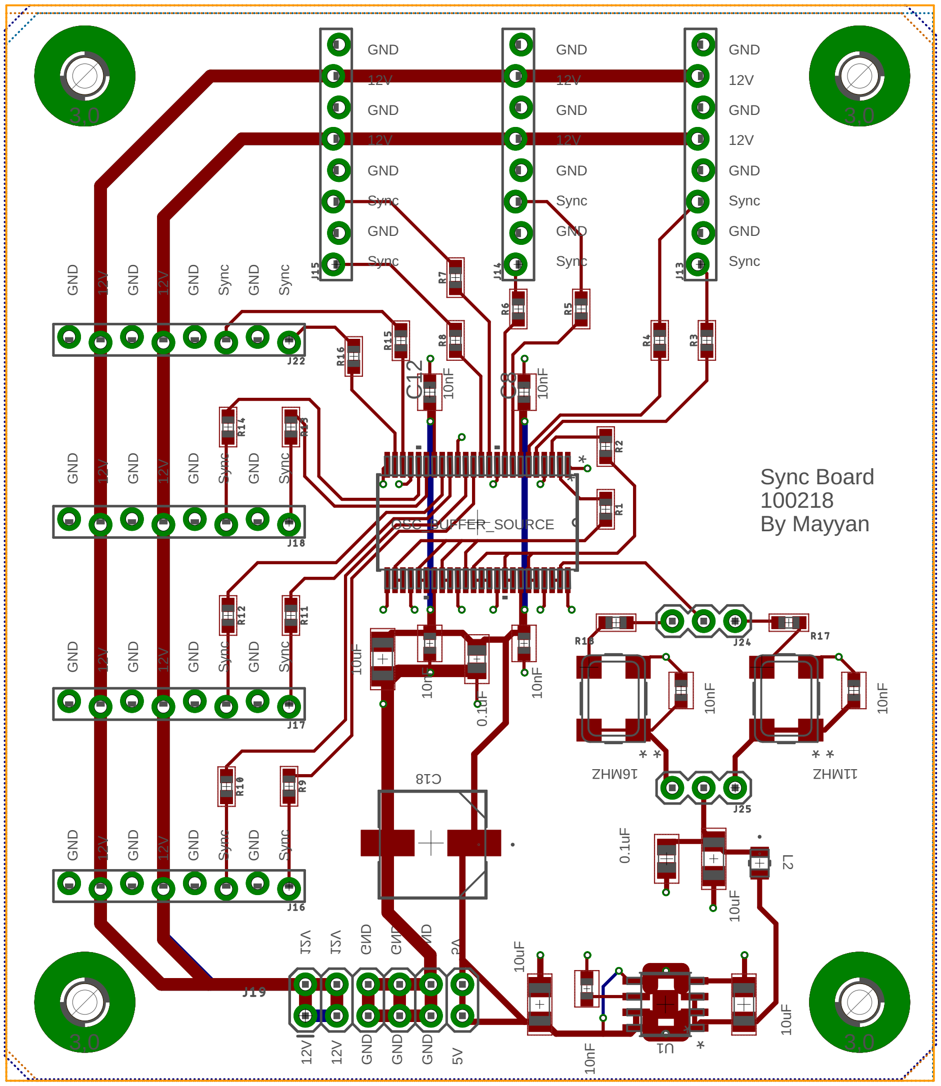

Figure C.2: Sync clock PCB.

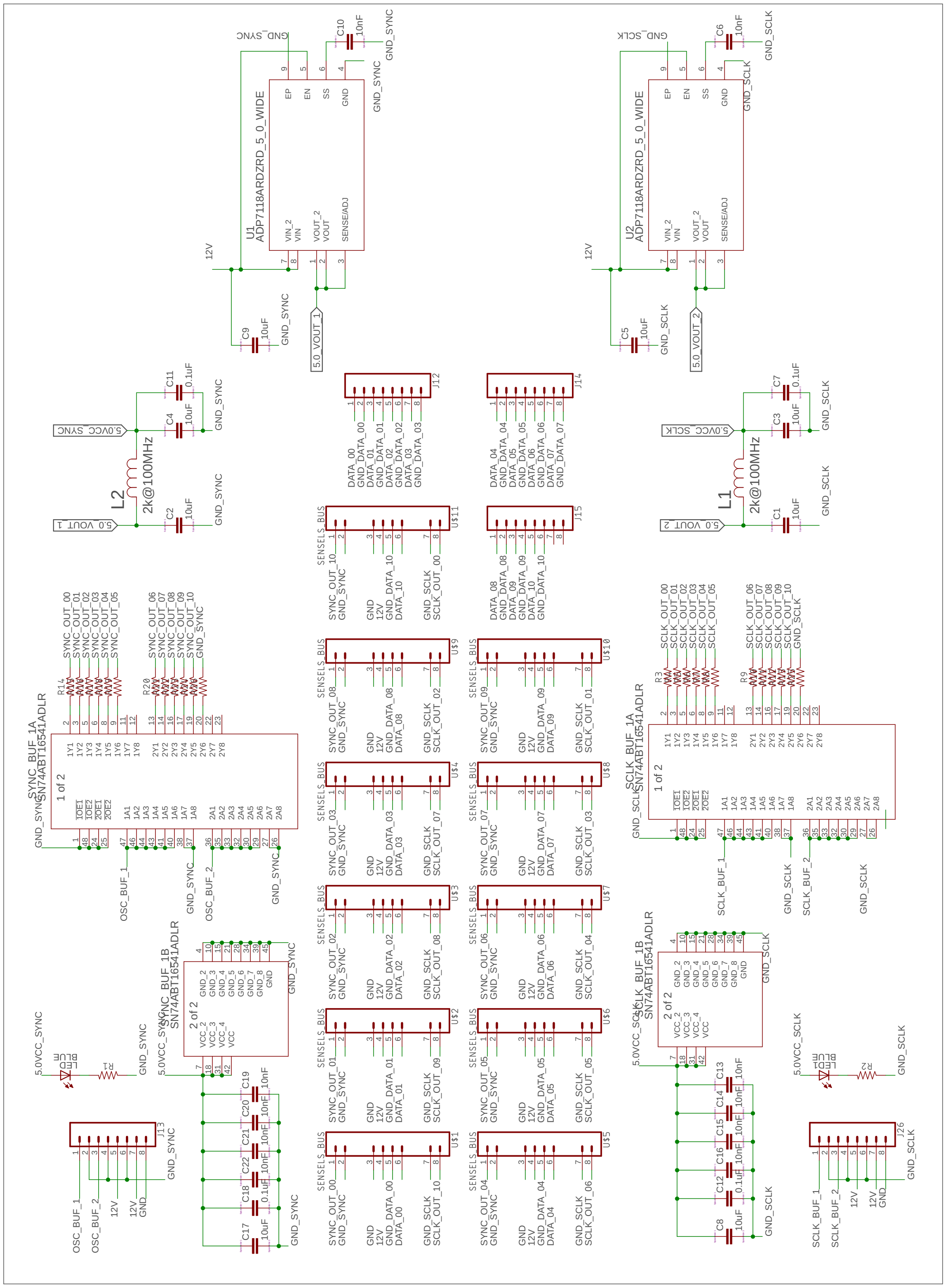

Figure C.3: Row Driver .

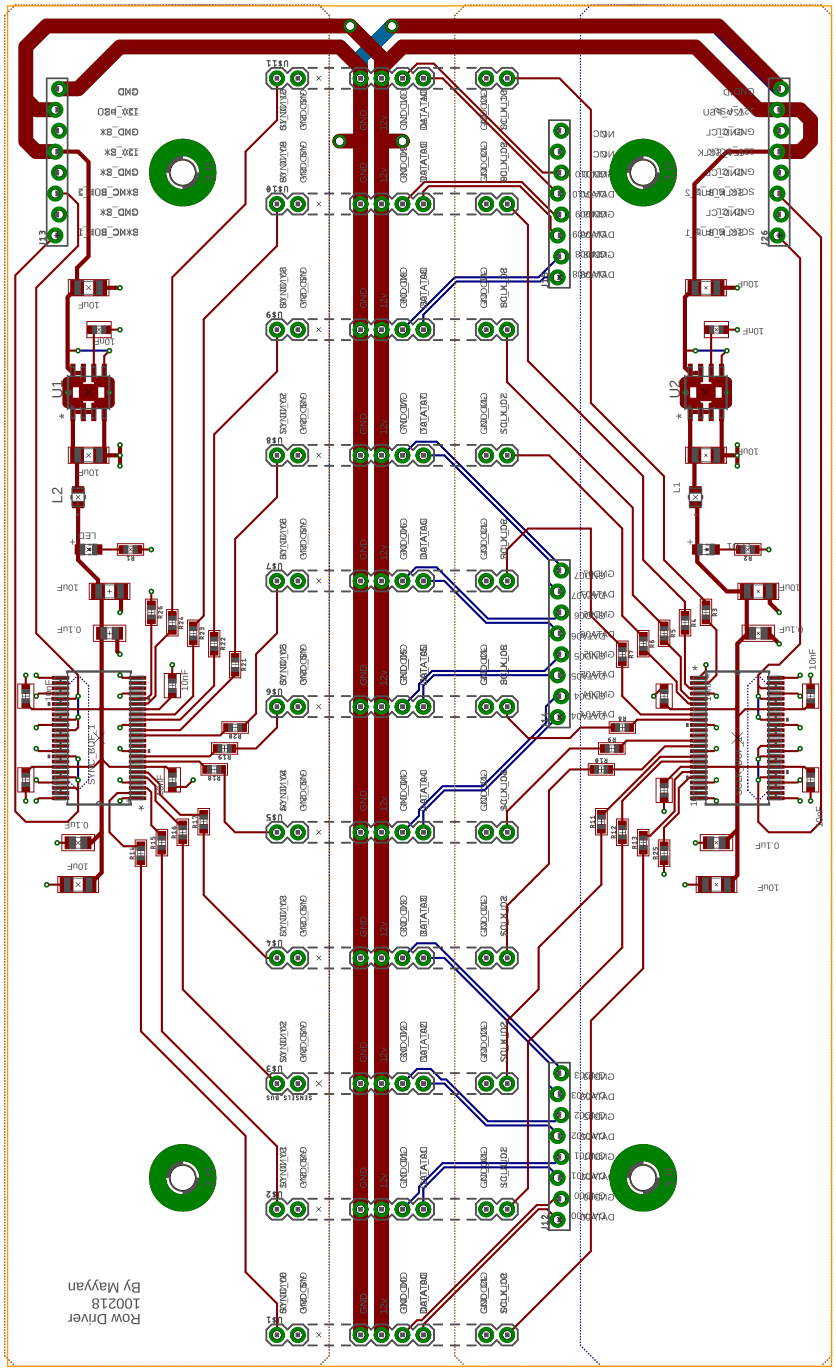

Figure C.4: Row Driver PCB.

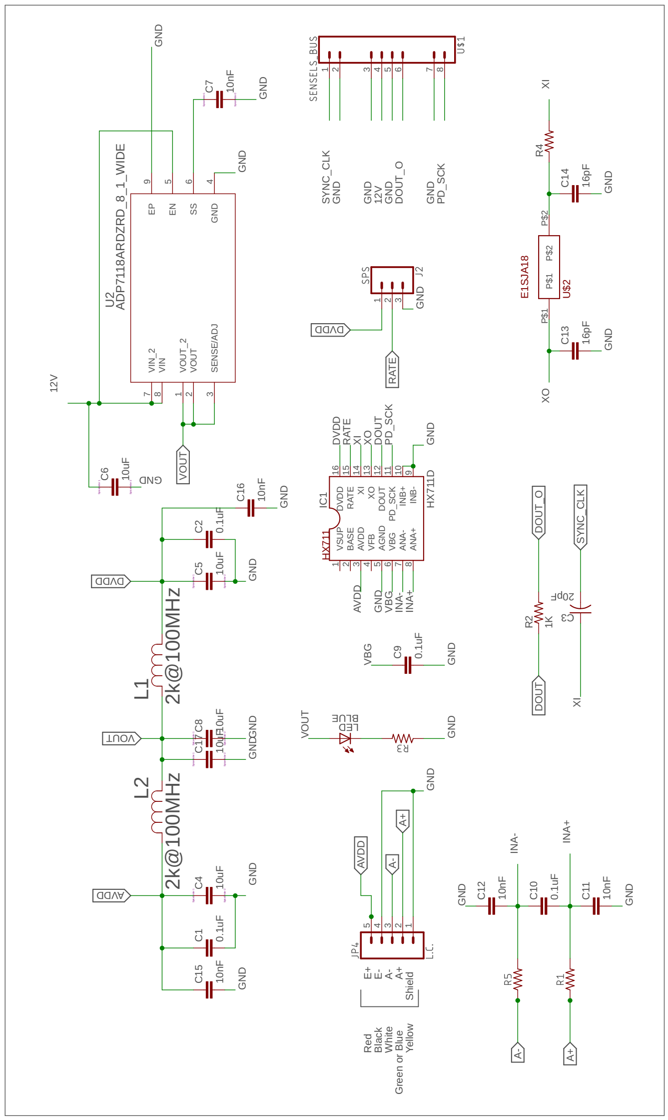

Figure C.5: Sensel board .

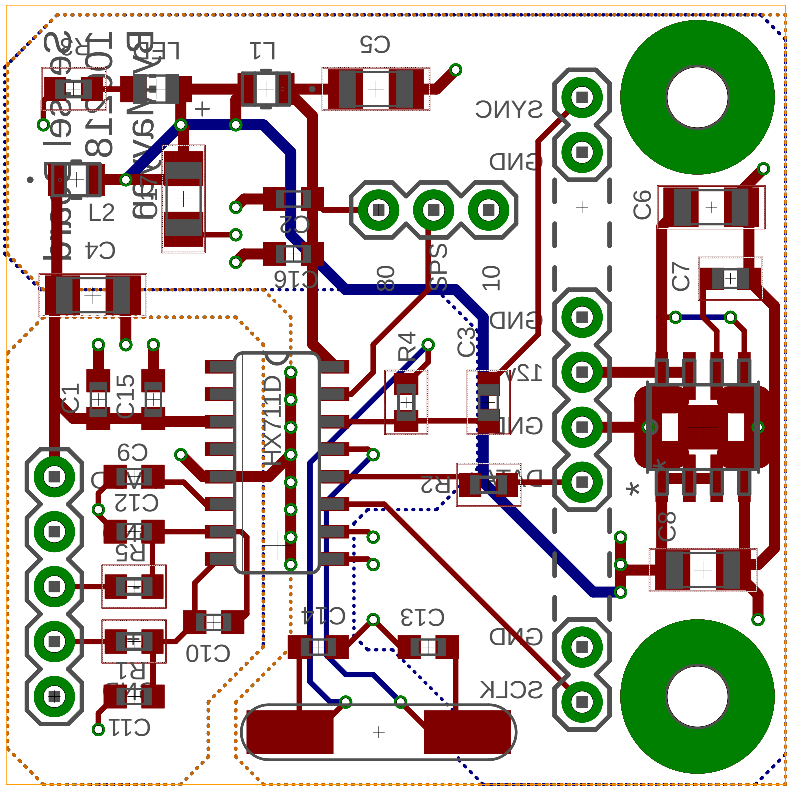

Figure C.6: Sensel board PCB.

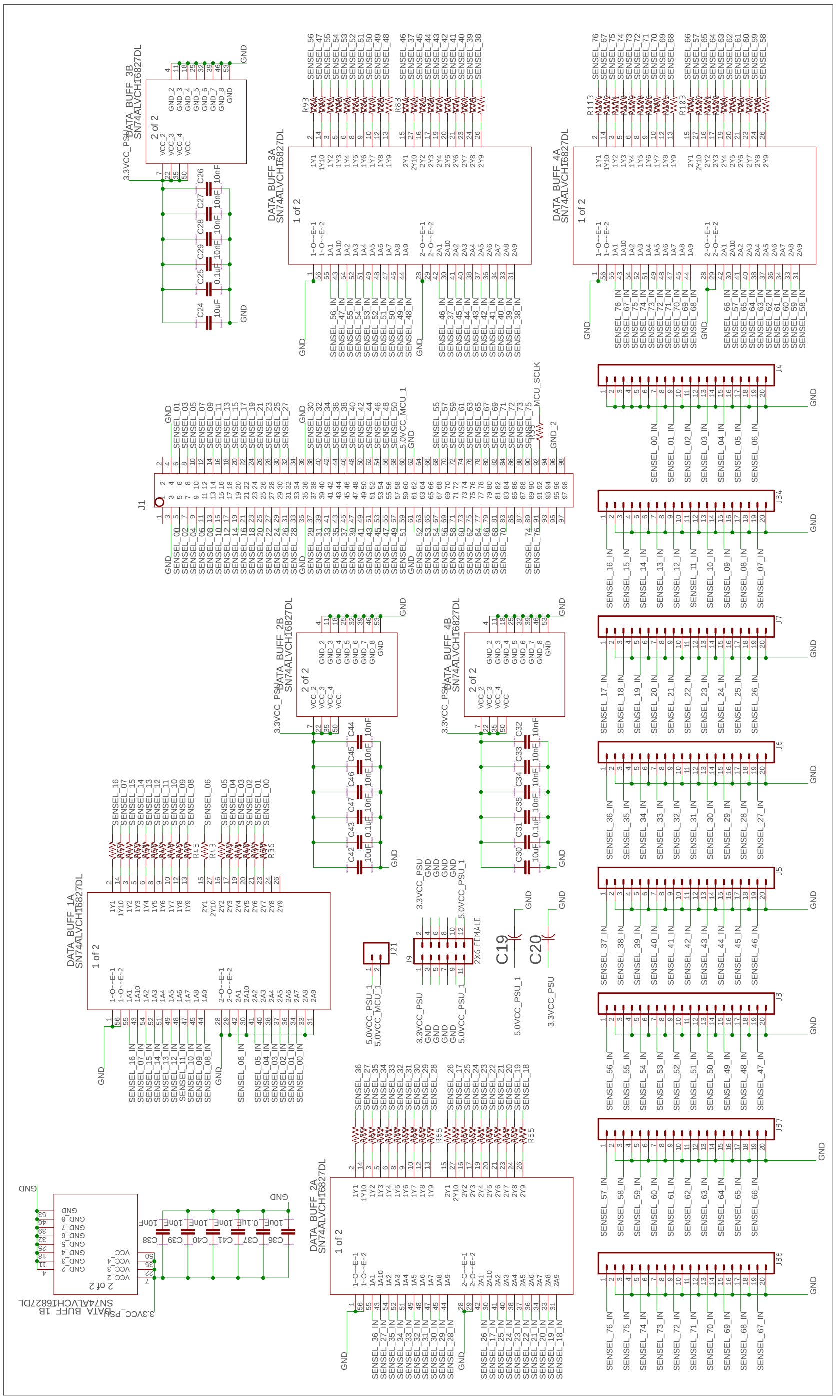

Figure C.7: Main board part 1.

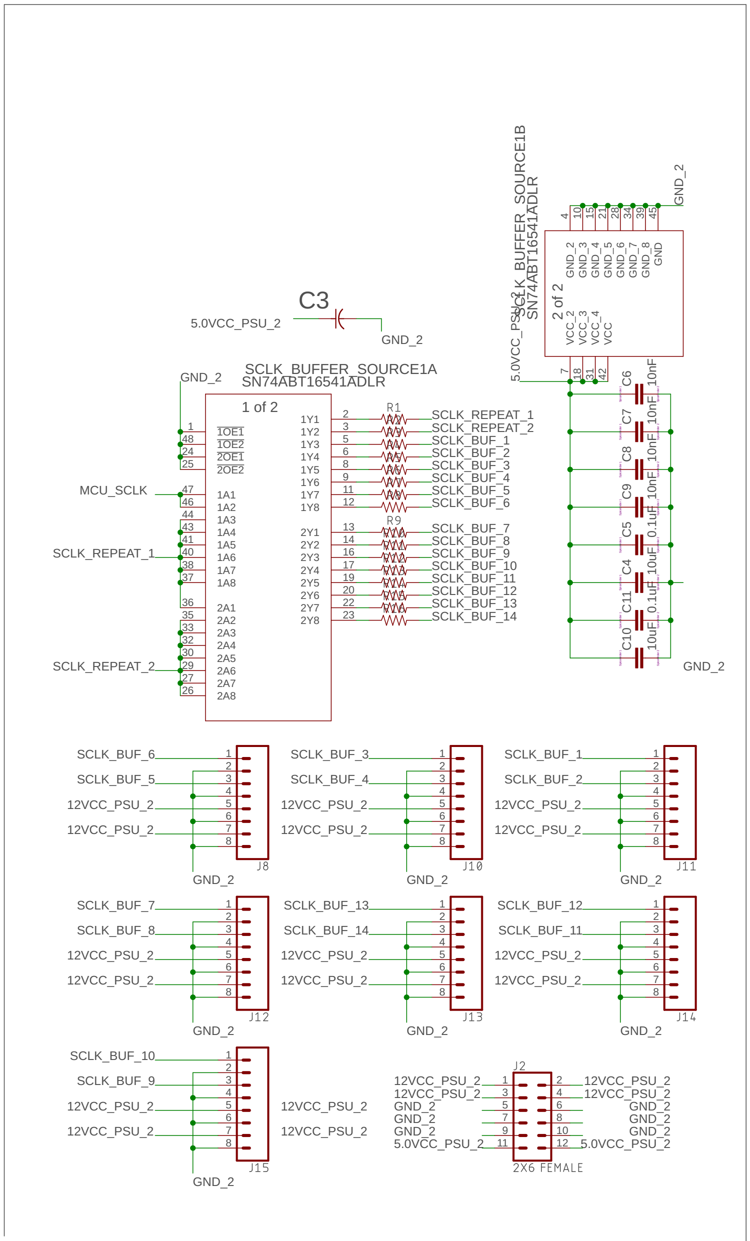

Figure C.8: Main board part 2.

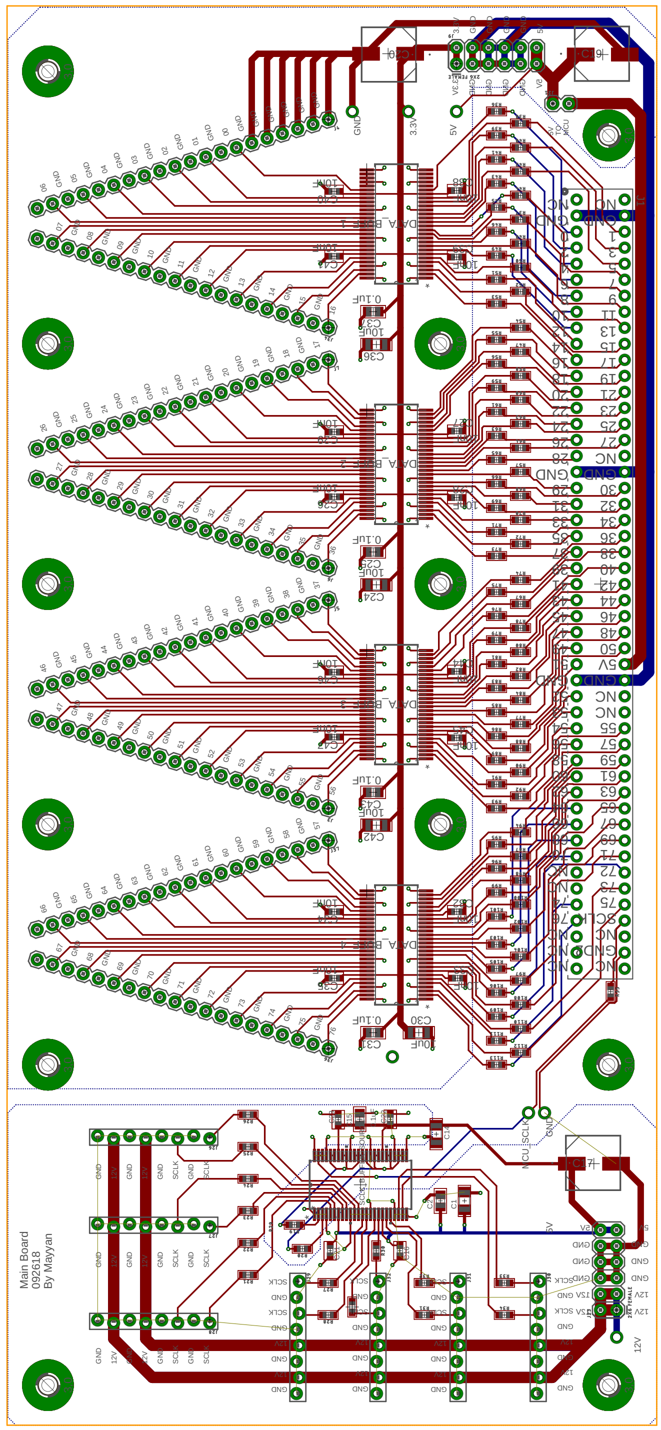

Figure C.9: Main board PCB.

Bibliography

[1] National Cancer Institutes, The Division of Cancer Control and Population Sciences (DCCPS), US, URL epi.grants.cancer.gov/asa24/ [Accessed 2022-04-04].

[2] National Institutes of Health (NIH), National Cancer Institute, US, "Automated Self-Administered 24-hour (ASA24®) Dietary Assessment Tool" URL asa24.nci.nih.gov/demo/ [Accessed 2022-04-04].

[3] Harvard T.H. Chan School of Public Health Nutrition Department's File Download Site URL regepi.bwh.harvard.edu/health/FFQ/files [Accessed 2022-04-04].

[4] World Health Organization. URL www.who.int/news-room/fact-sheets/detail/obesity-and-overweight [accessed 2022-02-09].

[5] Center of Disease Control and Prevention, US. URL www.cdc.gov/cdctv/diseaseandconditions/lifestyle/obesity-epidemic.html [Accessed 2022-03-24].

[6] World Health Organization, Regional Office for Europe. URL www.euro.who.int/en/media-centre/sections/press-releases/2022/new-who-report-europe-can-reverse-its-obesity-epidemic [accessed 2022-05-13].

[7] Center of Disease Control and Prevention, US. URL www.cdc.gov/healthyweight/effects/index.html [Accessed 2022-02-14].

[8] National Cancer Institute, US. URL www.cancer.gov/about-cancer/causes-prevention/risk/obesity/obesity-fact-sheet [Accessed 2022-02-14].

[9] World Health Organization. Diabetes. URL www.who.int/news-room/fact-sheets/detail/diabetes [Accessed 2022-03-20].

[10] National Institute of Diabetes and Digestive and Kidney Diseases (NIDDK), US. URL www.niddk.nih.gov/health-information/weight-management/adult-overweight-obesity/treatment [Accessed 2022-03-29].

[11] Clarifai, Inc. Clarifai URL www.clarifai.com [Accessed 2022-04-12].

[12] interFaceforce, URL www.interfaceforce.de/wp-content/uploads/2015/01/definitionen.pdf [Accessed 2022-02-22].

[13] Mahmoud Abdelaal, Carel W le Roux, and Neil G Docherty. Morbidity and mortality associated with obesity. *Annals of translational medicine*, 5(7), 2017.

[14] Abdullah S Al-Goblan, Mohammed A Al-Alfi, and Muhammad Z Khan. Mechanism linking diabetes mellitus and obesity. *Diabetes, metabolic syndrome and obesity: targets and therapy*, 7:587, 2014.

[15] Oliver Amft and Gerhard Troster. Methods for detection and classification of normal swallowing from muscle activation and sound. In *2006 Pervasive Health Conference and Workshops*, pages 1–10, 2006.

[16] Oliver Amft and Gerhard Tröster. Recognition of dietary activity events using on-body sensors. *Artificial Intelligence in Medicine*, 42(2):121–136, 2008. Wearable Computing and Artificial Intelligence for Healthcare Applications.

[17] Catherine J Andersen and Maria Luz Fernandez. Dietary strategies to reduce metabolic syndrome. *Reviews in Endocrine and Metabolic Disorders*, 14(3):241–254, 2013.

[18] David E Arterburn, Dana A Telem, Robert F Kushner, and Anita P Courcoulas. Benefits and risks of bariatric surgery in adults: a review. *Jama*, 324(9):879–887, 2020.

[19] Susan L Averett and David C Stifel. Race and gender differences in the cognitive effects of childhood overweight. *Applied Economics Letters*, 17(17):1673–1679, 2010.

[20] Adrienne R Barnosky, Kristin K Hoddy, Terry G Unterman, and Krista A Varady. Intermittent fasting vs daily calorie restriction for type 2 diabetes prevention: a review of human findings. *Translational Research*, 164(4):302–311, 2014.

[21] Brooke M Bell, Ridwan Alam, Nabil Alshurafa, Edison Thomaz, Abu S Mondol, Kayla de la Haye, John A Stankovic, John Lach, and Donna Spruijt-Metz. Automatic, wearable-based, in-field eating detection approaches for public health research: a scoping review. *NPJ digital medicine*, 3(1):1–14, 2020.

[22] Shengjie Bi, Tao Wang, Nicole Tobias, Josephine Nordrum, Shang Wang, George Halvorsen, Sougata Sen, Ronald Peterson, Kofi Odame, Kelly Caine, Ryan Halter, Jacob Sorber, and David Kotz. Auracle: Detecting eating episodes with an ear-mounted sensor. *Proc. ACM Interact. Mob. Wearable Ubiquitous Technol.*, 2(3), sep 2018.

[23] Yin Bi, Mingsong Lv, Chen Song, Wenyao Xu, Nan Guan, and Wang Yi. Autodietary: A wearable acoustic sensor system for food intake recognition in daily life. *IEEE Sensors Journal*, 16(3):806–816, 2015.

[24] Joan-Isaac Biel, Nathalie Martin, David Labbe, and Daniel Gatica-Perez. Bites 'n'bits: Inferring eating behavior from contextual mobile data. *Proceedings of the ACM on Interactive, Mobile, Wearable and Ubiquitous Technologies*, 1(4):1–33, 2018.

[25] Adam Biener, John Cawley, and Chad Meyerhoefer. The impact of obesity on medical care costs and labor market outcomes in the us. *Clinical chemistry*, 64(1):108–117, 2018.

[26] Sheila A Bingham. Urine nitrogen as a biomarker for the validation of dietary protein intake. *The Journal of nutrition*, 133(3):921S–924S, 2003.

[27] AE Black and TJ Cole. Within-and between-subject variation in energy expenditure measured by the doubly-labelled water technique: implications for validating reported dietary energy intake. *European journal of clinical nutrition*, 54(5):386–394, 2000.

[28] Nicole Black, David W Johnston, and Anna Peeters. Childhood obesity and cognitive achievement. *Health economics*, 24(9):1082–1100, 2015.

[29] J Blechert, M Liedlgruber, A Lender, J Reichenberger, and FH Wilhelm. Unobtrusive electromyography-based eating detection in daily life: A new tool to address underreporting? *Appetite*, 118:168–173, 2017.

[30] Maxence Bobin, Hamdi Amroun, Mehdi Boukalle, Margarita Anastassova, and Mehdi Ammi. Smart cup to monitor stroke patients activities during everyday life. In *2018 IEEE International Conference on Internet of Things (iThings) and IEEE Green Computing and Communications (GreenCom) and IEEE Cyber, Physical and Social Computing (CPSCom) and IEEE Smart Data (SmartData)*, pages 189–195. IEEE, 2018.

[31] Dieuwerke P Bolhuis, Ciaran G Forde, Yuejiao Cheng, Haohuan Xu, Nathalie Martin, and Cees de Graaf. Slow food: sustained impact of harder foods on the reduction in energy intake over the course of the day. *PloS one*, 9(4):e93370, 2014.

[32] James P Boyle, Theodore J Thompson, Edward W Gregg, Lawrence E Barker, and David F Williamson. Projection of the year 2050 burden of diabetes in the us adult population: dynamic modeling of incidence, mortality, and prediabetes prevalence. *Population health metrics*, 8(1):1–12, 2010.

[33] Maja Bramming, Maja B Jørgensen, Anne I Christensen, Cathrine J Lau, Kia K Egan, and Janne S Tolstrup. Bmi and labor market participation: a cohort study of transitions between work, unemployment, and sickness absence. *Obesity*, 27(10):1703–1710, 2019.

[34] Andrew W Brown, Stella Aslibekyan, Dennis Bier, Rafael Ferreira da Silva, Adam Hoover, David M Klurfeld, Eric Loken, Evan Mayo-Wilson, Nir Menachemi, Greg Pavela, et al. Toward more rigorous and informative nutritional epidemiology: The rational space between dismissal and defense of the status quo. *Critical Reviews in Food Science and Nutrition*, pages 1–18, 2021.

[35] Lora E Burke, Molly B Conroy, Susan M Sereika, Okan U Elci, Mindi A Styn, Sushama D Acharya, Mary A Sevick, Linda J Ewing, and Karen Glanz. The effect of electronic self-monitoring on weight loss and dietary intake: a randomized behavioral weight loss trial. *Obesity*, 19(2):338–344, 2011.

[36] Lora E Burke, Melanie Warziski, Terry Starrett, Jina Choo, Edvin Music, Susan Sereika, Susan Stark, and Mary Ann Sevick. Self-monitoring dietary intake: current and future practices. *Journal of Renal Nutrition*, 15(3):281–290, 2005.

[37] Tracy L Burrows, Rebecca J Martin, and Clare E Collins. A systematic review of the validity of dietary assessment methods in children when compared with the method of doubly labeled water. *Journal of the American Dietetic Association*, 110(10):1501–1510, 2010.

[38] Sydne J Carlson-Newberry and Rebecca B Costello. Emerging technologies for nutrition research: Potential for assessing military performance capability. 1997.

[39] John Cawley, Adam Biener, Chad Meyerhoefer, Yuchen Ding, Tracy Zvenyach, B NP, and Abhilasha Ramasamy. Job absenteeism costs of obesity in the united states. 2021.

[40] Simon Chakko, Manuel Mayor, Mark D Allison, Kenneth M Kessler, Barry J Materson, and Robert J Myerburg. Abnormal left ventricular diastolic filling in eccentric left ventricular hypertrophy of obesity. *The American journal of cardiology*, 68(1):95–98, 1991.

[41] June M Chan, Eric B Rimm, Graham A Colditz, Meir J Stampfer, and Walter C Willett. Obesity, fat distribution, and weight gain as risk factors for clinical diabetes in men. *Diabetes care*, 17(9):961–969, 1994.

[42] Keng-hao Chang, Shih-yen Liu, Hao-hua Chu, Jane Yung-jen Hsu, Cheryl Chen, Tung-yun Lin, Chieh-yu Chen, and Polly Huang. The diet-aware dining table: Observing dietary behaviors over a tabletop surface. In *International Conference on Pervasive Computing*, pages 366–382. Springer, 2006.

[43] Dinh-Toi Chu, Nguyen Thi Minh Nguyet, Thien Chu Dinh, Nguyen Vu Thai Lien, Khanh-Hoang Nguyen, Vo Truong Nhu Ngoc, Yang Tao, Duc-Hau Le, Vu Bich Nga, Adam Jurgoński, et al. An update on physical health and economic consequences of overweight and obesity. *Diabetes & Metabolic Syndrome: Clinical Research & Reviews*, 12(6):1095–1100, 2018.

[44] Keum San Chun, Sarnab Bhattacharya, and Edison Thomaz. Detecting eating episodes by tracking jawbone movements with a non-contact wearable sensor. *Proc. ACM Interact. Mob. Wearable Ubiquitous Technol.*, 2(1), mar 2018.

[45] Jungman Chung, Jungmin Chung, Wonjun Oh, Yongkyu Yoo, Won Gu Lee, and Hyunwoo Bang. A glasses-type wearable device for monitoring the patterns of food intake and facial activity. *Scientific Reports*, 7:41690, 2017.

[46] Rachel Cohen, Geoff Fernie, and Atena Roshan Fekr. Fluid intake monitoring systems for the elderly: a review of the literature. *Nutrients*, 13(6):2092, 2021.

[47] Graham A Colditz, Walter C Willett, Andrea Rotnitzky, and JoAnn E Manson. Weight gain as a risk factor for clinical diabetes mellitus in women. *Annals of internal medicine*, 122(7):481–486, 1995.

[48] Graham A Colditz, Walter C Willett, Meir J Stampfer, Joann E Manson, Charles H Hennekens, Ronald A Arky, and Frank E Speizer. Weight as a risk factor for clinical diabetes in women. *American journal of epidemiology*, 132(3):501–513, 1990.

[49] Anne Dahl Lassen, Sanne Poulsen, Lotte Ernst, Klaus Kaae Andersen, Anja Biltoft-Jensen, and Inge Tetens. Evaluation of a digital method to assess evening meal intake in a free-living adult population. *Food & nutrition research*, 54(1):5311, 2010.

[50] Andrew L Dannenberg, Deron C Burton, and Richard J Jackson. Economic and environmental costs of obesity: the impact on airlines. *American journal of preventive medicine*, 27(3):264, 2004.

[51] Maria Carlota Dao, Amy F Subar, Marisol Warthon-Medina, Janet E Cade, Tracy Burrows, Rebecca K Golley, Nita G Forouhi, Matthew Pearce, and Bridget A Holmes. Dietary assessment toolkits: an overview. *Public health nutrition*, 22(3):404–418, 2019.

[52] Bo Dong, Ryan Gallant, and Subir Biswas. A self-monitoring water bottle for tracking liquid intake. In *2014 IEEE Healthcare Innovation Conference (HIC)*, pages 311–314. IEEE, 2014.

[53] Yujie Dong, Adam Hoover, and Eric Muth. A device for detecting and counting bites of food taken by a person during eating. In *2009 IEEE International Conference on Bioinformatics and Biomedicine*, pages 265–268. IEEE, 2009.

[54] Yujie Dong, Adam Hoover, Jenna Scisco, and Eric Muth. A new method for measuring meal intake in humans via automated wrist motion tracking. *Applied psychophysiology and biofeedback*, 37(3):205–215, 2012.

[55] Yujie Dong, Jenna Scisco, Mike Wilson, Eric Muth, and Adam Hoover. Detecting periods of eating during free-living by tracking wrist motion. *IEEE journal of biomedical and health informatics*, 18(4):1253–1260, 2013.

[56] Robert H Eckel and Ronald M Krauss. American heart association call to action: obesity as a major risk factor for coronary heart disease. *Circulation*, 97(21):2099–2100, 1998.

[57] Kristina Elfhag, Britta Barkeling, Anna Maria Carlsson, and Stephan Rossner. Microstructure of eating behavior associated with rorschach characteristics in obesity. *Journal of Personality Assessment*, 81(1):40–50, 2003.

[58] Reynolette Ettienne-Gittens, Carol J Boushey, Donna Au, Suzanne P Murphy, Unhee Lim, and Lynne Wilkens. Evaluating the feasibility of utilizing the automated self-administered 24-hour (asa24) dietary recall in a sample of multiethnic older adults. *Procedia food science*, 2:134–144, 2013.

[59] Muhammad Farooq and Edward Sazonov. A novel wearable device for food intake and physical activity recognition. *Sensors*, 16(7):1067, 2016.

[60] Muhammad Farooq and Edward Sazonov. Accelerometer-based detection of food intake in free-living individuals. *IEEE sensors journal*, 18(9):3752–3758, 2018.

[61] Eric A Finkelstein, Marco daCosta DiBonaventura, Somali M Burgess, and Brent C Hale. The costs of obesity in the workplace. *Journal of Occupational and Environmental Medicine*, pages 971–976, 2010.

[62] Juan M Fontana, Muhammad Farooq, and Edward Sazonov. Automatic ingestion monitor: a novel wearable device for monitoring of ingestive behavior. *IEEE Transactions on Biomedical Engineering*, 61(6):1772–1779, 2014.

[63] Anna L Ford, Cecilia Bergh, Per Södersten, Matthew A Sabin, Sandra Hollinghurst, Linda P Hunt, and Julian PH Shield. Treatment of childhood obesity by retraining eating behaviour: randomised controlled trial. *Bmj*, 340, 2010.

[64] CG Forde, N Van Kuijk, T Thaler, C De Graaf, and N Martin. Oral processing characteristics of solid savoury meal components, and relationship with food composition, sensory attributes and expected satiation. *Appetite*, 60:208–219, 2013.

[65] Emma Foster, Clement Lee, Fumiaki Imamura, Stefanie E Hollidge, Kate L Westgate, Michelle C Venables, Ivan Poliakov, Maisie K Rowland, Timur Osadchiy, Jennifer C Bradley, et al. Validity and reliability of an online self-report 24-h dietary recall method (intake24): a doubly labelled water study and repeated-measures analysis. *Journal of nutritional science*, 8, 2019.

[66] Afful J. Fryar CD, Carroll MD. NCHS Health E-Stats, US. URL www.cdc.gov/nchs/data/hestat/obesity-adult-17-18/obesity-adult.htm [Accessed 2022-02-09].

[67] Sofiya Gancheva, Tomas Jelenik, Elisa Alvarez-Hernandez, and Michael Roden. Interorgan metabolic crosstalk in human insulin resistance. *Physiological reviews*, 98(3):1371–1415, 2018.

[68] Chuhan Gao, Yilong Li, and Xinyu Zhang. {LiveTag}: Sensing {Human-Object} interaction through passive chipless {WiFi} tags. In *15th USENIX Symposium on Networked Systems Design and Implementation (NSDI 18)*, pages 533–546, 2018.

[69] Yang Gao, Ning Zhang, Honghao Wang, Xiang Ding, Xu Ye, Guanling Chen, and Yu Cao. ihear food: eating detection using commodity bluetooth headsets. In *2016 IEEE First International Conference on Connected Health: Applications, Systems and Engineering Technologies (CHASE)*, pages 163–172. IEEE, 2016.

[70] Luke Gemming, Jennifer Utter, and Cliona Ni Mhurchu. Image-assisted dietary assessment: a systematic review of the evidence. *Journal of the Academy of Nutrition and Dietetics*, 115(1):64–77, 2015.

[71] Mitchell Gersovitz, J Patrick Madden, and Helen Smiciklas-Wright. Validity of the 24-hr. dietary recall and seven-day record for group comparisons. *Journal of the American Dietetic Association*, 73(1):48–55, 1978.

[72] Annelies HC Goris, Margriet S Westerterp-Plantenga, and Klaas R Westerterp. Undereating and underrecording of habitual food intake in obese men: selective underreporting of fat intake. *The American journal of clinical nutrition*, 71(1):130–134, 2000.

[73] Henry Griffith, Yan Shi, and Subir Biswas. A container-attachable inertial sensor for real-time hydration tracking. *Sensors*, 19(18), 2019.

[74] Erik J Groessl, Robert M Kaplan, Elizabeth Barrett-Connor, and Theodore G Ganiats. Body mass index and quality of well-being in a community of older adults. *American Journal of Preventive Medicine*, 26(2):126–129, 2004.

[75] Scott M Grundy. Obesity, metabolic syndrome, and cardiovascular disease. *The Journal of Clinical Endocrinology & Metabolism*, 89(6):2595–2600, 2004.

[76] Cagatay Gumus, Kadir Ozlem, Fidan Khalilbayli, Omur Fatmanur Erzurumluoglu, Gokhan Ince, Ozgur Atalay, and Asli Tuncay Atalay. Textile-based pressure sensor arrays: A novel scalable manufacturing technique. *Micro and Nano Engineering*, 15:100140, 2022.

[77] Juliet AM Haarman, Roelof AJ de Vries, Emiel C Harmsen, Hermie J Hermens, and Dirk KJ Heylen. Sensory interactive table (sit)—development of a measurement instrument to support healthy eating in a social dining setting. *Sensors*, 20(9):2636, 2020.

[78] Valisa E Hedrick, Andrea M Dietrich, Paul A Estabrooks, Jyoti Savla, Elena Serrano, and Brenda M Davy. Dietary biomarkers: advances, limitations and future directions. *Nutrition journal*, 11(1):1–14, 2012.

[79] Kelly A Hirko, Elizabeth D Kantor, Sarah S Cohen, William J Blot, Meir J Stampfer, and Lisa B Signorello. Body mass index in young adulthood, obesity trajectory, and premature mortality. *American journal of epidemiology*, 182(5):441–450, 2015.

[80] Kalon KL Ho, Joan L Pinsky, William B Kannel, and Daniel Levy. The epidemiology of heart failure: the framingham study. *Journal of the American College of Cardiology*, 22(4):A6–A13, 1993.

[81] Steve Hodges, Lyndsay Williams, Emma Berry, Shahram Izadi, James Srinivasan, Alex Butler, Gavin Smyth, Narinder Kapur, and Ken Wood. Sensecam: A retrospective memory aid. In Paul Dourish and Adrian Friday, editors, *UbiComp 2006: Ubiquitous Computing*, pages 177–193, Berlin, Heidelberg, 2006. Springer Berlin Heidelberg.

[82] Clemens Holzmann and Andreas Hader. Towards tabletop interaction with everyday artifacts via pressure imaging. In *Proceedings of the fourth international conference on Tangible, embedded, and embodied interaction*, pages 77–84. ACM, 2010.

[83] Adam Hoover and Edward Sazonov. Measuring human energy intake and ingestive behavior: Challenges and opportunities [from the technical committees]. *IEEE Pulse*, 7(6):6–7, 2016.

[84] Qianyi Huang, Wei Wang, and Qian Zhang. Your glasses know your diet: Dietary monitoring using electromyography sensors. *IEEE Internet of Things Journal*, 2017.

[85] Qianyi Huang, Zhice Yang, and Qian Zhang. Smart-u: Smart utensils know what you eat. In *IEEE INFOCOM 2018-IEEE Conference on Computer Communications*, pages 1439–1447. IEEE, 2018.

[86] Yan Huang, Yun Chen, Xiangyu Fan, Ningqi Luo, Shuang Zhou, Shih-Chi Chen, Ni Zhao, and Ching Ping Wong. Wood derived composites for high sensitivity and wide linear-range pressure sensing. *Small*, 14(31):1801520, 2018.

[87] Yan Huang, Xiangyu Fan, Shih-Chi Chen, and Ni Zhao. Emerging technologies of flexible pressure sensors: materials, modeling, devices, and manufacturing. *Advanced Functional Materials*, 29(12):1808509, 2019.

[88] R Hubel, RG Laessle, S Lehrke, and J Jass. Laboratory measurement of cumulative food intake in humans: Results on reliability. *Appetite*, 46(1):57–62, 2006.

[89] Helen B Hubert, Manning Feinleib, Patricia M McNamara, and William P Castelli. Obesity as an independent risk factor for cardiovascular disease: a 26-year follow-up of participants in the framingham heart study. *Circulation*, 67(5):968–977, 1983.

[90] Sheldon H Jacobson and Douglas M King. Measuring the potential for automobile fuel savings in the us: the impact of obesity. *Transportation research part D: transport and environment*, 14(1):6–13, 2009.

[91] Sheldon H Jacobson and Laura A McLay. The economic impact of obesity on automobile fuel consumption. *The Engineering Economist*, 51(4):307–323, 2006.

[92] Gunn Signe Jakobsen, Milada Cvancarova Småstuen, Rune Sandbu, Njord Nordstrand, Dag Hofsø, Morten Lindberg, Jens Kristoffer Hertel, and Jøran Hjelmesæth. Association of bariatric surgery vs medical obesity treatment with long-term medical complications and obesity-related comorbidities. *JAMA*, 319(3):291–301, 2018.

[93] Wenyan Jia, Yuecheng Li, Ruowei Qu, Thomas Baranowski, Lora E Burke, Hong Zhang, Yicheng Bai, Juliet M Mancino, Guizhi Xu, Zhi-Hong Mao, et al. Automatic food detection in egocentric images using artificial intelligence technology. *Public health nutrition*, 22(7):1168–1179, 2019.

[94] Azusa Kadomura, Cheng-Yuan Li, Koji Tsukada, Hao-Hua Chu, and Itiro Siio. Persuasive technology to improve eating behavior using a sensor-embedded fork. In *Proceedings of the 2014 acm international joint conference on pervasive and ubiquitous computing*, pages 319–329, 2014.

[95] Steven E Kahn, Rebecca L Hull, and Kristina M Utzschneider. Mechanisms linking obesity to insulin resistance and type 2 diabetes. *Nature*, 444(7121):840–846, 2006.

[96] Haik Kalantarian, Nabil Alshurafa, and Majid Sarrafzadeh. A survey of diet monitoring technology. *IEEE Pervasive Computing*, 16(1):57–65, 2017.

[97] Haik Kalantarian and Majid Sarrafzadeh. Audio-based detection and evaluation of eating behavior using the smartwatch platform. *Computers in biology and medicine*, 65:1–9, 2015.

[98] Dean M Karantonis, Michael R Narayanan, Merryn Mathie, Nigel H Lovell, and Branko G Celler. Implementation of a real-time human movement classifier using a triaxial accelerometer for ambulatory monitoring. *IEEE transactions on information technology in biomedicine*, 10(1):156–167, 2006.

[99] Erik A Karlsson and Melinda A Beck. The burden of obesity on infectious disease. *Experimental biology and medicine*, 235(12):1412–1424, 2010.

[100] Satish Kenchaiah, Jane C Evans, Daniel Levy, Peter WF Wilson, Emelia J Benjamin, Martin G Larson, William B Kannel, and Ramachandran S Vasan. Obesity and the risk of heart failure. *New England Journal of Medicine*, 347(5):305–313, 2002.

[101] Syed Afroz Keramat, Khorshed Alam, Jeff Gow, and Stuart JH Biddle. Gender differences in the longitudinal association between obesity, and disability with workplace absenteeism in the australian working population. *PloS one*, 15(5):e0233512, 2020.

[102] Sharon I Kirkpatrick, Anne M Gilsing, Erin Hobin, Nathan M Solbak, Angela Wallace, Jess Haines, Alexandra J Mayhew, Sarah K Orr, Parminder Raina, Paula J Robson, et al. Lessons from studies to evaluate an online 24-hour recall for use with children and adults in canada. *Nutrients*, 9(2):100, 2017.

[103] HARRY R Kissileff, GARY Klingsberg, and THEODORE B Van Itallie. Universal eating monitor for continuous recording of solid or liquid consumption in man. *American Journal of Physiology-Regulatory, Integrative and Comparative Physiology*, 238(1):R14–R22, 1980.

[104] Harry R Kissileff, F Xavier Pi-Sunyer, John Thornton, and Gerard P Smith. C-terminal octapeptide of cholecystokinin decreases food intake in man. *The American journal of clinical nutrition*, 34(2):154–160, 1981.

[105] Harry R Kissileff, John Thornton, and Emil Becker. A quadratic equation adequately describes the cumulative food intake curve in man. *Appetite*, 3(3):255–272, 1982.

[106] Pauline Koh-Banerjee, Youfa Wang, Frank B Hu, Donna Spiegelman, Walter C Willett, and Eric B Rimm. Changes in body weight and body fat distribution as risk factors for clinical diabetes in us men. *American journal of epidemiology*, 159(12):1150–1159, 2004.

[107] Chrysi Koliaki, Stavros Liatis, and Alexander Kokkinos. Obesity and cardiovascular disease: revisiting an old relationship. *Metabolism*, 92:98–107, 2019.

[108] Joachim F Kreutzer, Jannai Flaschberger, Christina M Hein, and Tim C Lueth. Capacitive detection of filling levels in a cup. In *2016 IEEE 13th International Conference on Wearable and Implantable Body Sensor Networks (BSN)*, pages 31–36. IEEE, 2016.

[109] Chayakrit Krittanawong, Anusith Tunhasiriwet, Zhen Wang, HongJu Zhang, Larry J Prokop, Sakkarin Chirapongsathorn, Tao Sun, Takeshi Kitai, and WH Wilson Tang. Meta-analysis comparing frequency of overweight versus normal weight in patients with new-onset heart failure. *The American Journal of Cardiology*, 121(7):836–843, 2018.

[110] Anja Kroke, Kerstin Klipstein-Grobusch, Susanne Voss, Jutta Möseneder, Frank Thielecke, Rudolf Noack, and Heiner Boeing. Validation of a self-administered food-frequency questionnaire administered in the european prospective investigation into cancer and nutrition (epic) study: comparison of energy, protein, and macronutrient intakes estimated with the doubly labeled water, urinary nitrogen, and repeated 24-h dietary recall methods. *The American journal of clinical nutrition*, 70(4):439–447, 1999.

[111] Emma M Krop, Marion M Hetherington, Chandani Nekitsing, Sophie Miquel, Luminita Postelnicu, and Anwesha Sarkar. Influence of oral processing on appetite and food intake–a systematic review and meta-analysis. *Appetite*, 125:253–269, 2018.

[112] Konstantinos Kyritsis, Christos Diou, and Anastasios Delopoulos. Food intake detection from inertial sensors using lstm networks. In *International conference on image analysis and processing*, pages 411–418. Springer, 2017.

[113] Konstantinos Kyritsis, Christos Diou, and Anastasios Delopoulos. Modeling wrist micromovements to measure in-meal eating behavior from inertial sensor data. *IEEE journal of biomedical and health informatics*, 23(6):2325–2334, 2019.

[114] Konstantinos Kyritsis, Christina Lefkothea Tatli, Christos Diou, and Anastasios Delopoulos. Automated analysis of in meal eating behavior using a commercial wristband imu sensor. In *2017 39th Annual International Conference of the IEEE Engineering in Medicine and Biology Society (EMBC)*, pages 2843–2846. IEEE, 2017.

[115] Béatrice Lauby-Secretan, Chiara Scoccianti, Dana Loomis, Yann Grosse, Franca Bianchini, and Kurt Straif. Body fatness and cancer—viewpoint of the iarc working group. *New England journal of medicine*, 375(8):794–798, 2016.

[116] Ki-Seung Lee. Joint audio-ultrasound food recognition for noisy environments. *IEEE Journal of Biomedical and Health Informatics*, 24(5):1477–1489, 2020.

[117] Zairan Li, Dan Wang, Nilanjan Dey, Amira S Ashour, R Simon Sherratt, and Fuqian Shi. Plantar pressure image fusion for comfort fusion in diabetes mellitus using an improved fuzzy hidden markov model. *Biocybernetics and Biomedical Engineering*, 39(3):742–752, 2019.

[118] Zhaoling Li, Miaomiao Zhu, Jiali Shen, Qian Qiu, Jianyong Yu, and Bin Ding. All-fiber structured electronic skin with high elasticity and breathability. *Advanced Functional Materials*, 30(6):1908411, 2020.

[119] Yvonne Linné, Britta Barkeling, Stephan Rössner, and Pål Rooth. Vision and eating behavior. *Obesity research*, 10(2):92–95, 2002.

[120] Jindong Liu, Edward Johns, Louis Atallah, Claire Pettitt, Benny Lo, Gary Frost, and Guang-Zhong Yang. An intelligent food-intake monitoring system using wearable sensors. In *2012 ninth international conference on wearable and implantable body sensor networks*, pages 154–160. IEEE, 2012.

[121] Yuhan Luo, Peiyi Liu, and Eun Kyoung Choe. Co-designing food trackers with dietitians: Identifying design opportunities for food tracker customization. In *Proceedings of the 2019 CHI Conference on Human Factors in Computing Systems*, pages 1–13, 2019.

[122] John I Malone and Barbara C Hansen. Does obesity cause type 2 diabetes mellitus (t2dm)? or is it the opposite? *Pediatric diabetes*, 20(1):5–9, 2019.

[123] JoAnn E Manson, Graham A Colditz, Meir J Stampfer, Walter C Willett, Bernard Rosner, Richard R Monson, Frank E Speizer, and Charles H Hennekens. A prospective study of obesity and risk of coronary heart disease in women. *New England journal of medicine*, 322(13):882–889, 1990.

[124] Sean Manton, Greta Magerowski, Laura Patriarca, and Miguel Alonso-Alonso. The "smart dining table": Automatic behavioral tracking of a meal with a multi-touch-computer. *Frontiers in psychology*, 7, 2016.

[125] Corby K Martin, John B Correa, Hongmei Han, H Raymond Allen, Jennifer C Rood, Catherine M Champagne, Bahadir K Gunturk, and George A Bray. Validity of the remote food photography method (rfpm) for estimating energy and nutrient intake in near real-time. *Obesity*, 20(4):891–899, 2012.

[126] Boban Mathew, Lisa Francis, Attila Kayalar, and Jesse Cone. Obesity: effects on cardiovascular disease and its diagnosis. *The Journal of the American Board of Family Medicine*, 21(6):562–568, 2008.

[127] Ryan S Mattfeld, Eric R Muth, and Adam Hoover. Measuring the consumption of individual solid and liquid bites using a table-embedded scale during unrestricted eating. *IEEE journal of biomedical and health informatics*, 21(6):1711–1718, 2016.

[128] Gert Mertes, Glenn Christiaensen, Hans Hallez, Sammy Verslype, Wei Chen, and Bart Vanrumste. Measuring weight and location of individual bites using a sensor augmented smart plate. In *2018 40th Annual International Conference of the IEEE Engineering in Medicine and Biology Society (EMBC)*, pages 5558–5561. IEEE, 2018.

[129] Gert Mertes, Li Ding, Wei Chen, Hans Hallez, Jie Jia, and Bart Vanrumste. Measuring and localizing individual bites using a sensor augmented plate during unrestricted eating for the aging population. *IEEE journal of biomedical and health informatics*, 24(5):1509–1518, 2019.

[130] Franz H Messerli, Hector O Ventura, Efrain Reisin, Gerald R Dreslinski, Francis G Dunn, Allan A MacPhee, and ED Frohlich. Borderline hypertension and obesity: two prehypertensive states with elevated cardiac output. *Circulation*, 66(1):55–60, 1982.

[131] Mark Mirtchouk, Drew Lustig, Alexandra Smith, Ivan Ching, Min Zheng, and Samantha Kleinberg. Recognizing eating from body-worn sensors: Combining free-living and laboratory data. *Proc. ACM Interact. Mob. Wearable Ubiquitous Technol.*, 1(3), sep 2017.

[132] Mark Mirtchouk, Christopher Merck, and Samantha Kleinberg. Automated estimation of food type and amount consumed from body-worn audio and motion sensors. In *Proceedings of the 2016 ACM International Joint Conference on Pervasive and Ubiquitous Computing*, pages 451–462. ACM, 2016.

[133] Ivan Muller, Renato Machado de Brito, Carlos Eduardo Pereira, and Valner Brusamarello. Load cells in force sensing analysis–theory and a novel application. *IEEE Instrumentation & Measurement Magazine*, 13(1):15–19, 2010.

[134] Ronald G Munger, Aaron R Folsom, Lawrence H Kushi, Susan A Kaye, and Thomas A Sellers. Dietary assessment of older iowa women with a food frequency questionnaire: nutrient intake, reproducibility, and comparison with 24-hour dietary recall interviews. *American journal of epidemiology*, 136(2):192–200, 1992.

[135] Kazuya Murao, Junna Imai, Tsutomu Terada, and Masahiko Tsukamoto. Activity recognition and user identification based on tabletop activities with load cells. *Journal of Information Processing*, 25:59–66, 2017.

[136] Christopher JL Murray, Aleksandr Y Aravkin, Peng Zheng, Cristiana Abbafati, Kaja M Abbas, Mohsen Abbasi-Kangevari, Foad Abd-Allah, Ahmed Abdelalim, Mohammad Abdollahi, Ibrahim Abdollahpour, et al. Global burden of 87 risk factors in 204 countries and territories, 1990–2019: a systematic analysis for the global burden of disease study 2019. *The Lancet*, 396(10258):1223–1249, 2020.

[137] Akihiro Nakamura, Takato Saito, Daizo Ikeda, Ken Ohta, Hiroshi Mineno, and Masafumi Nishimura. Automatic detection of chewing and swallowing using multichannel sound information. In *2021 IEEE 3rd Global Conference on Life Sciences and Technologies (LifeTech)*, pages 173–175, 2021.

[138] David C Nieman, Dru A Henson, Sandra L Nehlsen-Cannarella, Melinda Ekkens, Alan C Utter, Diane E Butterworth, and Omar R Fagoaga. Influence of obesity on immune function. *Journal of the American Dietetic Association*, 99(3):294–299, 1999.

[139] Gillian O'Loughlin, Sarah Jane Cullen, Adrian McGoldrick, Siobhan O'Connor, Richard Blain, Shane O'Malley, and Giles D. Warrington. Using a wearable camera to increase the accuracy of dietary analysis. *American Journal of Preventive Medicine*, 44(3):297–301, 2013.

[140] Temiloluwa Olubanjo and Maysam Ghovanloo. Real-time swallowing detection based on tracheal acoustics. In *2014 IEEE International Conference on Acoustics, Speech and Signal Processing (ICASSP)*, pages 4384–4388, 2014.

[141] Rosa M Ortega, Carmen Pérez-Rodrigo, and Ana M López-Sobaler. Dietary assessment methods: dietary records. *Nutricion hospitalaria*, 31(3):38–45, 2015.

[142] Lijia Pan, Alex Chortos, Guihua Yu, Yaqun Wang, Scott Isaacson, Ranulfo Allen, Yi Shi, Reinhold Dauskardt, and Zhenan Bao. An ultra-sensitive resistive pressure sensor based on hollow-sphere microstructure induced elasticity in conducting polymer film. *Nature communications*, 5(1):1–8, 2014.

[143] Vasileios Papapanagiotou, Christos Diou, and Anastasios Delopoulos. Chewing detection from an in-ear microphone using convolutional neural networks. In *2017 39th Annual International Conference of the IEEE Engineering in Medicine and Biology Society (EMBC)*, pages 1258–1261, 2017.

[144] Vasileios Papapanagiotou, Christos Diou, Ioannis Ioakimidis, Per Södersten, and Anastasios Delopoulos. Automatic analysis of food intake and meal microstructure based on continuous weight measurements. *IEEE journal of biomedical and health informatics*, 23(2):893–902, 2018.

[145] Vasileios Papapanagiotou, Christos Diou, Billy Langlet, Ioannis Ioakimidis, and Anastasios Delopoulos. Automated extraction of food intake indicators from continuous meal weight measurements. In *International Conference on Bioinformatics and Biomedical Engineering*, pages 35–46. Springer, 2015.

[146] Vasileios Papapanagiotou, Christos Diou, Billy Langlet, Ioannis Ioakimidis, and Anastasios Delopoulos. A parametric probabilistic context-free grammar for food intake analysis based on continuous meal weight measurements. In *2015 37th annual international conference of the IEEE Engineering in Medicine and Biology Society (EMBC)*, pages 7853–7856. IEEE, 2015.

[147] Sebastian Päßler, Matthias Wolff, and Wolf-Joachim Fischer. Food intake monitoring: an acoustical approach to automated food intake activity detection and classification of consumed food. *Physiological measurement*, 33(6):1073, 2012.

[148] Alaina L Pearce, Maria C Cevallos, Olivia Romano, Elodie Daoud, and Kathleen L Keller. Child meal microstructure and eating behaviors: A systematic review. *Appetite*, 168:105752, 2022.

[149] Erika L Pearce and Hao Shen. Making sense of inflammation, epigenetics, and memory cd8+ t-cell differentiation in the context of infection. *Immunological reviews*, 211(1):197–202, 2006.

[150] S. Pereira, R. Simoes, J. Fonseca, R. Carvalho, and J. Almeida. Textile embedded sensors matrix for pressure sensing and monitoring applications for the pressure ulcer prevention. In *2018 International Conference on Biomedical Engineering and Applications (ICBEA)*, pages 1–6, July 2018.

[151] Claire Pettitt, Jindong Liu, Richard M Kwasnicki, Guang-Zhong Yang, Thomas Preston, and Gary Frost. A pilot study to determine whether using a lightweight, wearable micro-camera improves dietary assessment accuracy and offers information on macronutrients and eating rate. *British Journal of Nutrition*, 115(1):160–167, 2016.

[152] Joshua C Pinkston. The dynamic effects of obesity on the wages of young workers. *Economics & Human Biology*, 27:154–166, 2017.

[153] Benoit Plourde, Jean-François Sarrazin, Isabelle Nault, and Paul Poirier. Sudden cardiac death and obesity. *Expert review of cardiovascular therapy*, 12(9):1099–1110, 2014.

[154] JMC Po, JA Kieser, Luigi M Gallo, AJ Tésenyi, P Herbison, and Mauro Farella. Time-frequency analysis of chewing activity in the natural environment. *Journal of dental research*, 90(10):1206–1210, 2011.

[155] Paul Poirier, Thomas D Giles, George A Bray, Yuling Hong, Judith S Stern, F Xavier Pi-Sunyer, and Robert H Eckel. Obesity and cardiovascular disease: pathophysiology, evaluation, and effect of weight loss: an update of the 1997 american heart association scientific statement on obesity and heart disease from the obesity committee of the council on nutrition, physical activity, and metabolism. *Circulation*, 113(6):898–918, 2006.

[156] Parisa Pouladzadeh, Shervin Shirmohammadi, and Rana Al-Maghrabi. Measuring calorie and nutrition from food image. *IEEE Transactions on Instrumentation and Measurement*, 63(8):1947–1956, 2014.

[157] Temiloluwa Prioleau, Elliot Moore, and Maysam Ghovanloo. Unobtrusive and Wearable Systems for Automatic Dietary Monitoring. *IEEE Transactions on Biomedical Engineering*, 2017.

[158] Nicolaas P Pronk, Michael J Goodman, Patrick J O'Connor, and Brian C Martinson. Relationship between modifiable health risks and short-term health care charges. *Jama*, 282(23):2235–2239, 1999.

[159] Simon W Rabkin, Francis AL Mathewson, and Ping-Hwa Hsu. Relation of body weight to development of ischemic heart disease in a cohort of young north american men after a 26 year observation period: the manitoba study. *The American journal of cardiology*, 39(3):452–458, 1977.

[160] Laavanya Rachakonda, Saraju P Mohanty, and Elias Kougianos. ilog: an intelligent device for automatic food intake monitoring and stress detection in the iomt. *IEEE Transactions on Consumer Electronics*, 66(2):115–124, 2020.

[161] Viprav B Raju and Edward Sazonov. A systematic review of sensor-based methodologies for food portion size estimation. *IEEE Sensors Journal*, 21(11):12882–12899, 2020.

[162] Abhilasha Ramasamy, François Laliberté, Shoghag A Aktavoukian, Dominique Lejeune, Maral DerSarkissian, Cristi Cavanaugh, B Gabriel Smolarz, Rahul Ganguly, and Mei Sheng Duh. Direct, absenteeism, and disability cost burden of obesity among privately insured employees: A comparison of healthcare industry versus other major industries in the united states. *Journal of Occupational and Environmental Medicine*, 62(2):98–107, 2020.

[163] Raul I. Ramos-Garcia and Adam W. Hoover. A study of temporal action sequencing during consumption of a meal. In *Proceedings of the International Conference on Bioinformatics, Computational Biology and Biomedical Informatics*, BCB'13, page 68–75, New York, NY, USA, 2013. Association for Computing Machinery.

[164] Raul I Ramos-Garcia, Eric R Muth, John N Gowdy, and Adam W Hoover. Improving the recognition of eating gestures using intergesture sequential dependencies. *IEEE journal of biomedical and health informatics*, 19(3):825–831, 2014.

[165] Alison E Ringel, Jefte M Drijvers, Gregory J Baker, Alessia Catozzi, Juan C García-Cañaveras, Brandon M Gassaway, Brian C Miller, Vikram R Juneja, Thao H Nguyen, Shakchhi Joshi, et al. Obesity shapes metabolism in the tumor microenvironment to suppress anti-tumor immunity. *Cell*, 183(7):1848–1866, 2020.

[166] Eric Robinson, Eva Almiron-Roig, Femke Rutters, Cees de Graaf, Ciarán G Forde, Catrin Tudur Smith, Sarah J Nolan, and Susan A Jebb. A systematic review and meta-analysis examining the effect of eating rate on energy intake and hunger. *The American journal of clinical nutrition*, 100(1):123–151, 2014.

[167] Joseph J Sabia and Daniel I Rees. Body weight, mental health capital, and academic achievement. *Review of Economics of the Household*, 13(3):653–684, 2015.

[168] Jose Francisco Saenz-Cogollo, Massimiliano Pau, Beatrice Fraboni, and Annalisa Bonfiglio. Pressure mapping mat for tele-home care applications. *Sensors*, 16(3):365, 2016.

[169] Nazir Savji, Wouter C Meijers, Traci M Bartz, Vijeta Bhambhani, Mary Cushman, Matthew Nayor, Jorge R Kizer, Amy Sarma, Michael J Blaha, Ron T Gansevoort, et al. The association of obesity and cardiometabolic traits with incident hfpef and hfref. *JACC: Heart Failure*, 6(8):701–709, 2018.

[170] Edward Sazonov, Stephanie Schuckers, Paulo Lopez-Meyer, Oleksandr Makeyev, Nadezhda Sazonova, Edward L Melanson, and Michael Neuman. Non-invasive monitoring of chewing and swallowing for objective quantification of ingestive behavior. *Physiological measurement*, 29(5):525, 2008.

[171] Edward S. Sazonov and Juan M. Fontana. A sensor system for automatic detection of food intake through non-invasive monitoring of chewing. *IEEE Sensors Journal*, 12(5):1340–1348, 2012.

[172] Giovanni Schiboni, Fabio Wasner, and Oliver Amft. A privacy-preserving wearable camera setup for dietary event spotting in free-living. In *2018 IEEE International Conference on Pervasive Computing and Communications Workshops (PerCom Workshops)*, pages 872–877, 2018.

[173] Albrecht Schmidt, Martin Strohbach, Kristof Van Laerhoven, and Gellersen Hans-W. Ubiquitous interaction—using surfaces in everyday environments as pointing devices. In *ERCIM Workshop on User Interfaces for All*, pages 263–279. Springer, 2002.

[174] Alexa Blair Segal, M Carmen Huerta, Elisabetta Aurino, and Franco Sassi. The impact of childhood obesity on human capital in high-income countries: a systematic review. *Obesity Reviews*, 22(1):e13104, 2021.

[175] Jaap C Seidell. Societal and personal costs of obesity. *Experimental and Clinical Endocrinology & Diabetes*, 106(S 02):7–10, 1998.

[176] Nur Asmiza Selamat and Sawal Hamid Md Ali. Automatic food intake monitoring based on chewing activity: A survey. *IEEE Access*, 8:48846–48869, 2020.

[177] Sougata Sen, Vigneshwaran Subbaraju, Archan Misra, Rajesh Balan, and Youngki Lee. Annapurna: Building a real-world smartwatch-based automated food journal. In *2018 IEEE 19th International Symposium on "A World of Wireless, Mobile and Multimedia Networks" (WoWMoM)*, pages 1–6, 2018.

[178] Sougata Sen, Vigneshwaran Subbaraju, Archan Misra, Rajesh Krishna Balan, and Youngki Lee. The case for smartwatch-based diet monitoring. In *2015 IEEE International Conference on Pervasive Computing and Communication Workshops (PerCom Workshops)*, pages 585–590, 2015.

[179] Edmund Seto, Jenna Hua, Lemuel Wu, Victor Shia, Sue Eom, May Wang, and Yan Li. Models of individual dietary behavior based on smartphone data: the influence of routine, physical activity, emotion, and food environment. *PLoS One*, 11(4):e0153085, 2016.

[180] Danit Shahar, Drora Fraser, Iris Shai, and Hillel Vardi. Development of a food frequency questionnaire (ffq) for an elderly population based on a population survey. *The Journal of nutrition*, 133(11):3625–3629, 2003.

[181] Arnold Slyper. Oral processing, satiation and obesity: overview and hypotheses. *Diabetes, Metabolic Syndrome and Obesity: Targets and Therapy*, 14:3399, 2021.

[182] Alexia G Smith, Patricia A Sheridan, Raymond J Tseng, John F Sheridan, and Melinda A Beck. Selective impairment in dendritic cell function and altered antigen-specific cd8+ t-cell responses in diet-induced obese mice infected with influenza virus. *Immunology*, 126(2):268–279, 2009.

[183] Pin Song, Haili Qin, Huai-Ling Gao, Huai-Ping Cong, and Shu-Hong Yu. Self-healing and superstretchable conductors from hierarchical nanowire assemblies. *Nature communications*, 9(1):1–9, 2018.

[184] John R Speakman. The history and theory of the doubly labeled water technique. *The American journal of clinical nutrition*, 68(4):932S–938S, 1998.

[185] Simon Stankoski, Marko Jordan, Hristijan Gjoreski, and Mitja Luštrek. Smartwatch-based eating detection: Data selection for machine learning from imbalanced data with imperfect labels. *Sensors*, 21(5), 2021.

[186] Norbert Stefan, Andreas L Birkenfeld, and Matthias B Schulze. Global pandemics interconnected—obesity, impaired metabolic health and covid-19. *Nature Reviews Endocrinology*, pages 1–15, 2021.

[187] Eliot Stellar and E Eileen Shrager. Chews and swallows and the microstructure of eating. *The American journal of clinical nutrition*, 42(5):973–982, 1985.

[188] Petra Stiegler, Stefanie Sausenthaler, Anette E Buyken, Peter Rzehak, Daniel Czech, Jakob Linseisen, Anja Kroke, Kurt Gedrich, Claire Robertson, and Joachim Heinrich. A new ffq designed to measure the intake of fatty acids and antioxidants in children. *Public health nutrition*, 13(1):38–46, 2010.

[189] Amy F Subar, Sharon I Kirkpatrick, Beth Mittl, Thea Palmer Zimmerman, Frances E Thompson, Christopher Bingley, Gordon Willis, Noemi G Islam, Tom Baranowski, Suzanne McNutt, et al. The automated self-administered 24-hour dietary recall (asa24): a resource for researchers, clinicians and educators from the national cancer institute. *Journal of the Academy of Nutrition and Dietetics*, 112(8):1134, 2012.

[190] Mingui Sun, Lora E Burke, Zhi-Hong Mao, Yiran Chen, Hsin-Chen Chen, Yicheng Bai, Yuecheng Li, Chengliu Li, and Wenyan Jia. ebutton: a wearable computer for health monitoring and personal assistance. In *Proceedings of the 51st annual design automation conference*, pages 1–6, 2014.

[191] Young Jin Tak and Sang Yeoup Lee. Long-term efficacy and safety of anti-obesity treatment: where do we stand? *Current obesity reports*, 10(1):14–30, 2021.

[192] Edison Thomaz, Irfan Essa, and Gregory D Abowd. A practical approach for recognizing eating moments with wrist-mounted inertial sensing. In *Proceedings of the 2015 ACM international joint conference on pervasive and ubiquitous computing*, pages 1029–1040, 2015.

[193] Frances E Thompson and Tim Byers. Dietary assessment resource manual. *The Journal of nutrition*, 124(suppl_11):2245s–2317s, 1994.

[194] Frances E Thompson and Amy F Subar. Dietary assessment methodology. *Nutrition in the Prevention and Treatment of Disease*, pages 5–48, 2017.

[195] Jillian Trabulsi and Dale A Schoeller. Evaluation of dietary assessment instruments against doubly labeled water, a biomarker of habitual energy intake. *American Journal of Physiology-Endocrinology And Metabolism*, 2001.

[196] Maximilian Tremmel, Ulf-G Gerdtham, Peter M Nilsson, and Sanjib Saha. Economic burden of obesity: a systematic literature review. *International journal of environmental research and public health*, 14(4):435, 2017.

[197] Janet van den Boer, Annemiek van der Lee, Lingchuan Zhou, Vasileios Papapanagiotou, Christos Diou, Anastasios Delopoulos, Monica Mars, et al. The splendid eating detection sensor: Development and feasibility study. *JMIR mHealth and uHealth*, 6(9):e9781, 2018.

[198] Luc F Van Gaal, Ilse L Mertens, and Christophe E De Block. Mechanisms linking obesity with cardiovascular disease. *Nature*, 444(7121):875–880, 2006.

[199] Mirre Viskaal-van Dongen, Frans J Kok, and Cees de Graaf. Eating rate of commonly consumed foods promotes food and energy intake. *Appetite*, 56(1):25–31, 2011.

[200] Theo Vos, Stephen S Lim, Cristiana Abbafati, Kaja M Abbas, Mohammad Abbasi, Mitra Abbasifard, Mohsen Abbasi-Kangevari, Hedayat Abbastabar, Foad Abd-Allah, Ahmed Abdelalim, et al. Global burden of 369 diseases and injuries in 204 countries and territories, 1990–2019: a systematic analysis for the global burden of disease study 2019. *The Lancet*, 396(10258):1204–1222, 2020.

[201] William P. Walker and Dinesh K. Bhatia. Automated ingestion detection for a health monitoring system. *IEEE Journal of Biomedical and Health Informatics*, 18(2):682–692, 2014.

[202] Yongbiao Wan, Yan Wang, and Chuan Fei Guo. Recent progresses on flexible tactile sensors. *Materials Today Physics*, 1:61–73, 2017.

[203] Nikolas Wanahita, Franz H Messerli, Sripal Bangalore, Apoor S Gami, Virend K Somers, and Jonathan S Steinberg. Atrial fibrillation and obesity—results of a meta-analysis. *American heart journal*, 155(2):310–315, 2008.

[204] Shuangquan Wang, Gang Zhou, Lisha Hu, Zhenyu Chen, and Yiqiang Chen. Care: Chewing activity recognition using noninvasive single axis accelerometer. In *Adjunct Proceedings of the 2015 ACM International Joint Conference on Pervasive and Ubiquitous Computing and Proceedings of the 2015 ACM International Symposium on Wearable Computers*, pages 109–112, 2015.

[205] Shuangquan Wang, Gang Zhou, Yongsen Ma, Lisha Hu, Zhenyu Chen, Yiqiang Chen, Hongyang Zhao, and Woosub Jung. Eating detection and chews counting through sensing mastication muscle contraction. *Smart Health*, 9:179–191, 2018.

[206] Danny Weathers, Jennifer Christie Siemens, and Steven W Kopp. Tracking food intake as bites: effects on cognitive resources, eating enjoyment, and self-control. *Appetite*, 111:23–31, 2017.

[207] Gary M. Weiss, Jessica L. Timko, Catherine M. Gallagher, Kenichi Yoneda, and Andrew J. Schreiber. Smartwatch-based activity recognition: A machine learning approach. In *2016 IEEE-EMBS International Conference on Biomedical and Health Informatics (BHI)*, pages 426–429, 2016.

[208] MS Westerterp-Plantenga, KR Westerterp, NA Nicolson, A Mordant, PFM Schoffelen, and F Ten Hoor. The shape of the cumulative food intake curve in humans, during basic and manipulated meals. *Physiology & behavior*, 47(3):569–576, 1990.

[209] Anne M Wolf. Economic outcomes of the obese patient. *Obesity*, 10(s11):58S, 2002.

[210] Thomas P Wycherley, Lisa J Moran, Peter M Clifton, Manny Noakes, and Grant D Brinkworth. Effects of energy-restricted high-protein, low-fat compared with standard-protein, low-fat diets: a meta-analysis of randomized controlled trials. *The American journal of clinical nutrition*, 96(6):1281–1298, 2012.

[211] Jie Xue, Jiawei Chen, Jizhong Song, Leimeng Xu, and Haibo Zeng. Wearable and visual pressure sensors based on zn 2 geo 4@ polypyrrole nanowire aerogels. *Journal of Materials Chemistry C*, 5(42):11018–11024, 2017.

[212] Xin Yang, Abul Doulah, Muhammad Farooq, Jason Parton, Megan A McCrory, Janine A Higgins, and Edward Sazonov. Statistical models for meal-level estimation of mass and energy intake using features derived from video observation and a chewing sensor. *Scientific reports*, 9(1):1–10, 2019.

[213] Modjtaba Zandian, Ioannis Ioakimidis, Cecilia Bergh, and Per Södersten. Linear eaters turned decelerated: Reduction of a risk for disordered eating? *Physiology & behavior*, 96(4-5):518–521, 2009.

[214] Federica Zatterale, Michele Longo, Jamal Naderi, Gregory Alexander Raciti, Antonella Desiderio, Claudia Miele, and Francesco Beguinot. Chronic adipose tissue inflammation linking obesity to insulin resistance and type 2 diabetes. *Frontiers in physiology*, 10:1607, 2020.

[215] Chunyan Zhang, Chanyu Yue, Andreas Herrmann, Jieun Song, Colt Egelston, Tianyi Wang, Zhifang Zhang, Wenzhao Li, Heehyoung Lee, Maryam Aftabizadeh, et al. Stat3 activation-induced fatty acid oxidation in cd8+ t effector cells is critical for obesity-promoted breast tumor growth. *Cell metabolism*, 31(1):148–161, 2020.

[216] Rui Zhang and Oliver Amft. Monitoring chewing and eating in free-living using smart eyeglasses. *IEEE Journal of Biomedical and Health Informatics*, 22(1):23–32, 2018.

[217] Rui Zhang and Oliver Amft. Retrieval and timing performance of chewing-based eating event detection in wearable sensors. *Sensors*, 20(2), 2020.

[218] Rui Zhang, Severin Bernhart, and Oliver Amft. Diet eyeglasses: Recognising food chewing using emg and smart eyeglasses. In *2016 IEEE 13th International Conference on Wearable and Implantable Body Sensor Networks (BSN)*, pages 7–12, 2016.

[219] Bo Zhou, Jingyuan Cheng, Mathias Sundholm, Attila Reiss, Wuhuang Huang, Oliver Amft, and Paul Lukowicz. Smart table surface: A novel approach to pervasive dining monitoring. In *2015 IEEE International Conference on Pervasive Computing and Communications (PerCom)*, pages 155–162. IEEE, 2015.

[220] Nicolien Zijlstra, René de Wijk, Monica Mars, Annette Stafleu, and Cees de Graaf. Effect of bite size and oral processing time of a semisolid food on satiation. *The American journal of clinical nutrition*, 90(2):269–275, 2009.

[221] C Zimmermann, J Zeilfelder, T Bloecher, M Diehl, S Essig, and Wilhelm Stork. Evaluation of a smart drink monitoring device. In *2017 IEEE Sensors Applications Symposium (SAS)*, pages 1–5. IEEE, 2017.